UC Irvine
UC Irvine Electronic Theses and Dissertations

Title
Phosphorylation of ribosomal protein S6 as a mechanism to regulate translation at activated synapses

Permalink
https://escholarship.org/uc/item/8hf7w1qt

Author
Pirbhoy, Patricia Salgado

Publication Date
2016

Peer reviewed|Thesis/dissertation

eScholarship.org Powered by the California Digital Library
University of California

UNIVERSITY OF CALIFORNIA,
IRVINE

Phosphorylation of ribosomal protein S6 as a mechanism to regulate translation at activated synapses

DISSERTATION

submitted in partial satisfaction of the requirements
for the degree of

DOCTOR OF PHILOSOPHY

in Neurobiology and Behavior

by

Patricia Salgado Pirbhoy

Dissertation Committee:
Professor Oswald Steward, Chair
Professor Christine Gall
Professor John Guzowski

2016

Chapter 2 © CSH Press
All other materials © 2016 Patricia Salgado Pirbhoy

DEDICATION

To

my loving parents, husband, brother, family and friends

in recognition of their worth

and their unwavering belief in me.

At the end of the day, all that is left is our memories.

We are who we are because of what we learn and what we remember.

Eric R. Kandel
"In search of Memory: The emergence of a new science of mind"

TABLE OF CONTENTS

LIST OF FIGURES

LIST OF TABLES

ACKNOWLEDGMENTS

I would like to express the deepest appreciation to my committee chair, Dr. Oswald Steward, who has been supportive every step of the way. I am thankful for the guidance and support he has provided throughout our time together. I would like to thank him for his continued guidance in helping me be a better scientist in all aspects, presentations, writing, and with experiments. I have enjoyed coming into the laboratory and seeing his passion for research. His constant enthusiasm and curiosity made being in the laboratory a wonderful experience. It is a great honor to have worked with such an inspirational scientist.

I would also like to express my deepest appreciation to the members of my dissertation committee, Dr. Christine Gall, and Dr. John Guzowski. I am thankful for their valuable input and discussions throughout my doctoral program. Their input helped me expand my view of the results and helped me become a better scientist. I would like to thank them for providing the necessary guidance to excel in this program.

I would also like to thank Dean Francis Leslie for being an incredible support throughout my undergraduate and graduate career. I feel blessed to have such strong support. I would like to thank her for her belief in me and guidance, which has helped shape my path. I would like to thank her for helping me navigate through important life decisions and always offering a helping hand.

I would also like to thank Dr. Marlene de la Cruz for the opportunity that she has given me to pursue higher education. I am the first member of my family to receive a doctorate from a University, and I could not have accomplished this without her. I am thankful for her advice and strong will and determination in helping me get to where I am now. I have learned many valuable skills under her wing and I would like to express my deepest appreciation for her guidance and support.

I would also like to thank my parents for always believing in me. Thank you for always offering a hand-to-hold at every moment. I would not be here without you. Thank you to my brother, George, whom I have always looked up to and am grateful to have in this life. Thank you for always being there. Thank you to my husband, Amir, who has been my rock, in this process. Thank you for your words of encouragement and love, every day. I am excited to see where life takes us. Thank you to my family and friends who are always there for me ready to cheer me on. You all give me strength and courage, and I am blessed to have you all.

I would also like to thank Cold Spring Harbor Laboratory Press for permission to include copyrighted photographs as part of my dissertation. The text of Chapter 2 is a reprint of material as it appears in Pirbhoy et al., 2016 in the Journal of Learning and Memory. Coauthors on the publication included Shannon Farris and Oswald Steward. Thank you to my collaborators in experimental procedures conducted in Chapter 4, which included Brian

Trieu, Dr. Yousheng Jia, Dr. Christine Gall, and Dr. Gary Lynch. Thank you for your advice and for your time and expertise in making this project possible.

This work was supported in part by a fellowship award to Patricia S. Pirbhoy, an NRSA predoctoral fellowship from NINDS (F31-NS083349), a T32 training grant (T32-NS045540), and a grant from the Minority Science Program (NIH MBRS-IMSD GM055246). Financial support was also provided from NIH NS-12333 to Oswald Steward.

CURRICULUM VITAE

Patricia Salgado Pirbhoy

EDUCATION

August 2016 — **Ph.D. in Biological Sciences**
Department of Neurobiology and Behavior
University of California, Irvine
Irvine, CA

December 2015 — **M.S. in Biological Sciences**
University of California, Irvine
Irvine, CA

June 2010 — **B.S. in Biological Sciences**
University of California, Irvine
Irvine, CA

RESEARCH EXPERIENCE

2010 – 16 — **Graduate Student Researcher**
Department of Neurobiology and Behavior, University of California, Irvine
Advisor: Oswald Steward, PhD
Thesis: Phosphorylation of ribosomal protein S6 as a mechanism to regulate translation at activated synapses

2010 — **International Research Training**
Minority Health and Health Disparities International Research Training
Center for Public Health Research (CSISP); Valencia, Spain
Advisor: Juan Jose Abellan, PhD
Project title: "Analysis of the relationship between microbiota composition of IBS patients and clinical, lifestyle and social-economic status variables"

2008-10 — **Undergraduate Research Assistant**
Department of Pharmacology, University of California, Irvine
Advisor: Frances Leslie, PhD
Mentor: Jasmin M. Dao, MD/PhD
Project title: "The role of 5-HT in modulating dopamine-mediated behaviors"

2008 — **International Research Training**
Minority Health and Health Disparities International Research Training
Department of Behavioral and Cognitive Neurobiology

Advisor: Victor Ramirez-Amaya, PhD
Mentor: Marisela Martinez Claros, MD/PhD
Project title: "Relationship between corticosterone and plastic changes in the adult rat hippocampus"

2008 **Undergraduate Research Assistant**
Minority Biomedical Research Support (MBRS) Program
Advisor: Luis Mota-Bravo, PhD
Mentor: Toai Nguyen
Project title: "Antibiotic gene transfer between humans and domestic dogs"

TEACHING EXPERIENCE

2012-13 Teaching Assistant for Neurobiology Laboratory course, N113L, University of California, Irvine

2014 Teaching Assistant for Brain Dysfunction and Repair course, Bio 37, University of California, Irvine

2014 Instructor for Power of Speech Workshop, communication workshop hosted by Graduate Division, University of California, Irvine

LEADERSHIP EXPERIENCE

2013-15 Vice President of affiliate chapter, Orange County Graduate Women in Science, University of California, Irvine

2014-15 Vice President for American Association of University Women Chapter at the University of California, Irvine

2014 Laboratory Tour Coordinator, Tech Trek Camp, University of California, Irvine

2013-14 Secretary for American Association of University Women Chapter at the University of California, Irvine

2013 Laboratory Tour Coordinator, Tech Trek Camp, University of California, Irvine

2012-13 Undergraduate Mentor: Supervised undergraduate research conducted by Christina Abundis (B.S., Developmental and Cell Biology, 2013).
Project Title: "Localization of ribosomal protein S6 and the immediate early gene, Arc, in animals exposed to a novel environment"
Honors: Undergraduate Research Opportunities Program Fellow (2012 - 2013)

FELLOWSHIPS

2013-2016 Ruth L. Kirschstein National Service Award (NRSA) for Individual Predoctoral Fellowships to Promote Diversity in Health-Related Research (Parent F31 - Diversity) - National Institute of Neurological Disorders and Stroke (NINDS), Grant FNS083349A

2013 NRSA Epilepsy Training Grant# 5T32NS045540-09

2010 NIH - Minority Health and Health Disparities International Research Training (MHIRT) NIH Grant # MD:-01485. Valencia, Spain.

2009-10 Minority Access for Research Careers (MARC), fellowship funded by National Institutes of Health (NIH)

2009-10 Undergraduate research and mentoring (URM), National Science Foundation (NSF) Grant #0731655

2008 NIH - Minority Health and Health Disparities International Research Training (MHIRT) NIH Grant # MD:-01485. Queretaro, Mexico.

PUBLICATIONS

1. **Pirbhoy PS,** Farris S, Steward O (2016). Synaptic activation of ribosomal protein S6 phosphorylation occurs locally in activated dendritic domains. Learn Memory, 23:1-16. Doi:10.1101/lm.041947.116

2. Steward O, Farris S, Darnell J, Van Driesche SJ, **Pirbhoy PS** (2015). Localization and local translation of Arc/Arg3.1 mRNA at synapses: some observations and paradoxes. Frontiers in Molecular Neuroscience,7. Doi: 10.3389/fnmol.2014.00101

3. Durban A, Abellan JJ, Jimenez-Hernandez N, **Salgado P,** Ponce M, Ponce J, Garigues V, Latorre A, Moya A (2012). Structural alterations of faecal and mucosa-associated bacterial communities in irritable bowel syndrome. Environ Microbiol. 4:242-247.

ABSTRACTS

1. **Pirbhoy PS,** Trieu B, Jia Y, Gall C, Lynch G, Steward O. Selective optogenetic activation of perforant path synapses in hippocampal slices. 2015. Society for Neuroscience, Chicago, IL. (Poster)

2. **Pirbhoy PS,** Trieu B, Jia Y, Gall C, Lynch G, Steward O. Optogenetic stimulation of the medial perforant path. 2015. Annual EpiCenter Symposium, UC Irvine, Irvine, CA. (Poster)

3. **Salgado P,** Steward O. Phosphorylation of ribosomal protein S6 as a mechanism to regulate translation at activated synapses. 2013. Society for Neuroscience, San Diego, California. (Poster)

4. **Salgado P,** Steward O. A learning experience activates phosphorylation of ribosomal protein S6 in the same group of neurons in which Arc mRNA is induced. 2013. American Association for the Advancement of Science (AAAS), Boston MA. (Poster)

5. **Salgado P,** Steward O. A learning experience activates phosphorylation of ribosomal protein S6 in the same group of neurons in which Arc mRNA is induced. 2012. Society for Neuroscience, New Orleans, LA. (Poster)

6. **Salgado P,** Farris S, Steward O. LTP induction triggers rapid but transient phosphorylation of ribosomal protein S6 in activated dendritic domains. 2011. Society for Neuroscience, Washington, D.C. (Poster)

7. Farris S, **Salgado P,** Steward O. Ribosomal protein S6 is phosphorylated at activated synapses in vivo in response to strong synaptic activity. 2011. Synapses: From Molecules to Circuits and Behavior, Cold Spring Harbor, New York. (Poster)

8. Durban A, Jimenez-Hernandez N, **Salgado P**, Latorre PA, Moya A. Structural Alterations of Fecal and Mucosa-Associated Bacteria in Irritable Bowel Syndrome. 2011. International Human Microbiome Congress, Vancouver in British Columbia, Canada. (Poster)

9. Dao JM, **Salgado P**, Albano JV, Belluzzi JD, Leslie FM. Effects of Brief Nicotine Exposure on the Developing Dopamine System. 2009. Society for Neuroscience Conference, Chicago, Illinois. (Poster)

10. **Salgado P,** Dao JM, Leslie FM. 4th year. WAY 100635's Potential to Modulate Nicotine's Addictive Effects. 2009. Sigma Xi Conference. Houston, Texas. (Poster)

11. **Salgado P,** Martinez M.C, Ramirez-Amaya V. 3rd year. Relationship between Corticosterone and Plastic Changes in the Adult Rat Hippocampus. 2009. American Association for the Advancement of Science (AAAS). Chicago, Illinois. (Poster)

12. **Salgado P,** Martinez M.C, Ramirez-Amaya V. 3rd year. Relationship between Corticosterone and Plastic Changes in the Adult Rat Hippocampus. 2008. Annual Biomedical Research Conference for Minority Students (ABRCMS). Orlando, Florida. (Poster)

PROFESSIONAL MEMBERSHIPS AND AFFILIATIONS

Graduate Women in Science

American Association of University Women

Society for Neuroscience

International Medical Fraternity, Phi Delta Epsilon

HONORS AND AWARDS

Dean's List: Fall 2006; Fall 2008; Spring 2009; Fall 2009; Winter 2010; Spring 2010

Minority Access for Research Careers (MARC) Scholar: awarded based on academic merit

TRAINING AND SKILLS

2014 Mentoring Excellence Program offered by Graduate Division at the University of California, Irvine. Development of mentoring skills.

2014 Certified Communication Trainer, preparation to teach workshop following Train the Trainers workshop by Bri McWhorter. Hosted by Graduate Division at the University of California, Irvine. Training prepared trainers to present a 2-3-hour workshop to department peers on communication tools to improve general communication and research presentations.

Laboratory Skills:

Neurobiology Techniques: performing behavioral experiments on rats (novel object recognition, object location memory, novel environment exploration, unsupervised learning, Morris water maze), and experienced in animal surgeries including, surgeries for intravenous delivery of treatments (insertion of catheter into jugular vein), intracranial injection of vectors using stereotaxic apparatus, stereotaxic *in vivo* electrophysiology (medial perforant path stimulation), *in vivo* delivery of pharmacological agents into entorhinal cortex and hippocampus.

Molecular Neurobiology Techniques: experienced in brain extraction, transcardial perfusions, brain sectioning (Vibratome and cryostat), subcellular fractionation, confocal microscopy, fluorescent immunohistochemistry, gel electrophoresis, western blotting.

COMMUNITY OUTREACH

2014 GIRLS INC (September-December)
Volunteer at "Girls Inc" Literacy Program hosted in local elementary school. Worked with 1st and 2nd grade girls to help improve their reading scores. The mission of the program is to inspire all girls to be strong, smart and bold to help them pursue professional careers by targeting them early in their youth.

2014 PANELIST (September)
Served as a panelist for the "Getting Involved: Leadership Opportunities Outside of Your Office or Lab" during the campus-wide new graduate student orientation.

2014 TECH TREK CAMP (July)
Dorm Mom Volunteer. During a week-long math and science camp, I worked with incoming 8th grade girls. The girls that attended the camp were generally low-income or underrepresented minority students who were nominated by their teachers for their exceptional achievements in math and science. The camp is designed to further develop interest and excitement in math and science as well as develop self-confidence.

2014 LABORATORY TOUR (January)
Volunteer for "Mission Viejo Christian School laboratory tour" hosted by the Reeve-Irvine Research Center. Third grade students from Mission Viejo Christian school were informed of research done in the Steward laboratory and educated about the brain and spinal cord injury.

2013-15 MEET THE SCIENTIST (March)
Volunteer for "Meet the Scientist" event hosted by the Reeve-Irvine Research Center. This event brings together scientists, researchers, clinicians, associates, and students offering the spinal cord injury community the opportunity to meet scientists directly, ask questions and understand on-going spinal cord research conducted at the University of California, Irvine.

2013 TECH TREK CAMP (July)
Served as a dorm mom during a week-long math and science camp (see description above).

2013 DIVERSITY FORUM (April)
Volunteered for "Southern California Forum for Diversity in Graduate Education" event hosted at the University of California, Irvine. This event is designed to meet the needs of diversity students interested in advanced degrees. The event allows participants to explore graduate opportunities and

participate in workshops to help prepare students for graduate school. The forum also hosts a graduate recruitment fair where participants can receive information from over 175 institutions from across the United States.

2012 PET RESCUE CENTER (July)
Volunteer for The Pet Rescue Center, a non-profit organization that rescues dogs and cats at risk of euthanasia by providing temporary sanctuary while they work to locate an adopting family.

2012 CAMP MED (May)
Volunteer for CampMed, a non-profit educational-enrichment program that educates socio-economically disadvantaged high school students interested in pursuing higher education in health science fields. Hosted at the University of California, Irvine.

2007-09 SALSA TEAM COORDINATOR
Volunteered as a co-coordinator of a performing salsa team at the University of California, Irvine.

2008 CHOC
Volunteer for Children's Hospital of Orange County (CHOC) walk.

ABSTRACT OF THE DISSERTATION

Phosphorylation of ribosomal protein S6 as a mechanism to regulate translation at activated synapses

By

Patricia Salgado Pirbhoy

Doctor of Philosophy in Biological Sciences

University of California, Irvine, 2016

Professor Oswald Steward, Chair

Long-term potentiation (LTP) is a key candidate for cellular and molecular mechanisms underlying memory formation. LTP induction results in functional and structural changes at synapses, but mechanisms connecting signal transduction pathways to processes responsible for these synaptic modifications remain obscure. The present studies investigate the induction of a post-translational modification, phosphorylation of ribosomal protein S6 (rpS6), in response to synaptic activity and its role in the initiation of translation. Using acute neurophysiological techniques, LTP was induced in the dentate gyrus (DG) of intact, anesthetized rats by delivering high-frequency stimulation (HFS) to the medial perforant path. Immunohistochemical analysis using phospho-specific antibodies that detect phosphorylation at subsets of serine residues, ser235/236, and ser240/244, were used to assess levels of rpS6 phosphorylation. Chapter 2 presents experiments detailing activation parameters of rpS6 phosphorylation in response to synaptic activity. Results show that HFS induces robust phosphorylation of rpS6 (p-rpS6) in granule cell bodies and a selective accumulation in the portion of the dendrites contacted

by active synapses. Surprisingly, the selective accumulation at activated synapses was primarily observed with ser235/236. Also, synaptically-driven rpS6 phosphorylation is dependent on NMDA receptor activation and persists for hours after LTP induction. Interestingly, despite the robust induction of p-rpS6 following HFS, assessment of protein synthesis by autoradiography revealed no increases in protein synthesis. Furthermore, a learning experience triggered p-rpS6 in individual neurons in a pattern similar to that of immediate early gene (IEG) induction. Chapter 3 presents studies that investigate the induction of p-rpS6 by PI3K/mTOR and MAPK/ERK-dependent signaling pathways. Local infusions of selective pharmacological agents were delivered into the DG to inhibit fundamental kinases. Results show that PI3K/mTOR and MAPK/ERK signaling pathways regulate p-rpS6 differentially in granule cell bodies and dendrites. Surprisingly, local delivery of the PI3-kinase inhibitor, wortmannin, abolished p-rpS6 specifically in the cell bodies, while sparing p-rpS6 in the dendrites. Results from the local infusion of the MEK inhibitor, U0126, provided further support by revealing a selective reduction of p-rpS6 in the dendrites. Together, these results point to phosphorylation of rpS6 as a mechanism by which PI3K/mTOR and MAPK/ERK signaling regulates translational control in response to neuronal activity.

CHAPTER 1

INTRODUCTION

1.1 Cellular and molecular mechanisms underlying memory formation

Long-term potentiation (LTP) induces activity-dependent modifications in synaptic strength and is extensively studied as a model of synaptic plasticity. The synaptic alterations induced by LTP are widely accepted as a cellular and molecular mechanism by which memory can be encoded in neuronal ensembles (Bliss and Collingridge, 1993). LTP was first characterized in the excitatory connections made by perforant path fibers onto granule cells of the hippocampus in the anesthetized rabbit, where long-lasting potentiation of evoked excitatory postsynaptic potentials (EPSPs) was observed to last from 30 minutes up to 10 hours post stimulation (Bliss and Lomo, 1973). This long-lasting potentiation, later termed long-term potentiation, is characterized by a persistent increase in synaptic strength between synapses following repetitive synaptic stimulation (Bliss and Lomo, 1973; Douglas and Goddard, 1975). LTP is commonly divided into two phases but at times may be divided into three temporal phases [reviewed in (Adams and Sweatt, 2002)]. The first phase is initial LTP and is characterized by a short-term potentiation lasting up to 30 minutes. Expression of initial LTP is protein kinase and protein synthesis-independent. The second phase consists of a transient, early phase (E-LTP), which lasts from 30 minutes to a few hours. E-LTP expression is mediated by persistent activation of post-translational modifications, such as activation of kinases and insertion of glutamate receptors into postsynaptic membranes (Adams and Sweatt, 2002), but is independent of cAMP-dependent protein kinase (PKA) activation and does not require protein or RNA synthesis (Nguyen and Kandel, 1996). The third phase is late-phase LTP (L-LTP), which lasts for a

prolonged period of time ranging from a few hours to weeks to a year (Abraham et al., 2002). L-LTP requires gene transcription and protein synthesis and can be blocked by PKA inhibitors (Nguyen and Kandel, 1996).

LTP has several characteristics that make it an attractive model for memory storage (Malenka and Nicoll, 1999). As mentioned above, LTP has two main phases, an early- and late-phase. Encoding of new memories is also categorized into short-term memory (STM) and long-term memory (LTM). Similarly, STM, lasting minutes to hours, is believed to require only covalent modification of pre-existing proteins, while LTM is believed to involve structural remodeling or the formation of new synaptic connections mediated by increased gene expression and protein synthesis (Bailey et al., 1996).

Other characteristics that make LTP an attractive model for memory storage include its properties of cooperativity, associativity, and input specificity [reviewed in (Bliss and Collingridge, 1993)]. Cooperativity refers to the intensity threshold that exists for LTP induction, where a weak stimulus that activates relatively few afferent fibers does not result in the induction of LTP. LTP is also associative in that strong activation of one set of synapses can facilitate LTP at an independent set of adjacent active synapses on the same cell if both sets of synapses are activated within a specific temporal window. LTP is also input-specific, meaning that LTP induction at one set of synapses results in an increase in synaptic strength at or near the activated synapses. Together these characteristics explain how a particular synapse can be selectively modified if and only if sufficient depolarization occurs. Furthermore, LTP-induced synaptic modifications have been shown to last for hours, days and in one particular case was recorded up to a year *in vivo* (Abraham et al., 2002*).* This long-lasting characteristic is an essential component that makes LTP an

attractive model that parallels long-term memory storage. Collectively, these features make LTP a key candidate mechanism underlying memory formation. Understanding the cellular and molecular mechanisms that underlie LTP is critical to delineating how memories are stored in neuronal ensembles.

1.1.1 Signal transduction pathways

Pharmacological blockade or genetic removal of N-methyl-D-aspartate (NMDA) receptors prevents LTP induction implicating the crucial role for NMDA receptor activation in synaptic plasticity (Collingridge and Bliss, 1987). To activate NMDA receptors glutamate binds the NMDA receptor accompanied by a substantial positive shift in the membrane potential of the postsynaptic cell sufficient to depolarize the cell. NMDA receptors exhibit a voltage-dependence due to the block of its channel by extracellular magnesium and thus contribute little to the basal postsynaptic response. On the other hand, the alpha-amino-3-hydroxy-5-methyl-4-isoxazolepropionic (AMPA) receptor, which is permeable to sodium and potassium, provides the majority of inward current for generating synaptic responses when the cell is close to its resting membrane potential. When the postsynaptic cell is depolarized during the induction of LTP, the magnesium block is released and dissociates from its binding site allowing an influx of calcium and sodium into the postsynaptic cell. This NMDAR-mediated increase in postsynaptic calcium triggers various biochemical processes responsible for LTP (Bliss and Collingridge, 1993; Malenka and Nicoll, 1999). Both, NMDA receptors and calcium/calmodulin-dependent protein kinase II (CaMKII) (Lisman and McIntyre, 2001) are critical players involved in LTP-induced synaptic plasticity.

CaMKII acts as a calcium detector in the postsynaptic neuron. CaMKII is highly

concentrated in the postsynaptic density (PSD), and several studies have shown that activation of CaMKII is a critical step for LTP induction. Pharmacological blockade or genetic removal of CaMKII has also been shown to block LTP induction (Silva et al., 1992). Furthermore, introducing an active form of CaMKII into the postsynaptic neuron induces potentiation and prevents subsequent LTP induction suggesting that CaMKII is both necessary and sufficient for LTP induction (Lisman and McIntyre, 2001). Manipulations of calcium alone demonstrate that calcium signaling is essential in initiating processes responsible for LTP induction [reviewed in (Bliss and Collingridge, 1993)]. Studies show that preventing a rise in postsynaptic calcium with the calcium chelator, EGTA, blocks induction of LTP (Lynch et al., 1983) and raising the amount of postsynaptic calcium by photolysis of caged calcium mimics LTP induction (Malenka et al., 1988).

Several calcium-sensitive enzymes also play a critical role in converting the NMDA receptor-mediated induction signal into processes that initiate synaptic modifications. These calcium-sensitive enzymes include the protease, calpain, the phosphatase, calcineurin, and phospholipases, and protein kinases (Bliss and Collingridge, 1993). Some of the signal transduction pathways activated by these enzymes include protein kinase C (PKC), cyclic adenosine 3',5'-monophosphate (cAMP)-dependent protein kinase A (PKA), the tyrosine kinase Src, and mitogen-activated protein kinase/extracellular signal-regulated kinase (MAPK/ERK). Precise mechanisms defining the contribution of these signal transduction pathways in synaptic plasticity following the induction of LTP or LTM remains elusive. Studies exploring the role of PKC have reported that inhibitors of PKC block LTP (Malenka and Nicoll, 1999) and increasing PKC postsynaptic activity enhances

synaptic transmission (Hu et al., 1987). Studies investigating the role of PKA suggest that it contributes to activation of cAMP and transcription, but precise roles remain elusive.

The MAPK/ERK signaling pathway was first implicated in cell differentiation and proliferation in mitotic cells (Boulton et al., 1991). Over the years it has been attributed a role in LTP-induced synaptic plasticity (English and Sweatt, 1997; Coogan et al., 1999) and LTM (Atkins et al., 1998). In hippocampal slice experiments, LTP induction increases ERK2 activation in area CA1 following NMDA receptor stimulation (English and Sweatt, 1996). Behavioral studies also show that inhibition of MAPK/ERK results in impaired long-term fear memory (Atkins et al., 1998), long-term spatial memory (Blum et al., 1999; Selcher et al., 1999), and long-term taste memory (Berman et al., 1998). Overall, NMDA receptor activation is crucial for the induction of LTP. NMDA receptor activation allows for the influx of postsynaptic calcium, which is responsible for activating a series of biochemical processes that play a major role in NMDA receptor-mediated synaptic plasticity and learning and memory, yet the molecular connections linking NMDA receptor activation to synaptic modifications remains unclear.

1.1.2 Morphological modifications

Establishing mechanisms of how synaptic activity results in structural and functional changes at activated synapses is a leading goal in the field. It is hypothesized that synaptic modifications occur at both pre- and postsynaptic cells. At the presynaptic synapse, increased neurotransmitter release (i.e. glutamate) is proposed to explain the enhancement of synaptic strength observed following LTP induction. At the postsynaptic synapse, hypotheses include an increase in the number of receptors or alterations in the receptor's functional state (i.e. AMPA receptors), and/or structural modifications in spine

shape [reviewed in (Bliss and Collingridge, 1993)]. For example, modification of AMPA receptor function is proposed as a mechanism underlying the enhancement of synaptic transmission observed following LTP induction (Malenka and Nicoll, 1999). Studies report an increase in phosphorylation of ser831 of the GluR1 AMPA receptor, which has been shown to be phosphorylated by CaMKII (Mammen et al., 1997), following LTP induction. Phosphorylation of ser831 is proposed to result in increases in single-channel conductance of GluR1 AMPA receptors (Derkach et al., 1999). These findings provide compelling evidence that changes in AMPA receptor function underlie the persistent increase in synaptic transmission observed following LTP induction (Benke et al., 1998) at the postsynaptic cell. But it is likely that multiple modifications are required to accomplish enhanced synaptic transmission between synapses and these findings provide a small piece of the entire process.

Structural modifications of the postsynaptic cell may also serve as a mechanism by which enhanced synaptic transmission occurs between synapses and also as a mechanism for stabilization of LTP. Synaptic potentiation is accompanied by changes in spine size and shape, changes that are observed as early as 10 minutes post stimulation (Fifková and Van Harreveld, 1977). But specific mechanisms by which this occurs remains obscure. One hypothesis proposes the remodeling of the actin cytoskeleton as a mechanism to alter dendritic morphology. Dendritic spines contain high levels of cytoskeletal actin (Fischer et al., 1998), particularly, in the spine head and PSD (Capani et al., 2001). Studies report that synaptic potentiation triggers reorganization of the actin cytoskeleton, which may facilitate alterations in dendritic spine shape (Fukazawa et al., 2003; Chen et al., 2007). Inhibition of actin polymerization results in the inhibition of L-LTP indicating that the late phase is

dependent on the restructuring of the actin cytoskeleton. It is also reported that LTP persistence correlates with the duration of filamentous actin (F-actin) increase (Fukazawa et al., 2003) indicating that F-actin increase may facilitate spine enlargement or the formation of new synapses (Colicos et al., 2001). Together, the high concentrations of actin in dendritic spines and their dynamic state, provide support for actin cytoskeletal reorganization as a mechanism to mediate structural changes in dendritic spines (Fischer et al., 1998; Fukazawa et al., 2003; Herring and Nicoll, 2016).

LTP induction also activates the induction of immediate early genes (IEGs), including c-fos (Lamprecht and Dudai, 1996), zif268 (Jones et al., 2001), and activity-regulated cytoskeleton associated (Arc/Arg3.1) (Link et al., 1995; Lyford et al., 1995). Arc is a unique IEG that localizes to activated dendritic regions (Steward et al., 1998) and is implicated in the maintenance of L-LTP (Guzowski et al., 2000) and memory consolidation (Guzowski et al., 2000; Guzowski et al., 2001; Plath et al., 2006). Exploration of a novel environment is associated with increases in IEG expression (Guzowski et al., 1999; Ramirez-Amaya et al., 2005) and is also reported to result in structural changes in a subset of neurons, specifically in neurons that express Arc (Kitanishi et al., 2009). Studies also indicate that other behavioral tasks, such as contextual fear conditioning results in an increase in spine elimination in Arc-expressing CA1 neurons (Nakayama et al., 2015). Overall, accumulating evidence shows that both synaptic potentiation induced by repetitive stimulation and behavioral learning tasks result in dendritic spine changes at activated synapses. These studies provide compelling evidence that synaptic activity initiates processes in neurons that lead to structural changes in dendritic morphology that underlie learning and memory.

1.1.3 Local protein synthesis

At one time, it was thought that all proteins were synthesized in the cell body (Grafstein and Forman, 1980). Once synthesized, these proteins are transported out to target regions. This view was challenged by the discovery of ergastoplasm, which consists of ribosome particles, associated with the endoplasmic reticulum, near zones of synaptic contact (Bodian, 1965). This observation prompted the hypothesis that translational machinery near proximal dendrites may have a role in the formation of new synaptic contacts. Further evidence for this hypothesis was later observed with the discovery of polyribosome rosettes near the base of dendritic spines in postsynaptic neurons (Steward and Levy, 1982). This study provided strong evidence that the translational machinery needed for protein synthesis was selectively located near synapses, and thus individual synapses could regulate the synthesis of its synaptic constituents. These studies revolutionized the traditional view of protein synthesis prompting a mechanism of local protein synthesis, which would allow for rapid modifications of synapses and local regulation of protein composition as polyribosomes would be able to synthesize key molecular constituents near synapses.

Several studies have separated dendrites or axons from neuronal cell bodies to confirm the ability of dendrites to synthesize proteins without a cell body. This process is complicated due to contamination of cell body fragments and glia. But subcellular fractionation studies, which allows the isolation of synaptosomes with attached fragments of dendrites that retain their cytoplasmic constituents, have provided convincing data that local protein synthesis occurs in the absence of neuronal cell bodies (Rao and Steward, 1991; Torre and Steward, 1992).

1.1.4 Overview of translation

The process of protein synthesis is a highly energy-dependent process. In periods of nutrient or amino acid deprivation, protein synthesis is halted to enhance cell survival. Currently, clearly defined mechanisms of how protein synthesis is regulated following activity-dependent stimulation remains unclear. Several studies point to translation initiation as the rate limiting step for translational control. This section will provide a brief description of translation with a focus on initiation of translation, as mechanisms involved in elongation and termination are beyond the scope of this project.

Translation occurs in three phases: initiation, elongation, and termination. Initiation is commonly targeted for translational control (Sonenberg and Hinnebusch, 2009). mRNA translation is initiated by the assembly of the 43S pre-initiation complex (PIC), which consists of the 40S ribosome subunit, the initiator methionyl-tRNA (met-tRNA) and GTP-bound form of eukaryotic initiation factor 2 (eIF2). PIC assembly is stimulated by eIFs 1, 1A, 3 and 5 (Hinnebusch et al., 2016). The PIC then binds to the 5' end of the m7-G-capped mRNA, a process facilitated by the eIF4F complex, which consists of eIF4E, eIF4A, eIF4G and the poly(A)-binding protein (PABP). The PIC then scans the mRNA from 5' to 3' in search for the AUG start codon. During this process, eIF4F catalyzes the unwinding of the secondary structures in the 5' untranslated region (5'UTR). Recognition of the AUG start codon, triggers eIF2-specific GTPase activated protein (GAP), eIF5B. eIF5B then hydrolyzes GTP, reducing affinity for met-tRNA and resulting in the eIF2-GDP to dissociate from the ribosome (Chakrabarti and Maitra, 1991). The dissociation of eIF1, eIF1A, eIF3, eIF2-GDP must occur for the 40S and 60S subunits to join and form the 80S ribosomal complex. The joining of the 60S subunit activates the GTPase activity of eIF5B leading to its release from

the 80S ribosome, completing the initiation phase of translation and priming the ribosome to accept the first elongating aminoacyl-tRNA (Dever, 2002) to begin the elongation phase. During the elongation phase, amino acids are added to the growing protein chain as specified by the sequence of codons in the mRNA. The polypeptide continues to grow until the ribosome encounters an in-frame stop codon that signals the termination of translation.

1.1.5 Translational machinery at the base of dendritic spines

The discovery of polyribosome rosettes near dendritic spines paved the way for the discovery of other translation associated substrates such as, mRNAs (Steward et al., 1998; Cajigas et al., 2012), mRNA binding proteins (Hoek et al., 1998), tRNA (Tiedge and Brosius, 1996), initiation and elongation factors (Tiedge and Brosius, 1996) in dendrites. Initial studies visualized mRNAs using *in situ* hybridization techniques. Some of the initial mRNAs visualized included Ca^{2+} - calmodulin-dependent protein kinase (CaMKII)-alpha subunit (Burgin et al., 1990), Shank (Böckers et al., 2004), beta-actin (Tiruchinapalli et al., 2003), dendrin (Herb, 1997), Arc (Link et al., 1995; Lyford et al., 1995) , microtubule-associated protein 2 (MAP2) (Garner et al., 1988) and PKM-zeta (Muslimov et al., 2004). Recently, new techniques have allowed for the identification of a more sophisticated list of dendritic mRNAs. Using deep sequencing techniques, a study identified 2,550 mRNAs that are associated with the dendrites and/or axons in the hippocampal neuropil (Cajigas et al., 2012). Several different types of mRNAs were detected, including mRNAs for ionotropic and metabotropic neurotransmitter receptors, adhesion molecules, synaptic scaffolding molecules, signaling molecules, regulators of degradation machinery as well as mRNAs associated with the presynaptic terminal (Cajigas et al., 2012). The continuing growing list of mRNAs identified in dendrites/axons provides substantial evidence in support of local

mRNA translation near synapses.

In analyzing the distribution of some of these mRNAs, it becomes apparent that each mRNA has a unique pattern of subcellular distribution, is expressed in specific cell types, and may even be expressed differentially during development relative to its expression in mature neurons. For example, CaMKII is highly expressed in neurons more than in glia. The mRNAs for the alpha- and beta-subunit of CaMKII are both found throughout the pyramidal and granule cell layers of the hippocampus, but only the CaMKII alpha-subunit is found in dendrites (Burgin et al., 1990). Some mRNAs also have a different subcellular localization compared to its encoded protein. For example, dendrin mRNA is localized in dendrites and cell bodies of forebrain neurons while its protein is limited to dendrites (Herb, 1997). The localization of these mRNAs certainly provides hints regarding their function. The localization of mRNAs near dendritic spines suggests a role in synaptic modifications.

Additional support for local protein synthesis has been provided by the identification of several components involved in mRNA metabolism in dendrites. Zipcode-binding-protein 1 (ZBP1) has been shown to be required for dendritic targeting of beta-actin mRNA (Tiruchinapalli et al., 2003) and ZBP2 has been implicated in the cytoplasmic mRNA localization of MAP2 mRNA in dendrites (Rehbein et al., 2004; Giorgi and Moore, 2007). Heterogeneous nuclear ribonucleoproteins (hnRNPs), which are complexes of a diverse set of proteins that couple with RNA, bind mRNA in the nucleus and accompany mRNAs to the cytoplasm where they modulate mRNA localization, translational efficiency and mRNA stability (Giorgi and Moore, 2007). Most importantly, hnRNPs have been identified in transport granules found in dendrites where they associate with dendritically targeted mRNAs and trans-acting factors that regulate their translation (Kiebler and Bassell, 2006).

Another set of proteins that binds to mRNA and travels to the cytoplasm is the exon junction complex (EJC). The EJC is deposited on mRNAs as a consequence of pre-mRNA splicing and is implicated in subcellular mRNA localization, mRNA translational efficiency and mRNA decay (Palacios et al., 2004). The main RNA anchoring protein found in the EJC is eukaryotic initiation factor 4A-III (eIF4AIII). eIF4AIII is found in dendritic layers of hippocampal neurons and has been shown to colocalize with dendritic messenger ribonucleoprotein particle (mRNP) proteins, Staufen 1 (STAU 1) and fragile X mental retardation protein (FMRP) (Giorgi et al., 2007). eIF4AIII has also been shown to associate with dendritic mRNAs, such as Arc, dendrin, MAP2, CaMKII-alpha, and GluR1 (Giorgi et al., 2007). Identification of these mRNA binding proteins and EJC factors provides insights on underlying mechanism regulating localization of dendritically targeted mRNAs. These studies hint that there are separate mechanisms regulating localization of different types of mRNAs. Furthermore, some of these complexes show dual functions in mRNA transport and localization, allowing for efficient regulation of local translation.

Lastly, translational factors including tRNA, aminoacyl-tRNA synthetase, eukaryotic initiation factor 2 (eIF2), which mediates the binding of the methionyl initiator tRNA to the small ribosomal subunit, and eukaryotic elongation factor 2 (eEF2), which catalyzes translocation from the A to the P site on the ribosome, have also been identified in somata and dendrites of mature hippocampal neurons in culture (Tiedge and Brosius, 1996; Tcherkezian et al., 2010). Support for local protein synthesis continues to grow as more and more protein synthesis-related factors are identified in dendrites and are found to be regulated by synaptic activity (Ostroff et al., 2002).

1.1.3 Transcription of 5'TOP mRNAs

mRNAs that encode ribosomal proteins, initiation factors, and elongation factors, make up the translational machinery of the cell (Hornstein et al., 2001) and are characterized by the presence of a 5'terminal oligopyrimidine (5'TOP) motif (Tsokas, 2005). Under favorable growth conditions, the cell enhances its protein synthesis capability by upregulating transcription the translational apparatus. 5'TOP mRNAs are regulated in an mTOR-dependent manner (Jefferies, 1997; Tcherkezian et al., 2014) and evidence shows that induction of LTP in area CA1 of hippocampal slices results in increased expression of 5'TOP encoded proteins, including ribosomal protein S6 (rpS6), eukaryotic initiation factor-1A (eIF-1A), ribosomal protein L32 (rpL32) (Tang et al., 2002; Tsokas, 2005), eukaryotic elongation factor 2 (eEF2), and Poly(A) binding protein (PABP) (Tsokas et al., 2007). Furthermore, eIF-1A has been shown to localize selectively to activated synapses (Tsokas, 2005). These studies indicate that 5'TOP mRNAs are present in dendrites where they are locally translated (Tang et al., 2002; Tsokas et al., 2007).

Despite the evidence suggesting the localization of 5'TOP mRNAs in dendrites, little is known about the signal transduction pathways that regulate their translation in neurons. Studies that explore the role of 5'TOP mRNAs often focus on signal transduction pathways activated following LTP induction. For example, studies implicate a role for phosphatidylinositol 3-kinase (PI3-kinase) in LTP induction as inhibition of PI3-kinase has been shown to block the induction and expression of LTP (Sanna et al., 2002; Opazo et al., 2003). MAPK/ERK activation has also been implicated in LTP induction and in regulating 5'TOP mRNA translation (Tsokas et al., 2007). In fact, it is proposed that MAPK/ERK regulates translation by directly phosphorylating mTOR-dependent substrates critical in translational control (Opazo et al., 2003; Kelleher et al., 2004a; Tsokas et al., 2007). These

studies provide compelling evidence of the involvement of PI3-kinase/mTOR signaling and MAPK/ERK in regulating local 5'TOP mRNA translation and synaptic plasticity underlying learning and memory.

1.1.7 Proposed models to regulate local protein synthesis

While there is an extensive list of translation-related factors identified in dendrites, the signals that regulate translation following synaptic stimulation are still not well-understood. Several proposed mechanistic models defining regulation of local protein synthesis involve transport of mRNAs to activated regions. For example, in the model of diffusion and entrapment, it is suggested that diffusion allows mRNAs to move from the nucleus to target regions without active transport allowing for entrapment of mRNAs at target regions by localized anchors. In a separate model, it is proposed that mRNAs are not diffusely located but are instead actively transported. In this model of active transport, motor proteins are involved in transporting mRNAs along the cytoskeleton to their final destination following the recruitment of motor proteins by trans-acting factors that bind to specific localization sequences found in mRNAs (Palacios, 2007). Other models proposes localized mRNA degradation and nonsense-mediated mRNA decay (NMD) as mechanisms to regulate mRNA translation (Giorgi et al., 2007). In the model of localized degradation, the mRNA is degraded if not protected by a signal. NMD regulation is proposed to occur in a specific subset of mRNAs, and it serves as a post-transcriptional mechanism that eliminates abnormal transcripts containing premature termination codons to prevent the production of truncated and dominant-negative proteins (Lejeune and Maquat, 2005; Giorgi et al., 2007). Natural NMD targets are mRNAs with upstream open reading frames and those produced from transcripts with introns in the 3'-UTR (Hillman et al., 2004; Mendell et al.,

2004; Wittmann et al., 2006).

Other models propose that mRNAs are transported to target regions in a translationally silent manner due to the presence of binding proteins that act as translational repressors. A well-known translational repressor is FMRP, which has been shown to associate with neuronal mRNA transport granules (Kanai et al., 2004; Vanderklish and Edelman, 2005) and bind to several mRNAs including CaMKII-alpha, MAP1b, and PSD-95 (Doyle and Kiebler, 2011). The translational repression is then relieved locally at activated synapses (Dahm and Kiebler, 2005; Meignin and Davis, 2010).

A critical question that arises in these models is – What is the signal that regulates the transport of mRNAs? One model proposes synaptic tagging (Frey and Morris, 1997). This model predicts that newly synthesized proteins are delivered by non-directed transport from the cell body and are captured locally at activated synapses to function in an input-specific manner (Okada et al., 2009). There are several proposed models to describe possible mechanisms that lead to the creation of synaptic tags. These synaptic tags can potentially be created through post-translational modifications at activated synapses; a prion-like switch in protein conformation; or the initiation of local translation may generate a platform for further translation (Doyle and Kiebler, 2011). Further research is needed to understand what signals lead to specific mRNA targeting to activated synapses.

Additional mechanisms implicated in regulating local protein synthesis include post-translational modifications such as promoting translation initiation by increasing poly (A) tail length via cytoplasmic polyadenylation element (CPE) (Jiang and Schuman, 2002). These factors have been found to be present in dendrites and regulated by NMDA receptor-dependent signaling (Huang, 2002). While there are several models to describe potential

mechanisms of local protein synthesis, studies have failed to provide sufficient evidence for the use of a single model in regulating local translation. Several studies report evidence for pieces of each model suggesting that these models may be specific to particular stimulation patterns, mRNAs or neuronal cell types. Overall, these models reveal how we are barely starting to piece together mechanisms of local protein synthesis.

1.1.8 Dysregulation of protein synthesis

Loss of translational control is found in disorders associated with mutations in FMRP, tuberous sclerosis complex (TSC), and phosphatase and tensin homolog (PTEN). Mutations in these genes are associated with altered dendritic spine morphology and synaptic function underlying neurological disorders such as fragile X syndrome (FXS) and other autism spectrum disorders (ASD) (Bassell and Warren, 2008). The loss of translational control may represent a possible mechanism leading to autistic phenotypes such as cognitive impairment, epilepsy and familial hamartoma-tumor syndromes (Kelleher and Bear, 2008). These findings highlight the critical role translational regulation plays in maintaining proper synaptic function and cognition.

1.2 Inducible phosphorylation of ribosomal protein S6

An important ribosomal protein that has attracted attention as a key mediator of translation is ribosomal protein S6 (rpS6). Early studies revealed inducible phosphorylation with a temporal correlation matching the initiation of protein synthesis in response to mitogenic or nutritional stimuli (Wettenhall and Howlett, 1979; Meyuhas, 2008). These early reports initiated a large-scale investigation to define the role of rpS6 phosphorylation in cell growth and proliferation. One seminal study reported increased phosphorylation of rpS6 that correlated to activation of protein synthesis and increased

cell growth in the rat regenerating rat liver after partial hepatectomy (Gressner and Wool, 1974; Ferrari and Thomas, 1994). Additional studies went on to propose that 40S ribosomes with the highest proportion of phosphorylated rpS6 were preferentially mobilized into polysomes (Thomas et al., 1982; Duncan and McConkey, 2005). Others proposed that phosphorylation of rpS6 served as a mechanism to stabilize the initiation complex (Gressner and van de Leur, 1980). Despite the growing number of studies performed to investigate the function of rpS6 phosphorylation little is still known regarding the exact function and the mechanisms by which rpS6 phosphorylation contributes to translation.

Regarding rpS6 biogenesis, rpS6 is transcribed in the nucleus, translated in the cytoplasm and imported into the nucleus via a nuclear localization signal (NLS)-dependent mechanism. In the nucleoli, it associates with rRNA and other proteins into premature 40S ribosomal subunits. Small rpS6 containing ribosomal subunits are exported to the cytoplasm where they fuse to form mature ribosomes (Rosner et al., 2010). The majority of rpS6 is found in the cytoplasm as an integral component of the 40S subunit, but it is also present in nucleoli (Pende et al., 2004). Higher eukaryotic ribosomes consist of two subunits, the small 40S, and large 60S ribosomal subunits. The 40S ribosomal subunit comprises a single 18S rRNA and 33 proteins. The 60S ribosomal subunit has the 5S, 5.8S, and 28S rRNA and 46 proteins (Wool, 1996).

RpS6 consists of five evolutionarily conserved serine residues: ser235, ser236, ser240, ser244, ser247, each located at the carboxy terminus (Wettenhall et al., 1992). Phosphorylation of rpS6 is activated by multiple stimuli including hormones (Gressner and Wool, 1974), mitogens (Wettenhall and Howlett, 1979), serum (Jeno et al., 1988; Bandi et

al., 1993), growth factors (Lastick and McConkey, 1980) and HFS (Panja et al., 2009; Pirbhoy et al., 2016). Furthermore, studies have found that rpS6 is localized to the small head region of the 40S subunit placing it precisely in the interface between the small and large ribosomal subunits (Nygard and Nilsson, 1990). It has also been shown that rpS6 interacts with tRNA, initiation factors and mRNA (Nygard and Nilsson, 1990). The inducible phosphorylation of rpS6 in response to various stimuli, its location on the 40S subunit, and its interaction with protein synthesis-related factors, provide compelling evidence supporting a role for phosphorylation of rpS6 as a mechanism to regulate the initiation of translation in response to a range of stimuli.

1.2.1 Current implicated roles for rpS6 phosphorylation

One seminal study proposed phosphorylation of rpS6 as a regulator of 5'TOP mRNA translation (Jefferies et al., 1994). In a series of studies, they revealed that rapamycin treatment suppressed 5'TOP mRNA translation and phosphorylation of rpS6. They proposed that rapamycin treatment inhibited the recruitment of mRNAs into polysomes, an effect that was mediated by activation of p70S6K and phosphorylation of rpS6 (Jefferies, 1997), and resulted in a 10-15% inhibition of global protein synthesis (Jefferies et al., 1994). These observations led to the attractive hypothesis that rpS6 phosphorylation increased the affinity of phosphorylated 40S ribosomes to the 5'TOP mRNA tract facilitating initiation of their translation (Jefferies et al., 1994; Jefferies, 1997). Since, 5'TOP mRNAs encode proteins associated with the translational apparatus of higher eukaryotes such as ribosomal proteins, elongation factors, and poly(A)-binding protein (Hornstein et al., 2001) it is proposed that rpS6 phosphorylation regulates synthesis of the translational machinery (Meyuhas, 2000).

In contrast to studies that implicate a role for rpS6 in regulating translation of 5'TOP mRNAs, other studies suggest that rpS6 phosphorylation is dispensable for 5'TOP translation. In a study where all phosphorylatable serine residues were substituted by alanines, it was found that rpS6 phosphorylation was dispensable for efficient translation of TOP mRNAs (Ruvinsky et al., 2005). In fact, it was found that rpS6 phosphorylation was necessary for the regulation of cell size in specific cell types, specifically beta-cells. Furthermore, the study found that rates of global protein synthesis were significantly increased in mouse embryonic fibroblasts (MEFs) derived from the knock-in mice, relative to those measured in wild-type MEFs (Ruvinsky et al., 2005). This provided evidence that protein synthesis in this cell type is downregulated by rpS6 phosphorylation. While these studies suggest that rpS6 is dispensable for the translation of 5'TOP mRNAs, it is important to keep in mind that they only assessed three different mRNAs, rpL32, rpS6, and rpS16. It is possible that these specific 5'TOP mRNAs are not regulated by rpS6 phosphorylation, while other 5'TOP mRNAs may depend on rpS6 phosphorylation.

Other studies have also presented opposing results stating that increased rpS6 phosphorylation alone is not sufficient to enhance the mobilization of 40S subunits into polysomes (Kruppa and Clemens, 1984; Tas and Martini, 1987; Montine and Henshaw, 1990). But it is important to keep in mind that results may vary depending on the model system used, for example, *in vivo* versus cultured cells. Overall, rpS6 phosphorylation is implicated as a critical effector of mTOR, a regulator of cell growth (Ruvinsky et al., 2005), but the exact role of rpS6 phosphorylation is unclear. This project aims to explore the role of rpS6 phosphorylation in regulating mTOR-dependent protein synthesis in the hippocampus. Determining activation patterns of rpS6 phosphorylation following synaptic

activation in dentate granule cells will provide necessary information regarding its activation in neurons, information that is currently lacking in the field. Furthermore, using *in vivo* medial perforant path stimulation provides an optimal model where neural circuits remain intact and where synapses can be selectively activated to study how rpS6 phosphorylation is differentially regulated in granule cell bodies and at activated dendritic domains.

1.2.2 Signaling pathways regulating phosphorylation of rpS6

Initial studies implicating a role for rpS6 phosphorylation in translational control proposed this hypothesis based on studies conducted exploring the role of ribosomal protein S6 kinase 1 (S6K1), a downstream target of mTOR that directly phosphorylates rpS6 (Jefferies, 1997). S6K1 has two isoforms, p70S6K, and p85S6K (Lee-Fruman et al., 1999) and is implicated in cell proliferation and growth by regulating translation, ribosome biogenesis and autophagy (Dennis et al., 1999; Dennis, 2001; Sharma et al., 2010). Additional mTOR-dependent substrates implicated in translational control include eukaryotic initiation factor 4E (eIF4E) (Mèndez et al., 1996) and 4E-binding protein (4E-BP) (Beretta et al., 1996). eIF4E is essential for ribosome recruitment (Gingras et al., 1999) and binds to the 7-methylguanosine cap structure at the 5'-end of nearly all transcribed mRNAs to initiate cap-dependent translation. Activation of mTOR leads to eIF4E initiating the assembly of the translation preinitiation complex via the recruitment of numerous initiation factors, resulting in the association of the ribosomal subunits to the mRNA. 4E-binding protein (4E-BP) competes with the scaffold protein eIF4G for binding to the 7-methyl cap-binding protein eIF4E, preventing the formation of the preinitiation complex that catalyzes the recruitment of mRNAs to the ribosome. Sequential phosphorylation of all

four sites, T37, T46, S65, and T70, is required to block eIF4E binding and activate translation (Gingras, 2001). It is possible that other translation-related substrates or that the interaction of substrates that form the preinitiation complex acts as a signal to control the initiation of translation. In fact, evidence suggests that the interaction of phosphorylated forms of rpS6 with mRNAs functions to increase the possibility of forming a stable initiation complex (Gressner and van de Leur, 1980; Jefferies, 1997). Overall, evidence supports a role for mTOR-dependent regulation of translation and specifically, regulation of its downstream effectors are indicated to play prominent roles in regulating the initiation of translation.

As mentioned above, phosphorylation of rpS6 has attracted attention as a key mediator of mTOR-dependent protein synthesis. One study assessed the phosphorylation of rpS6 in MEFs lacking S6K1$^{-/-}$ and S6K2$^{-/-}$ to define mTOR-dependent mechanisms involved in cell growth, proliferation, and 5'TOPmRNA translation. The study showed that MEFs lacking both S6K1$^{-/-}$ and S6K2$^{-/-}$ genes possessed low levels of rpS6 phosphorylation at ser235 and ser236 providing evidence that an mTOR-independent pathway was involved in regulating rpS6 phosphorylation (Pende et al., 2004). To determine additional kinases regulating rpS6 phosphorylation, primary hepatocytes were serum and nutrient deprived to reduce the high basal level of rpS6 phosphorylation then treated with rapamycin and PD184352, an MKK1/ERK1/ERK2 pathway inhibitor. This study revealed that rapamycin treatment alone abolished the insulin-induced increase in ser240/244 but only attenuated ser235/236 phosphorylation. PD184352 treatment alone had little effect but when combined with rapamycin the insulin-induced increase in rpS6 phosphorylation was completely abolished. This study provided some of the initial observations indicating

the involvement of an MAPK/ERK-dependent kinase in regulating rpS6 phosphorylation (Pende et al., 2004).

In addition to the observations reported in cells in culture, this study also revealed phenotypic observations of mice lacking S6K1$^{-/-}$, S6K2$^{-/-}$, and both S6K1$^{-/-}$/S6K2$^{-/-}$ genes. S6K1$^{-/-}$ mice were found to be 15-20% smaller in body weight compared to wild-type (WT) mice. S6K1$^{-/-}$ were viable and fertile but hypoinsulinemic with reduced beta-cell size. S6K1$^{-/-}$ mice also possessed rpS6 phosphorylation levels comparable to WT mice. S6K2$^{-/-}$ mice, surprisingly, were viable with no phenotypic abnormalities and no significant differences in body weight when compared to WT mice. With regards to rpS6 phosphorylation, S6K2$^{-/-}$ mice expressed rpS6 phosphorylation but to a lesser extent than WT and S6K1$^{-/-}$ mice. Deletion of both S6K1$^{-/-}$/S6K2$^{-/-}$ genes was semilethal with only 10 out of 536 viable offspring, and 1/3 of the mice were born dead. These mice also develop cyanosis, a bluish discoloration of the skin. Analysis of rpS6 phosphorylation levels revealed severely suppressed levels that were rapamycin-resistant (Pende et al., 2004). These phenotypic observations of S6K1/2 deficient mice point to different functions for S6K1 and S6K2 mediated by phosphorylation of rpS6. S6K2 is reported to play a more dominant role in regulating levels of rpS6 phosphorylation, while S6K1 may regulate insulin resistance (Um et al., 2006). In fact, studies show differential localization of S6K1 and S6K2 isoforms with S6K1 being localized to the nucleus and cytoplasm of cells and S6K2 being largely localized to the nucleus of cells (Lee-Fruman et al., 1999). S6K1 has also been localized at nerve endings as observed by its presence in the soluble fraction of synaptosomes following subcellular fractionation indicating a potential role in neurite outgrowth (Burnett et al., 1998). This evidence supports a mechanism by which S6-kinases may carry out specific

functions via the phosphorylation of rpS6 at different subcellular compartments in response to changes in the local environment.

The discovery that cells lacking both S6 kinases contained residual rpS6 phosphorylation that was resistant to rapamycin, but completely abolished by MEK inhibitors, supported the hypothesis that MAPK/ERK regulates rpS6 phosphorylation at ser235 and ser236 (Pende et al., 2004). Further evidence for MAPK/ERK regulating rpS6 phosphorylation was revealed in a study with serum-stimulated HEK293E cells. When these cells were pretreated with rapamycin, there was no increase in serum-induced phosphorylation of rpS6 at ser240/244. Phosphorylation at ser235/236, though, remained partly phosphorylated, supporting that an mTOR-independent pathway activated phosphorylation at these sites. When the cells were pretreated with U0126 before serum stimulation, ser240/244 was not significantly affected while ser235/236 phosphorylation was strongly reduced. When U0126 and rapamycin treatment were administered together before serum stimulation, rpS6 phosphorylation was completely inhibited. This seminal study provided supporting evidence to indicate that ser235/236 phosphorylation occurs through an mTOR and MAPK/ERK-dependent mechanism, while ser240/244 occurs predominately through an mTOR-dependent mechanism (Roux et al., 2007).

Compelling evidence suggests that mTOR and ERK signaling pathways interact to regulate synaptic plasticity (Wang et al., 2001; Shahbazian et al., 2006; Roux et al., 2007; Hoang et al., 2012). Phosphorylation of rpS6 at ser235/236 emerges as a key candidate for the integration of inputs from these signal transduction pathways to accomplish various functions. Several downstream mTOR and MAPK/ERK substrates are implicated in the regulation of rpS6 phosphorylation. Some studies suggest that interaction between mTOR

and ERK pathways results from phosphorylation at TSC2 by ERK or by its downstream effector, RSK (Roux, 2004; Ma et al., 2005). But the interaction between these pathways remains controversial. It is apparent that additional studies are needed to assess the interaction between mTOR and ERK signaling pathways in regulating synaptic plasticity.

Accumulating evidence suggest that the MAPK/ERK signaling pathway regulates rpS6 phosphorylation. This possibility extended the list of possible contributions that rpS6 phosphorylation may facilitate in synaptic plasticity. The MAPK family consists of seven kinases: ERK1, ERK2 and ERK5, c-Jun N-terminal kinases (JNKs) 1-3, and p38. MAPK/ERK is implicated in regulating local dendritic protein synthesis (Kelleher et al., 2004a; Kelleher et al., 2004b) and is transiently activated during different memory tasks (Adams and Sweatt, 2002; Davis and Laroche, 2006) implicating a role for MAPK/ERK in learning and memory (Sweatt, 2004). Upregulation of ERK1/2 activity leads to enhanced GABA release as well as impaired LTP induction (Costa et al., 2002; Cui et al., 2008). Since MAPK/ERK-dependent pathways are implicated in synaptic plasticity and memory related tasks, regulation of rpS6 phosphorylation by MAPK/ERK suggests that rpS6 phosphorylation may be involved in similar functions.

One study, directly investigated the involvement of S6K1 and S6K2 in learning and memory and synaptic plasticity by using genetically engineered mice deficient in S6K1 and S6K2. In the study, mice underwent a series of behavioral tasks. The study reported that the majority of the effects were observed in mice lacking S6K1. These mice exhibited a deficit in contextual fear conditioning as early as 1 hour after training. In a spatial learning task assessed by the Morris Water Maze (MWM), S6K1 deficient mice made fewer platform crossings and spent less time at the precise target location during a probe trial

administered at day-3, but performed comparable to WT mice during a probe trial administered on day-7. In LTP experiments in S6K1 deficient mice, no reduction in L-LTP potentiation was observed three hours post LTP induction, which was comparable to WT mice. Surprisingly, E-LTP was more transient in S6K1 deficient mice than E-LTP in WT mice. S6K1 mice exhibited decreased potentiation 20-60 min after LTP induction and reached baseline levels 60-80min post LTP induction, while WT mice returned to baseline levels 80-100min post LTP induction (Antion et al., 2008). S6K2 knockout mice demonstrated impaired long-term contextual fear memory. In the MWM, S6K2 deficient mice performed at levels comparable to WT mice. In LTP experiments, S6K2 deficient mice exhibited normal E-LTP and L-LTP comparable to WT mice (Antion et al., 2008). These findings support previous findings where S6K1-deficient mice have more abnormal phenotypes compared to S6K2-deficient mice (Pende et al., 2004). The results of this study point to S6K2 as a regulator of behaviors that rely on long-term memory encoding, while S6K1 may be involved in the early phases of enduring synaptic modifications involved in memory and plasticity (Antion et al., 2008). With these single knockout studies, though, it is also important to keep in mind that a compensatory alteration of other genes may occur. For example, a dramatic enhancement of basal Akt phosphorylation was observed, which was further enhanced following L-LTP (Antion et al., 2008). Alterations in other genes complicate the interpretation of the results.

1.2.3 Phosphorylation of rpS6 as a mechanism to regulate translation

The current project addresses a relatively unexplored aspect of synaptic protein synthesis -- how the translation of mRNAs is regulated by synaptic activity. My studies to date have shown that induction of perforant path LTP in vivo triggers rapid

phosphorylation of rpS6 in dentate granule cells and selective activation of rpS6 phosphorylation in the laminae activated by medial perforant path stimulation (Pirbhoy et al., 2016). Both the mTOR and the MAPK/ERK signaling pathways have been identified as key players in activity-dependent synaptic changes (Xia et al., 1996; Qi et al., 2010), both of which target rpS6 phosphorylation sites. Phosphorylation of rpS6 at ser235/236 has been shown to be targeted by both MAPK/ERK and mTOR, while ser240/244 is predominately mTOR-dependent. This study, therefore, investigates the role of rpS6 phosphorylation in the initiation of translation in response to signal transduction pathways that activate rpS6 phosphorylation in the dentate gyrus of the hippocampus. My findings uniquely show selective activation of rpS6 phosphorylation in the activated portion of dendrites implicating a role for rpS6 phosphorylation in activity-dependent synaptic modifications. It is known that phosphorylation of rpS6 progresses in an ordered fashion, with ser236 as the primary phosphorylation site followed by ser235, ser240, ser244 and ser247 (Krieg et al., 1988; Flotow and Thomas, 1992; Wettenhall et al., 1992), but the exact contributions of each phosphorylation site are not well-understood. This study will assess the differential role of rpS6 phosphorylation at ser235/236 and ser240/244 in different subcellular compartments (cell body vs. dendrites) in response to synaptic activation using an *in vivo* rat model. It is hypothesized that phosphorylation of rpS6 serves as an initiation switch to regulate the translation of activity-dependent proteins involved in LTP-induced synaptic modifications.

1.2.4 Significance and therapeutic applications

Altered dendritic spine morphology, synaptic function, and loss of translation-dependent synaptic plasticity has been observed in patients with disorders in which there

is a loss of translational control, for example, Fragile X Syndrome (FXS) (Bagni and Greenough, 2005; Bassell and Warren, 2008). These synaptic alterations observed in FXS are attributed to dysregulation of mRNA translation and are associated with cognitive deficits (Bagni and Greenough, 2005; Bassell and Warren, 2008). Learning impairments are also present in a mouse model of Angelman syndrome. These hippocampal learning impairments are attributed to reduced activity of alpha-CaMKII as a result of increased inhibitory phosphorylation at T305/T306 (Weeber et al., 2003). One study that addressed the contribution of this increased inhibitory phosphorylation demonstrated that the cognitive deficits could be rescued by decreasing the inhibitory phosphorylation on alpha-CaMKII (van Woerden et al., 2007). This is one example that demonstrates the importance of phosphorylation events in synaptic plasticity and cognition. Most importantly, it shows that cognitive deficits can be rescued by altering phosphorylation of specific targets. Therefore, understanding how translation is regulated in the non-diseased brain is critical to identify target mechanisms that may serve as therapeutic targets to help regain translational control and rescue cognitive deficits in disorders where there is a loss of translational control.

1.3 Summary

LTP induction initiates a series of processes that result in enhanced synaptic transmission and structural changes at activated synapses. It has been over 40 years since the discovery of LTP and the field remains unclear as to how these processes occur. The proposed dissertation sets out to investigate the role of a post-translational modification, phosphorylation of ribosomal protein S6, and its role in synaptic plasticity in the dentate gyrus, specifically its role in regulating the initiation of translation at activated synapses.

Several questions remain in the field regarding mRNA translation at synapses. A large number of studies have focused on identifying mRNAs localized to dendrites, but relatively few studies focus on how mRNA translation is regulated by synaptic activity. The present studies propose that phosphorylation of rpS6 may function as a mechanism to regulate the initiation of translation at activated synapses. The studies of Chapter 2 provide several new findings regarding activation of rpS6 phosphorylation in neurons following synaptic activity and a behavioral learning experience. Results also demonstrate that phosphorylation of rpS6 is dependent on NMDA receptor activation. NMDA receptors are strongly implicated in learning and memory suggesting that rpS6 phosphorylation may be involved in NMDA receptor-dependent synaptic plasticity. Furthermore, results reveal the surprising finding that phosphorylation of rpS6 is not associated with increases in protein synthesis. The studies in Chapter 3 report new findings regarding the differential phosphorylation of rpS6 in granule cell bodies and dendrites. Specifically, results suggest that PI3-kinase/Akt signaling regulates phosphorylation in granule cell bodies, while MAPK/ERK signaling regulates rpS6 phosphorylation in dendrites. This finding implicates regulation of rpS6 phosphorylation as a mechanism by which PI3-kinase/mTOR and MAPK/ERK may regulate the initiation of translation at different subcellular compartments, cell bodies vs. dendrites, in response to synaptic activity. The studies of Chapter 4 provide results demonstrating the feasibility of using optogenetic stimulation of the medial perforant path in the hippocampal slice preparation to study mechanisms of mRNA targeting following synaptic stimulation.

REFERENCES

Abraham WC, Logan B, Greenwood JM, Dragunow M (2002) Induction and experience-dependent consolidation of stable long-term potentiation lasting months in the hippocampus. J Neurosci 22:9626-9634.

Adams JP, Sweatt JD (2002) Roles for the ERK MAP Kinase Cascade in Memory. Annual Review of Pharmacology and Toxicology 42:135-163.

Antion MD, Merhav M, Hoeffer CA, Reis G, Kozma SC, Thomas G, Schuman EM, Rosenblum K, Klann E (2008) Removal of S6K1 and S6K2 leads to divergent alterations in learning, memory, and synaptic plasticity. Learn Mem 15:29-38.

Atkins CM, Selcher JC, Petraitis JJ, Trzaskos JM, Sweatt JD (1998) The MAPK cascade is required for mammalian associative learning. Nat Neurosci 1:602-609.

Bagni C, Greenough WT (2005) From mRNP trafficking to spine dysmorphogenesis: the roots of fragile X syndrome. Nature Reviews Neuroscience 6:376-387.

Bailey CH, Bartsch D, Kandel ER (1996) Toward a molecular definition of long-term memory storage. Proc Natl Acad Sci USA 93:13445-13452.

Bandi HR, Ferrari S, Krieg J, Meyer HE, Thomas G (1993) Identification of 40 S ribosomal protein S6 phosphorylation sites in Swiss mouse 3T3 fibroblasts stimulated with serum. J Biol Chem 268:4530-4533.

Bassell GJ, Warren ST (2008) Fragile X Syndrome: Loss of Local mRNA Regulation Alters Synaptic Development and Function. Neuron 60:201-214.

Benke TA, Luthi A, Isaac JT, Collingridge GL (1998) Modulation of AMPA receptor unitary conductance by synaptic activity. Nature 393:793-797.

Beretta L, Gingras AC, Svitkin YV, Hall MN, Sonenberg N (1996) Rapamycin blocks the phosphorylation of 4E-BP1 and inhibits cap-dependent initiation of translation. EMBO J 15:658-664.

Berman DE, Hazvi S, Rosenblum K, Seger R, Dudai Y (1998) Specific and differential activation of mitogen-activated protein kinase cascades by unfamiliar taste in the insular cortex of the behaving rat. J Neurosci 18:10037-10044.

Bliss TV, Lomo T (1973) Long-lasting potentiation of synaptic transmission in the dentate area of the anaesthetized rabbit following stimulation of the perforant path. J Physiol (Lond) 232:331-356.

Bliss TV, Collingridge GL (1993) A synaptic model of memory: long-term potentiation in the hippocampus. Nature 361:31-39.

Blum S, Moore AN, Adams F, Dash PK (1999) A mitogen-activated protein kinase cascade in the CA1/CA2 subfield of the dorsal hippocampus is essential for long-term spatial memory. J Neurosci 19:3535-3544.

Böckers TM, Segger-Junius M, Iglauer P, Bockmann J, Gundelfinger ED, Kreutz MR, Richter D, Kindler S, Kreienkamp H-J (2004) Differential expression and dendritic transcript localization of Shank family members: identification of a dendritic targeting element in the 3′ untranslated region of Shank1 mRNA. Molecular and Cellular Neuroscience 26:182-190.

Bodian D (1965) A suggestive relationship of nerve cell RNA with specific synaptic sites Proc Natl Acad Sci USA 53:418-425.

Boulton TG, Nye SH, Robbins DJ, Ip NY, Radziejewska E, Morgenbesser SD, DePinho RA, Panayotatos N, Cobb MH, Yancopoulos GD (1991) ERKs: a family of protein-

serine/threonine kinases that are activated and tyrosine phosphorylated in response to insulin and NGF. Cell 65:663-675.
Burgin KE, Waxham MN, Rickling S, Westgate SA, Mobley WC, Kelly PT (1990) In situ hybridization histochemistry of Ca2+/calmodulin-dependent protein kinase in developing rat brain. J Neurosci 10:1788-1798.
Burnett PE, Blackshaw S, Lai MM, Qureshi IA, Burnett AF, Sabatini DM, Snyder SH (1998) Neurabin is a synaptic protein linking p70 S6 kinase and the neuronal cytoskeleton. Pro Natl Acad Sci USA 95:8351-8356.
Cajigas IJ, Tushev G, Will TJ, tom Dieck S, Fuerst N, Schuman EM (2012) The local transcriptome in the synaptic neuropil revealed by deep sequencing and high-resolution imaging. Neuron 74:453-466.
Capani F, Martone ME, Deerinck TJ, Ellisman MH (2001) Selective localization of high concentrations of F-actin in subpopulations of dendritic spines in rat central nervous system: a three-dimensional electron microscopic study. J Comp Neurol 435:156-170.
Chakrabarti A, Maitra U (1991) Function of eukaryotic initiation factor 5 in the formation of an 80 S ribosomal polypeptide chain initiation complex. J Biol Chem 266:14039-14045.
Chen LY, Rex CS, Casale MS, Gall CM, Lynch G (2007) Changes in Synaptic Morphology Accompany Actin Signaling during LTP. J Neurosci 27:5363-5372.
Colicos MA, Collins BE, Sailor MJ, Goda Y (2001) Remodeling of synaptic actin induced by photoconductive stimulation. Cell 107:605-616.
Collingridge GL, Bliss TVP (1987) NMDA receptors - their role in long-term potentiation. Trends in Neurosciences 10:288-293.
Coogan AN, O'Leary DM, O'Connor JJ (1999) P42/44 MAP kinase inhibitor PD98059 attenuates multiple forms of synaptic plasticity in rat dentate gyrus in vitro. J Neurophysiol 81:103-110.
Costa RM, Federov NB, Kogan JH, Murphy GG, Stern J, Ohno M, Kucherlapati R, Jacks T, Silva AJ (2002) Mechanism for the learning deficits in a mouse model of neurofibromatosis type 1. Nature 415:526-530.
Cui Y, Costa RM, Murphy GG, Elgersma Y, Zhu Y, Gutmann DH, Parada LF, Mody I, Silva AJ (2008) Neurofibromin Regulation of ERK Signaling Modulates GABA Release and Learning. Cell 135:549-560.
Dahm R, Kiebler M (2005) Cell biology: Silenced RNA on the move. Nature 438:432-435.
Davis S, Laroche S (2006) Mitogen-activated protein kinase/extracellular regulated kinase signalling and memory stabilization: a review. Genes, Brain and Behavior 5:61-72.
Dennis PB (2001) Mammalian TOR: A Homeostatic ATP Sensor. Science 294:1102-1105.
Dennis PB, Fumagalli S, Thomas G (1999) Target of rapamycin (TOR): balancing the opposing forces of protein synthesis and degradation. Current Opinion in Genetics & Development 9:49-54.
Derkach V, Barria A, Soderling TR (1999) Ca2+/calmodulin-kinase II enhances channel conductance of alpha-amino-3-hydroxy-5-methyl-4-isoxazolepropionate type glutamate receptors. Pro Natl Acad Sci USA 96:3269-3274.
Dever TE (2002) Gene-Specific Regulation by General Translation Factors. Cell 108:545-556.

Douglas RM, Goddard GV (1975) Long-term potentiation of the perforant path-granule cell synapse in the rat hippocampus. Brain Res 86:205-215.
Doyle M, Kiebler MA (2011) Mechanisms of dendritic mRNA transport and its role in synaptic tagging. EMBO J 30:3540-3552.
Duncan R, McConkey EH (2005) Preferential Utilization of Phosphorylated 40-S Ribosomal Subunits during Initiation Complex Formation. Eur J Biochem 123:535-538.
English JD, Sweatt JD (1996) Activation of p42 mitogen-activated protein kinase in hippocampal long term potentiation. J Biol Chem 271:24329-24332.
English JD, Sweatt JD (1997) A requirement for the mitogen-activated protein kinase cascade in hippocampal long term potentiation. J Biol Chem 272:19103-19106.
Ferrari S, Thomas G (1994) S6 Phosphorylation and the p70s6k /p85s6k. Critical Reviews in Biochemistry and Molecular Biology 29:385-413.
Fifková E, Van Harreveld A (1977) Long-lasting morphological changes in dendritic spines of dentate granular cells following stimulation of the entorhinal area. J Neurocytol 6:211-230.
Fischer M, Kaech S, Knutti D, Matus A (1998) Rapid actin-based plasticity in dendritic spines. Neuron 20:847-854.
Flotow H, Thomas G (1992) Substrate recognition determinants of the mitogen-activated 70K S6 kinase from rat liver. J Biol Chem 267:3074-3078.
Frey U, Morris RGM (1997) Synaptic tagging and long-term potentiation. Nature 385:533-536.
Fukazawa Y, Saitoh Y, Ozawa F, Ohta Y, Mizuno K, Inokuchi K (2003) Hippocampal LTP is accompanied by enhanced F-actin content within the dendritic spine that is essential for late LTP maintenance in vivo. Neuron 38:447-460.
Garner CC, Tucker RP, Matus A (1988) Selective localization of messenger RNA for cytoskeletal protein MAP2 in dendrites. Nature 336:674-677.
Gingras A-C, Raught B, Sonenberg N (1999) eIF4 INITIATION FACTORS: Effectors of mRNA Recruitment to Ribosomes and Regulators of Translation. Annual Review of Biochemistry 68:913-963.
Gingras AC (2001) Regulation of translation initiation by FRAP/mTOR. Genes & Development 15:807-826.
Giorgi C, Moore MJ (2007) The nuclear nurture and cytoplasmic nature of localized mRNPs. Seminars in Cell & Developmental Biology 18:186-193.
Giorgi C, Yeo GW, Stone ME, Katz DB, Burge C, Turrigiano G, Moore MJ (2007) The EJC Factor eIF4AIII Modulates Synaptic Strength and Neuronal Protein Expression. Cell 130:179-191.
Grafstein B, Forman DS (1980) Intracellular transport in neurons. Physiol Rev 60:1167-1283.
Gressner AM, Wool IG (1974) The phosphorylation of liver ribosomal proteins in vivo. Evidence that only a single small subunit protein (S6) is phosphorylated. J Biol Chem 249:6917-6925.
Gressner AM, van de Leur E (1980) Interaction of synthetic polynucleotides with small rat liver ribosomal subunits possessing low and highly phosphorylated protein S6. Biochim Biophys Acta 608:459-468.

Guzowski JF, McNaughton BL, Barnes CA, Worley PF (1999) Environment-specific expression of the immediate-early gene Arc in hippocampal neuronal ensembles. Nat Neurosci 2:1120-1124.
Guzowski JF, Setlow B, Wagner EK, McGaugh JL (2001) Experience-dependent gene expression in the rat hippocampus after spatial learning: a comparison of the immediate-early genes Arc, c-fos, and zif268. J Neurosci 21:5089-5098.
Guzowski JF, Lyford GL, Stevenson GD, Houston FP, McGaugh JL, Worley PF, Barnes CA (2000) Inhibition of activity-dependent arc protein expression in the rat hippocampus impairs the maintenance of long-term potentiation and the consolidation of long-term memory. J Neurosci 20:3993-4001.
Herb A (1997) Prominent Dendritic Localization in Forebrain Neurons of a Novel mRNA and Its Product, Dendrin. Molecular and Cellular Neuroscience 8:367-374.
Herring BE, Nicoll RA (2016) Long-Term Potentiation: From CaMKII to AMPA Receptor Trafficking. Annu Rev Physiol 78:351-365.
Hillman RT, Green RE, Brenner SE (2004) An unappreciated role for RNA surveillance. Genome Biol 5.
Hinnebusch AG, Ivanov IP, Sonenberg N (2016) Translational control by 5'-untranslated regions of eukaryotic mRNAs. Science 352:1413-1416.
Hoang B, Benavides A, Shi Y, Yang Y, Frost P, Gera J, Lichtenstein A (2012) The PP242 Mammalian Target of Rapamycin (mTOR) Inhibitor Activates Extracellular Signal-regulated Kinase (ERK) in Multiple Myeloma Cells via a Target of Rapamycin Complex 1 (TORC1)/ Eukaryotic Translation Initiation Factor 4E (eIF-4E)/RAF Pathway and Activation Is a Mechanism of Resistance. J Biol Chem 287:21796-21805.
Hoek KS, Kidd GJ, Carson JH, Smith R (1998) hnRNP A2 selectively binds the cytoplasmic transport sequence of myelin basic protein mRNA. Biochemistry 37:7021-7029.
Hornstein E, Tang H, Meyuhas O (2001) Mitogenic and Nutritional Signals Are Transduced into Translational Efficiency of TOP mRNAs. Cold Spring Harbor Symposia on Quantitative Biology 66:477-484.
Hu GY, Hvalby O, Walaas SI, Albert KA, Skjeflo P, Andersen P, Greengard P (1987) Protein kinase C injection into hippocampal pyramidal cells elicits features of long term potentiation. Nature 328:426-429.
Huang YS (2002) N-methyl-D-aspartate receptor signaling results in Aurora kinase-catalyzed CPEB phosphorylation and alphaCaMKII mRNA polyadenylation at synapses. EMBO J 21:2139-2148.
Jefferies HB, Reinhard C, Kozma SC, Thomas G (1994) Rapamycin selectively represses translation of the "polypyrimidine tract" mRNA family. Proc Natl Acad Sci USA 91:4441-4445.
Jefferies HBJ (1997) Rapamycin suppresses 5'TOP mRNA translation through inhibition of p70s6k. EMBO J 16:3693-3704.
Jeno P, Ballou LM, Novak-Hofer I, Thomas G (1988) Identification and characterization of a mitogen-activated S6 kinase. Pro Natl Acad Sci USA 85:406-410.
Jiang C, Schuman EM (2002) Regulation and function of local protein synthesis in neuronal dendrites. Trends Biochem Sci 27:506-513.

Jones MW, Errington ML, French PJ, Fine A, Bliss TV, Garel S, Charnay P, Bozon B, Laroche S, Davis S (2001) A requirement for the immediate early gene Zif268 in the expression of late LTP and long-term memories. Nat Neurosci 4:289-296.
Kanai Y, Dohmae N, Hirokawa N (2004) Kinesin Transports RNA: isolation and characterization of an RNA-transporting granule. Neuron 43:513-525.
Kelleher RJ, Bear MF (2008) The Autistic Neuron: Troubled Translation? Cell 135:401-406.
Kelleher RJ, Govindarajan A, Jung H-Y, Kang H, Tonegawa S (2004a) Translational control by MAPK signaling in long-term synaptic plasticity and memory. Cell 116:467-479.
Kelleher RJ, 3rd, Govindarajan A, Tonegawa S (2004b) Translational regulatory mechanisms in persistent forms of synaptic plasticity. Neuron 44:59-73.
Kiebler MA, Bassell GJ (2006) Neuronal RNA Granules: Movers and Makers. Neuron 51:685-690.
Kitanishi T, Ikegaya Y, Matsuki N, Yamada MK (2009) Experience-dependent, rapid structural changes in hippocampal pyramidal cell spines. Cereb Cortex 19:2572-2578.
Krieg J, Hofsteenge J, Thomas G (1988) Identification of the 40 S ribosomal protein S6 phosphorylation sites induced by cycloheximide. J Biol Chem 263:11473-11477.
Kruppa J, Clemens MJ (1984) Differential kinetics of changes in the state of phosphorylation of ribosomal protein S6 and in the rate of protein synthesis in MPC 11 cells during tonicity shifts. EMBO J 3:95-100.
Lamprecht R, Dudai Y (1996) Transient expression of c-Fos in rat amygdala during training is required for encoding conditioned taste aversion memory. Learn Mem 3:31-41.
Lastick SM, McConkey EH (1980) Control of ribosomal protein phosphorylation in HeLa cells. Biochemical and Biophysical Research Communications 95:917-923.
Lee-Fruman KK, Kuo CJ, Lippincott J, Terada N, Blenis J (1999) Characterization of S6K2, a novel kinase homologous to S6K1. Oncogene 18:5108-5114.
Lejeune F, Maquat LE (2005) Mechanistic links between nonsense-mediated mRNA decay and pre-mRNA splicing in mammalian cells. Current Opinion in Cell Biology 17:309-315.
Link W, Konietzko U, Kauselmann G, Krug M, Schwanke B, Frey U, Kuhl D (1995) Somatodendritic expression of an immediate early gene is regulated by synaptic activity. Proc Natl Acad Sci USA 92:5734-5738.
Lisman JE, McIntyre CC (2001) Synaptic plasticity: A molecular memory switch. Current Biology 11:R788-R791.
Lyford GL, Yamagata K, Kaufmann WE, Barnes CA, Sanders LK, Copeland NG, Gilbert DJ, Jenkins NA, Lanahan AA, Worley PF (1995) Arc, a growth factor and activity-regulated gene, encodes a novel cytoskeleton-associated protein that is enriched in neuronal dendrites. Neuron 14:433-445.
Lynch G, Larson J, Kelso S, Barrionuevo G, Schottler F (1983) Intracellular injections of EGTA block induction of hippocampal long-term potentiation. Nature 305:719-721.
Ma L, Chen Z, Erdjument-Bromage H, Tempst P, Pandolfi PP (2005) Phosphorylation and Functional Inactivation of TSC2 by Erk. Cell 121:179-193.
Malenka RC, Nicoll RA (1999) Long-term potentiation--a decade of progress? Science 285:1870-1874.
Malenka RC, Kauer JA, Zucker RS, Nicoll RA (1988) Postsynaptic calcium is sufficient for potentiation of hippocampal synaptic transmission. Science 242:81-84.

Mammen AL, Kameyama K, Roche KW, Huganir RL (1997) Phosphorylation of the alpha-amino-3-hydroxy-5-methylisoxazole4-propionic acid receptor GluR1 subunit by calcium/calmodulin-dependent kinase II. J Biol Chem 272:32528-32533.
Meignin C, Davis I (2010) Transmitting the message: intracellular mRNA localization. Current Opinion in Cell Biology 22:112-119.
Mendell JT, Sharifi NA, Meyers JL, Martinez-Murillo F, Dietz HC (2004) Nonsense surveillance regulates expression of diverse classes of mammalian transcripts and mutes genomic noise. Nature Genetics 36:1073-1078.
Mèndez R, Myers MG, Jr., White MF, Rhoads RE (1996) Stimulation of protein synthesis, eukaryotic translation initiation factor 4E phosphorylation, and PHAS-I phosphorylation by insulin requires insulin receptor substrate 1 and phosphatidylinositol 3-kinase. Mol Cell Biol 16:2857-2864.
Meyuhas O (2000) Synthesis of the translational apparatus is regulated at the translational level. Eur J Biochem 267:6321-6330.
Meyuhas O (2008) Chapter 1 Physiological Roles of Ribosomal Protein S6: One of Its Kind. In: International Review of Cell and Molecular Biology, pp 1-37: Elsevier.
Montine KS, Henshaw EC (1990) TPA stimulates S6 phosphorylation but not protein synthesis in ehrlich cells. Biochemical and Biophysical Research Communications 166:1340-1345.
Muslimov IA, Nimmrich V, Hernandez AI, Tcherepanov A, Sacktor TC, Tiedge H (2004) Dendritic Transport and Localization of Protein Kinase M mRNA: implications for molecular memory consolidation J Biol Chem 279:52613-52622.
Nakayama D, Iwata H, Teshirogi C, Ikegaya Y, Matsuki N, Nomura H (2015) Long-delayed expression of the immediate early gene Arc/Arg3.1 refines neuronal circuits to perpetuate fear memory. J Neurosci 35:819-830.
Nguyen PV, Kandel ER (1996) A macromolecular synthesis-dependent late phase of long-term potentiation requiring cAMP in the medial perforant pathway of rat hippocampal slices. J Neurosci 16:3189-3198.
Nygard O, Nilsson L (1990) Translational dynamics. Interactions between the translational factors, tRNA and ribosomes during eukaryotic protein synthesis. Eur J Biochem 191:1-17.
Okada D, Ozawa F, Inokuchi K (2009) Input-Specific Spine Entry of Soma-Derived Vesl-1S Protein Conforms to Synaptic Tagging. Science 324:904-909.
Opazo P, Watabe AM, Grant SG, O'Dell TJ (2003) Phosphatidylinositol 3-kinase regulates the induction of long-term potentiation through extracellular signal-related kinase-independent mechanisms. J Neurosci 23:3679-3688.
Ostroff LE, Fiala JC, Allwardt B, Harris KM (2002) Polyribosomes Redistribute from Dendritic Shafts into Spines with Enlarged Synapses during LTP in Developing Rat Hippocampal Slices. Neuron 35:535-545.
Palacios IM (2007) How does an mRNA find its way? Intracellular localisation of transcripts. Seminars in Cell & Developmental Biology 18:163-170.
Palacios IM, Gatfield D, St Johnston D, Izaurralde E (2004) An eIF4AIII-containing complex required for mRNA localization and nonsense-mediated mRNA decay. Nature 427:753-757.

Panja D, Dagyte G, Bidinosti M, Wibrand K, Kristiansen AM, Sonenberg N, Bramham CR (2009) Novel translational control in Arc-dependent long term potentiation consolidation in vivo. J Biol Chem 284:31498-31511.
Pende M, Um SH, Mieulet V, Sticker M, Goss VL, Mestan J, Mueller M, Fumagalli S, Kozma SC, Thomas G (2004) S6K1-/-/S6K2-/- Mice Exhibit Perinatal Lethality and Rapamycin-Sensitive 5'-Terminal Oligopyrimidine mRNA Translation and Reveal a Mitogen-Activated Protein Kinase-Dependent S6 Kinase Pathway. Mol Cell Biol 24:3112-3124.
Pirbhoy PS, Farris S, Steward O (2016) Synaptic activation of ribosomal protein S6 phosphorylation occurs locally in activated dendritic domains. Learn Mem 23:255-269.
Plath N, Ohana O, Dammermann B, Errington ML, Schmitz D, Gross C, Mao X, Engelsberg A, Mahlke C, Welzl H (2006) Arc/Arg3.1 Is Essential for the Consolidation of Synaptic Plasticity and Memories. Neuron 52:437-444.
Qi S, Mizuno M, Yonezawa K, Nawa H, Takei N (2010) Activation of mammalian target of rapamycin signaling in spatial learning. Neurosci Res 68:88-93.
Ramirez-Amaya V, Vazdarjanova A, Mikhael D, Rosi S, Worley PF, Barnes CA (2005) Spatial exploration-induced Arc mRNA and protein expression: evidence for selective, network-specific reactivation. J Neurosci 25:1761-1768.
Rao A, Steward O (1991) Evidence that protein constituents of postsynaptic membrane specializations are locally synthesized: analysis of proteins synthesized within synaptosomes. J Neurosci 11:2881-2895.
Rehbein M, Wege K, Buck F, Schweizer M, Richter D, Kindler S (2004) Molecular characterization of MARTA1, a protein interacting with the dendritic targeting element of MAP2 mRNAs: MARTA1, a trans-factor of the MAP2-DTE. Journal of Neurochemistry 82:1039-1046.
Rosner M, Fuchs C, Dolznig H, Hengstschläger M (2010) Different cytoplasmic/nuclear distribution of S6 protein phosphorylated at S240/244 and S235/236. Amino Acids 40:595-600.
Roux PP (2004) Tumor-promoting phorbol esters and activated Ras inactivate the tuberous sclerosis tumor suppressor complex via p90 ribosomal S6 kinase. Pro Natl Acad Sci USA 101:13489-13494.
Roux PP, Shahbazian D, Vu H, Holz MK, Cohen MS, Taunton J, Sonenberg N, Blenis J (2007) RAS/ERK signaling promotes site-specific ribosomal protein S6 phosphorylation via RSK and stimulates cap-dependent translation. J Biol Chem 282:14056-14064.
Ruvinsky I, Sharon N, Lerer T, Cohen H, Stolovich-Rain M, Nir T, Dor Y, Zisman P, Meyuhas O (2005) Ribosomal protein S6 phosphorylation is a determinant of cell size and glucose homeostasis. Genes & development 19:2199-2211.
Sanna PP, Cammalleri M, Berton F, Simpson C, Lutjens R, Bloom FE, Francesconi W (2002) Phosphatidylinositol 3-kinase is required for the expression but not for the induction or the maintenance of long-term potentiation in the hippocampal CA1 region. J Neurosci 22:3359-3365.
Selcher JC, Atkins CM, Trzaskos JM, Paylor R, Sweatt JD (1999) A necessity for MAP kinase activation in mammalian spatial learning. Learn Mem 6:478-490.

Shahbazian D, Roux PP, Mieulet V, Cohen MS, Raught B, Taunton J, Hershey JWB, Blenis J, Pende M, Sonenberg N (2006) The mTOR/PI3K and MAPK pathways converge on eIF4B to control its phosphorylation and activity. EMBO J 25:2781-2791.
Sharma A, Hoeffer CA, Takayasu Y, Miyawaki T, McBride SM, Klann E, Zukin RS (2010) Dysregulation of mTOR Signaling in Fragile X Syndrome. J Neurosci 30:694-702.
Silva AJ, Stevens CF, Tonegawa S, Wang Y (1992) Deficient hippocampal long-term potentiation in alpha-calcium-calmodulin kinase II mutant mice. Science 257:201-206.
Sonenberg N, Hinnebusch AG (2009) Regulation of Translation Initiation in Eukaryotes: Mechanisms and Biological Targets. Cell 136:731-745.
Steward O, Levy WB (1982) Preferential localization of polyribosomes under the base of dendritic spines in granule cells of the dentate gyrus. J Neurosci 2:284-291.
Steward O, Wallace C, Lyford G, Worley P (1998) Synaptic activation causes the mRNA for the IEG Arc to localize selectively near activated postsynaptic sites on dendrites. Neuron 21:741-751.
Sweatt JD (2004) Mitogen-activated protein kinases in synaptic plasticity and memory. Curr Opin Neurbiol 14:311-317.
Tang SJ, Reis G, Kang H, Gingras AC, Sonenberg N, Schuman EM (2002) A rapamycin-sensitive signaling pathway contributes to long-term synaptic plasticity in the hippocampus. Pro Natl Acad Sci USA 99:467-472.
Tas PW, Martini OH (1987) Are highly phosphorylated 40-S subunits preferentially utilized during protein synthesis in a cell-free system from HeLa cells? European journal of biochemistry / FEBS 163:561-567.
Tcherkezian J, Brittis PA, Thomas F, Roux PP, Flanagan JG (2010) Transmembrane Receptor DCC Associates with Protein Synthesis Machinery and Regulates Translation. Cell 141:632-644.
Tcherkezian J, Cargnello M, Romeo Y, Huttlin EL, Lavoie G, Gygi SP, Roux PP (2014) Proteomic analysis of cap-dependent translation identifies LARP1 as a key regulator of 5'TOP mRNA translation. Genes Dev 28:357-371.
Thomas G, Martin-Perez J, Siegmann M, Otto AM (1982) The effect of serum, EGF, PGF2α and insulin on S6 phosphorylation and the initiation of protein and DNA synthesis. Cell 30:235-242.
Tiedge H, Brosius J (1996) Translational machinery in dendrites of hippocampal neurons in culture. J Neurosci 16:7171-7181.
Tiruchinapalli DM, Oleynikov Y, Kelic S, Shenoy SM, Hartley A, Stanton PK, Singer RH, Bassell GJ (2003) Activity-dependent trafficking and dynamic localization of zipcode binding protein 1 and beta-actin mRNA in dendrites and spines of hippocampal neurons. J Neurosci 23:3251-3261.
Torre ER, Steward O (1992) Demonstration of local protein synthesis within dendrites using a new cell culture system that permits the isolation of living axons and dendrites from their cell bodies. J Neurosci 12:762-772.
Tsokas P (2005) Local Protein Synthesis Mediates a Rapid Increase in Dendritic Elongation Factor 1A after Induction of Late Long-Term Potentiation. J Neurosci 25:5833-5843.
Tsokas P, Ma T, Iyengar R, Landau EM, Blitzer RD (2007) Mitogen-Activated Protein Kinase Upregulates the Dendritic Translation Machinery in Long-Term Potentiation by

Controlling the Mammalian Target of Rapamycin Pathway. J Neurosci 27:5885-5894.
Um SH, D'Alessio D, Thomas G (2006) Nutrient overload, insulin resistance, and ribosomal protein S6 kinase 1, S6K1. Cell Metab 3:393-402.
van Woerden GM, Harris KD, Hojjati MR, Gustin RM, Qiu S, de Avila Freire R, Jiang Y-h, Elgersma Y, Weeber EJ (2007) Rescue of neurological deficits in a mouse model for Angelman syndrome by reduction of αCaMKII inhibitory phosphorylation. Nat Neurosci 10:280-282.
Vanderklish PW, Edelman GM (2005) Differential translation and fragile X syndrome. Genes, Brain and Behavior 4:360-384.
Wang L, Gout I, Proud CG (2001) Cross-talk between the ERK and p70 S6 kinase (S6K) signaling pathways. MEK-dependent activation of S6K2 in cardiomyocytes. J Biol Chem 276:32670-32677.
Weeber EJ, Jiang YH, Elgersma Y, Varga AW, Carrasquillo Y, Brown SE, Christian JM, Mirnikjoo B, Silva A, Beaudet AL, Sweatt JD (2003) Derangements of hippocampal calcium/calmodulin-dependent protein kinase II in a mouse model for Angelman mental retardation syndrome. J Neurosci 23:2634-2644.
Wettenhall RE, Howlett GJ (1979) Phosphorylation of a specific ribosomal protein during stimulation of thymocytes by concanavalin A and prostaglandin E1. J Biol Chem 254:9317-9323.
Wettenhall RE, Erikson E, Maller JL (1992) Ordered multisite phosphorylation of Xenopus ribosomal protein S6 by S6 kinase II. J Biol Chem 267:9021-9027.
Wittmann J, Hol EM, Jack HM (2006) hUPF2 Silencing Identifies Physiologic Substrates of Mammalian Nonsense-Mediated mRNA Decay. Mol Cell Biol 26:1272-1287.
Wool IG (1996) Extraribosomal functions of ribosomal proteins. Trends Biochem Sci 21:164-165.
Xia Z, Dudek H, Miranti CK, Greenberg ME (1996) Calcium influx via the NMDA receptor induces immediate early gene transcription by a MAP kinase/ERK-dependent mechanism. J Neurosci 16:5425-5436.

CHAPTER 2

Synaptic activation of ribosomal protein S6 phosphorylation occurs locally in activated dendritic domains

ABSTRACT

Previous studies have shown that induction of long-term potentiation (LTP) induces phosphorylation of ribosomal protein S6 (rpS6) in postsynaptic neurons, but the functional significance of rpS6 phosphorylation is poorly understood. Here, we show that synaptic stimulation that induces perforant path LTP triggers phosphorylation of rpS6 (p-rpS6) locally near active synapses. Using antibodies specific for phosphorylation at different sites (ser235/236 vs. ser240/244), we show that strong synaptic activation led to dramatic increases in immunostaining throughout postsynaptic neurons with selectively higher staining for p-ser235/236 in the activated dendritic lamina. Following LTP induction, phosphorylation at ser235/236 was detectable by 5 minutes, peaked at 30 minutes, and was maintained for hours. Phosphorylation at both sites was completely blocked by local infusion of the NMDA receptor antagonist, APV. Despite robust induction of p-rpS6 following high frequency stimulation, assessment of protein synthesis by autoradiography revealed no detectable increases. Exploration of a novel environment led to increases in the number of p-rpS6-positive neurons throughout the forebrain in a pattern reminiscent of immediate early gene induction and many individual neurons that were p-rpS6-positive co-expressed Arc protein. Our results constrain hypotheses about the possible role of rpS6 phosphorylation in regulating postsynaptic protein synthesis during induction of synaptic plasticity.

INTRODUCTION

Long-term potentiation (LTP) was first characterized in the perforant path, which is the major extrinsic input pathway from the entorhinal cortex to the dentate gyrus (Bliss and Lomo 1973; Douglas and Goddard 1975). Subsequently, it was shown that induction of perforant path LTP initiates a number of processes in postsynaptic neurons in the dentate gyrus (DG), including activation of intracellular signaling cascades (Davis et al. 2000; Chotiner et al. 2010), induction of gene transcription (Abraham and Williams 2003; Ryan et al. 2011), actin polymerization at active synapses (Fukazawa et al. 2003; Lin et al. 2005; Huang et al. 2007), and changes in synapse morphology (Fifková and Van Harreveld 1977; Desmond and Levy 1983; Harris et al. 2003; Medvedev et al. 2010).

Although LTP was first discovered in the perforant path, mechanistic studies have largely involved studies of LTP in the CA1 region of hippocampal slices *in vitro*. Key conclusions are that late-phase LTP in CA1 involves transcription of mRNAs (Nguyen et al. 1994; Kandel 2001) and de novo protein synthesis (Nguyen and Kandel 1996) and that some of the mRNAs critical for synaptic modification are translated locally at synapses [for a review see (Steward and Schuman 2001)]. Elements necessary for local protein synthesis localize at synapses, including polyribosomes (Steward and Levy 1982), tRNA (Tiedge and Brosius 1996), and mRNAs (Burgin et al. 1990; Steward et al. 1998; Cajigas et al. 2012). Also, some mRNAs, including the mRNA for the immediate early gene (IEG), Arc/Arg3.1 (Link et al. 1995; Lyford et al. 1995), and CAMKII localize selectively near active synapses (Steward et al. 1998; Farris et al. 2014), supporting other evidence that the proteins encoded by these mRNAs are important for activity-dependent synaptic modifications.

Despite considerable information on mRNA localization in dendrites and at activated synapses, mechanisms controlling local translation of mRNAs are relatively un-explored. One interesting lead comes from a study showing that induction of perforant path LTP *in vivo* triggers phosphorylation of eukaryotic initiation factor 4E (eIF4E) and ribosomal protein S6 and de-phosphorylation of eIF2-alpha (Panja et al. 2009) in dentate granule cells. These alterations in phosphorylation state were maintained during the critical time window that stimulation-induced mRNA transcripts for the IEG, Arc, were being translated. Ribosomal protein S6 (rpS6) is of particular interest because it undergoes inducible phosphorylation in response to various stimuli (Meyuhas 2008) and is implicated in the regulation of translation initiation and protein synthesis (Thomas et al. 1982; Jefferies and Thomas 1996). RpS6 is localized near the mRNA/tRNA binding site junction between the 40S and 60S ribosomal subunits (Nygard and Nilsson 1990) making it a prime candidate to regulate recruitment of mRNA into polysomes (Nielsen et al. 1981).

In cells in culture, induction of rpS6 phosphorylation is associated with translation initiation of protein synthesis (Thomas et al. 1982; Jefferies and Thomas 1996) and preferential mobilization of specific mRNAs into polysomes (Duncan and McConkey 1982; Jefferies and Thomas 1996; Meyuhas 2000). Phosphorylation of rpS6 (p-rpS6) enhances translation of mRNAs containing a 5'-terminal tract of oligopyrimidines (5'TOP mRNAs), which encode elements of the translational machinery (Jefferies et al. 1994). Nevertheless, p-rpS6 alone is not always sufficient for activation of 5'TOP mRNA translation (Tang et al. 2001; Barth-Baus et al. 2002; Stolovich et al. 2002) and has been shown to be dispensable for the rate of protein synthesis (Kruppa and Clemens 1984; Mieulet et al. 2007). Thus, the significance of synaptically-induced p-rpS6 on mRNA translation remains to be defined.

Although Panja et al showed activity-dependent induction of p-rpS6, little is known, about the subcellular location within postsynaptic neurons where changes in phosphorylation occur, especially whether they occur near activated synapses. We explored this question here using phospho-specific antibodies for different phosphorylation sites on rpS6 (ser235/236 and ser240/244). We show that high frequency activation of the perforant path triggers robust induction of p-rpS6 in dentate granule cells with stronger induction of p-ser235/236 in the portion of the dendrite contacted by activated synapses. We further show that synaptically-driven induction of p-rpS6 is NMDA receptor-dependent, and persists for hours after LTP induction. Moreover, a learning experience (exploration of a novel environment) also triggers p-rpS6 in individual neurons in a particular pattern similar to that of IEG induction. Surprisingly, the striking increases in p-rpS6 following high frequency stimulation were not accompanied by detectable increases in postsynaptic protein synthesis. Taken together, our results provide new insights into how S6 phosphorylation is regulated by synaptic activity and during learning and suggest the need for a reassessment of how synaptic activity regulates postsynaptic protein synthesis during the consolidation phase of LTP.

MATERIALS AND METHODS

Animals: Experimental animals were adult female (150-300g) Sprague-Dawley rats from Harlan laboratories (Hsd). Rats were anesthetized with 20% urethane and positioned in a stereotaxic apparatus as described previously (Steward et al. 1998). All experimental procedures were approved by the Institutional Animal Care and Use Committee (IACUC) of the University of California, Irvine.

Acute neurophysiology preparation: Acute neurophysiological techniques were used to unilaterally stimulate the medial perforant path projections to the dentate gyrus. Projections from the entorhinal cortex to the dentate gyrus are predominately unilateral so the contralateral side serves as an intra-animal control. A stimulating electrode, an insulated tungsten microelectrode, was stereotaxically positioned in the medial entorhinal cortex (4.0mm lateral, 1.0mm anterior to lambda within a 3.0-4.0mm range below the cortical surface). Electrode depth was adjusted to obtain a maximal evoked response in the dentate gyrus with minimal stimulus intensity. Stimulus intensity was set to evoke an approximately 1.5mV population spike. The recording electrode, a glass micropipette filled with 0.9% saline, was positioned in the cell body layer of the dentate gyrus (3.5mm posterior, 1.7mm lateral to bregma and approximately 3.0mm below the cortical surface). The depth of the recording electrode was adjusted to record the positive-going field potential generated by perforant path stimulation.

Experimental Procedure: After positioning electrodes, test stimulation was delivered at a rate of 1/10sec to determine baseline response amplitude. Then high frequency stimulation was initiated as described below.

High Frequency Stimulation (HFS): Two HFS paradigms were used. One was our standard paradigm to induce perforant path LTP; the other involved longer periods of continuous HFS (5min to 2hrs), which is our standard paradigm to cause *Arc* mRNA to localize selectively in activated dendritic domains (Steward et al. 1998).

To induce LTP, 3 bouts of 10 400Hz trains (20msec in duration for a total of 8 pulses per train) were delivered at a rate of 1/10sec. 10 test responses were collected between each bout. Animals were euthanized at different times post LTP induction (5min, 15min, 30min, 60min, 120min, 240min, and 360min, N=5 per time point). Times are from the delivery of the first train of HFS. For the 5min time point, only 10 trains were delivered and the rats were perfused 5 minutes after the first train. For the 4hr and 6hr cases, the first 60 test responses were taken at a rate of 1/10sec and then test responses were taken at 1/30sec for the remaining time.

Longer periods of HFS involved delivery of 3 bouts of 10 400Hz trains followed by test stimulation to determine extent of LTP, then continuing HFS at a rate of 1/10sec for periods ranging up to 2hrs. For the 5min time point, 30 400Hz trains were delivered at 1/10 sec. At the designated survival interval, rats received a lethal dose of Euthasol (0.5ml) or Fatal plus (1.0ml) and were perfused with 4% paraformaldehyde.

Local Drug Infusions: Stimulating and recording electrodes were positioned as described above, and baseline response amplitude was assessed using a saline-filled recording electrode. The saline filled microelectrode was then replaced with a microelectrode filled with the NMDAR antagonist, APV, (51mM (10mg/ml) in saline; Tocris, Cat. 0106) and response amplitude was again monitored for a minimum of 10 minutes. After assessing response amplitude post-drug delivery, HFS was delivered as described above.

Unsupervised learning: Adult female rats (N=18) were handled for 10 minutes 2x a day for 3 days. On the day of the experiment, rats were habituated to the room for 15 minutes in their home cage. For the unsupervised learning paradigm, rats were placed in a large tank filled with numerous toys scattered inside and were allowed to explore the novel environment for 30 or 60 minutes. At the end of the exploration period, rats immediately received 0.5ml Euthasol and were perfused with 4% paraformaldehyde.

Immunohistochemistry: Brains were sectioned in the coronal plane on a Vibratome® at 40µm and sections were stored in phosphate buffer (pH 7.4). Prior to immunostaining, free-floating sections were placed in microfuge tubes with nano pure water and then the microfuge tubes were placed in boiling water for 3 minutes for antigen retrieval. Sections were then treated with H_2O_2 for 15 minutes to block endogenous peroxidase activity, transferred to 0.01% Tween in PBS for 15 minutes, blocked for 1-2 hours at room temperature in tyramide signal amplification blocking buffer and then incubated for 18-20 hours in a 1:100 dilution of rpS6 phospho-specific antibodies that recognize phosphorylated ser235/236 (Cell Signaling, #4858) or ser240/244 (Cell Signaling, #2215) or in a 1:100 dilution of total rpS6 (Cell Signaling, #2217). Sections were then incubated in a 1:250 dilution of biotinylated donkey anti rabbit IgG for 2 hours (Jackson Laboratories, 711-065-152), treated with ABC for 2 hours (Vector, PK-6100), stained for 5 minutes in DAB (Vector, SK-4100) and mounted on 0.5% gelatin subbed slides. Slides were dehydrated through washes of graded ethanol, cleared in 3 changes of xylene and cover slipped with DPX mountant for histology.

For immunofluorescence, free-floating sections underwent the same antigen retrieval and blocking of peroxidase activity but were then blocked for 1 hour in 0.1% Triton-X100 and 10% natural goat serum in PBS and then incubated for 18-20 hours in a 1:100 dilution of p-ser235/236, 1:100 dilution of Arc antibody (SCB, sc17839), 1:300 dilution of GFAP antibody (Cell Signaling, #3670) or 1:3000 dilution of anti-parvalbumin antibody (Sigma, P3088). Sections were then incubated for 2 hours in appropriate secondary antibody (ThermoFisher, 1:250), mounted on 0.5% gelatin subbed slides and cover slipped with Vectashield.

Image Quantification: Optical density (OD) across the granule cell layer and molecular layers of the dentate gyrus was quantified using NIH ImageJ as described in detail previously (Farris et al. 2014). Images were taken at 20X using the same acquisition parameters. A line region of interest (ROI) was aligned perpendicular to the cell body layer extending through the dendritic laminae and OD was measured at every 20μm. The OD at each level was averaged across the total number of line measurements per image to obtain an average value along the line ROI for each section. Figure 1 represents quantification of a single animal with ~19 line measurements averaged. For all other quantifications, the average line ROI values were then averaged across rats to generate an "average optical density vs. distance" graph where N=number of rats. Values are presented as mean ± SEM.

For the assessment of changes in immunostaining after HFS across time points, values were obtained as described above except that only OD measures from two sites, the cell body layer and middle molecular layer, for both ipsilateral and contralateral sides to the stimulation are shown. The average values were plotted to represent each time point.

For quantification following APV infusion, OD was measured at four sites, the cell body later, inner molecular layer, middle molecular layer and outer molecular layer.

For quantification of p-rpS6 immunofluorescence following experience, images were collected at 20X magnification. P-rpS6 positive granule cells were counted along the length of the granule cell layer of the dorsal blade of the dentate gyrus (~400 µm length). Levels of immunofluorescence for p-rpS6 in the pyramidal cell layers of CA1 and CA3 were assessed by centering a measuring frame (40µ x 40µm, CA1; 50µm x 50µm, CA3) over the pyramidal cell layer (see Figure 5G and 5J, respectively); fluorescence intensity was averaged along the length of the pyramidal cell layer using ImageJ software.

Film autoradiography to assess protein synthesis: To assess levels of protein precursor incorporation, rats received 30 minutes or 90 minutes of continuous HFS to induce rpS6 phosphorylation and then received injections of C14-leucine (50-70µCi per 250g of body weight) via tail vein injection immediately before HFS for the 30-minute time point or approximately 30 minutes before the end of the stimulation for the 90-minute time point. Rats were perfused with 4% paraformaldehyde immediately post stimulation and 20µm coronal brain sections were cut on a cryostat and mounted on glass coverslips. The glass coverslips were affixed to a cardboard sheet with rubber cement. The sheet was placed in a cassette with C14-sensitive film. Exposure times ranged from 8-12wks.

Quantification of film autoradiographs: Images of the dentate gyrus on the autoradiographic films were acquired at 10X on an upright microscope keeping exposure constant. OD was measured across the granule cell layer and molecular layers of the

dentate gyrus using NIH ImageJ software. Images were converted to 8-bit grayscale and inverted so that higher density equated to a greater intensity value. Since stimulation is unilateral, comparisons were done between the stimulated vs. the contralateral (control) side of the brain. A ROI was measured to be the length of the cell body layer and the dendritic laminae, aligned perpendicular to the cell body layer and line intensities were measured every 100μm along the length of the 10X image (~8 line measurements per image). The intensity value for each point in the line ROI was averaged across the total number of line measurements per image to obtain an average value along the line ROI for each section. Measures from 4 sections per animal were averaged. Intensity values for granule cell layer and molecular layers were averaged across rats then calculated as an ipsilateral/contralateral (I/C) ratio and then the values were expressed as a percent change to generate an "average grain density (% of contralateral) vs. region" graph where N=number of rats. Values are presented as mean ± SEM.

Image Adjustments: The only adjustments of images were for brightness and contrast. Images of light micrographs were adjusted only to make the images appear as they do in the microscope. Paired images taken at different parts of the same section (i.e. ipsi- and contralateral to the stimulation) are shown with identical adjustments. Images of fluorescence were adjusted for the figures so that background fluorescence is comparable; images used for quantitative analysis were not adjusted.

Statistical Analysis: Statistical analyses were done using Prism (GraphPad Software, San Diego, USA). For all analyses, "N"=number of animals.

RESULTS

High frequency activation of the perforant path triggers rapid and robust phosphorylation of ribosomal protein S6 in activated dendritic laminae

We discovered the selective phosphorylation of rpS6 (p-rpS6) in the activated dendritic lamina as a result of immunostaining sections from rats in which repeated HFS was delivered to induce targeting of *Arc* mRNA to active synapses (8 pulses at 400Hz at 1/10 seconds for 60 minutes). Sections from these cases were immunostained using phospho-specific antibodies for p-rpS6 at ser235/236 and ser240/244 (Figure 1). One hour of continuous HFS resulted in robust immunostaining throughout the cell body and dendritic lamina (Figure 1A). Most strikingly, there was a distinct band of increased immunostaining in the middle molecular layer (MML) in exactly the part of the dendritic lamina contacted by medial perforant path synapses (Figure 1C). On the side contralateral to the stimulation, which serves as an internal control, overall levels of immunostaining for p-ser235/236 were low (Figure 1B), although some individual granule cells exhibited high levels of immunostaining (more on this below). To quantify changes in immunostaining for p-rpS6, we measured optical density (OD) across the granule cell layer (GCL) and molecular layer ipsilateral and contralateral to the stimulation. Figure 1D plots the average OD along the dorsal blade of the dentate gyrus (DG) from GCL to outer molecular layer (OML) for the high-magnification image illustrated in Figure 1C and the corresponding contralateral side. The band of increased labeling in the zone of activated synapses (middle molecular layer) is evident.

It should be noted that immunostaining for p-rpS6 varies in a way much like IEG expression in that patterns of activation depend on the animal's behavior in the period

prior to death. When awake behaving animals are euthanized and prepared for p-rpS6 immunostaining, some individual neurons scattered throughout the brain are p-rpS6 positive, and the number of p-rpS6 neurons increases if the animals are exposed to a novel environment (see below). When animals have been anesthetized for an hour or more, overall levels of immunostaining are lower than for brains collected without prolonged anesthesia. In this regard, the pattern of immunostaining on the contralateral (non-stimulated) side in Figure 1B is noteworthy because of the number of p-rpS6-positive dentate granule cells. This is a relatively rostral section, and it should be noted that there is a sparse crossed projection from the entorhinal cortex of one side to the rostral dentate gyrus on the contralateral side which does activate dentate granule neurons (Levy and Steward 1979). It is possible that immunostaining of granule cells evident in Figure 1B reflects activation by the crossed pathway.

The pattern of immunostaining for p-ser240/244 was different than that observed for p-ser235/236 on both the stimulated and control (non-stimulated) sides (Figure 1E and 1F). On the stimulated side (Figure 1E), there was intense immunostaining of the majority of granule cell bodies and increased staining throughout the dendritic lamina. Although discernable, the band of increased immunostaining for p-rpS6 in the MML was less pronounced for p-ser240/244 than for p-ser235/236. Instead of a distinct band, quantitative assessment of the average OD over the dorsal blade of the dentate gyrus revealed a general increase in immunostaining for p-ser240/244 throughout the dendritic lamina (Figure 1H). On the non-stimulated side (Figure 1F), basal levels of immunostaining in the molecular layer of the dentate gyrus were higher for p-ser240/244 than for p-ser235/236 (Figure 1B) in the cell bodies and dendritic layers.

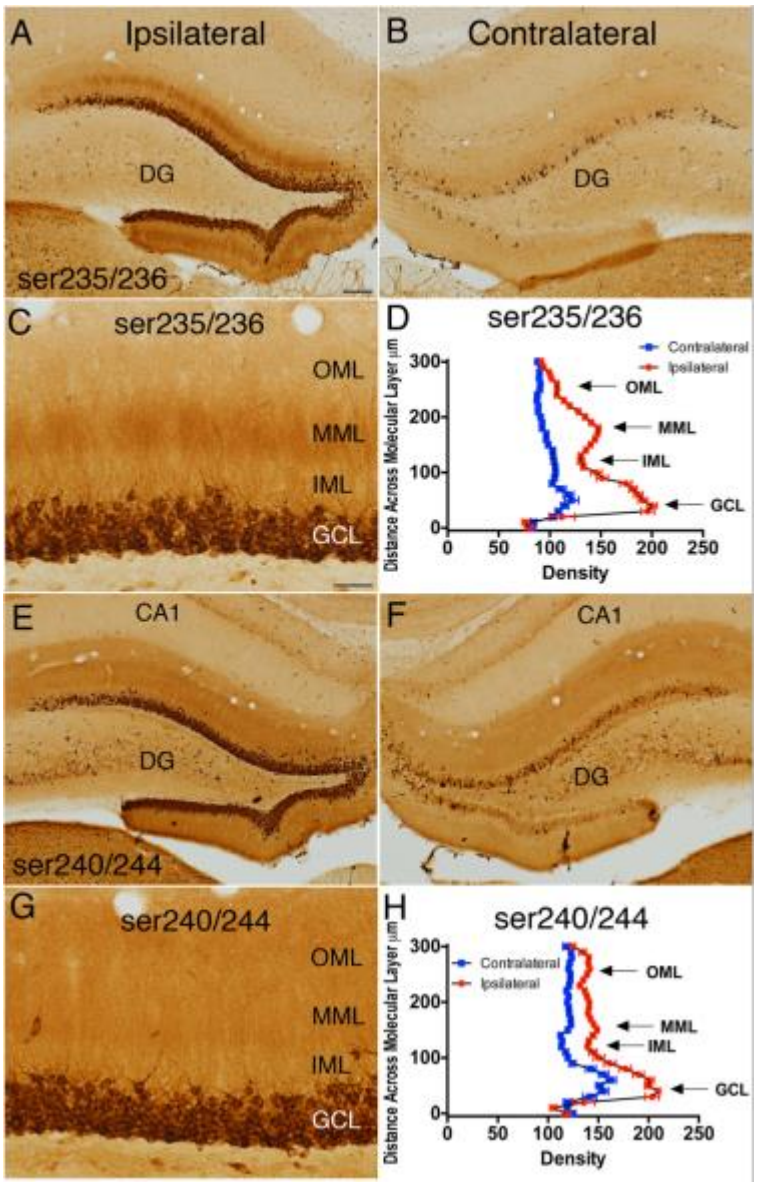

Figure 2.1. Unilateral HFS of the MPP triggers rapid and robust immunostaining of rpS6 phosphorylation. A, Immunostaining of p-ser235/236 in a section ipsilateral to MPP stimulation following 60 minutes of HFS. **B,** Immunostaining of p-ser235/236 contralateral (non-stimulated) to the stimulation. **C,** High-magnification image of A. Note the prominent band of rpS6 phosphorylation precisely in the middle molecular layer, the layer that is selectively activated with stimulation. **D,** Quantification of average OD across the dorsal blade of the dentate gyrus in both ipsilateral and contralateral sections for p-ser235/236. **E,** Immunostaining of p-ser240/244 in a section ipsilateral to MPP stimulation following 60 minutes of HFS. **F,** Immunostaining of p-ser240/244 contralateral to the stimulation. **G,** High-magnification image of E. Note that p-ser240/244 immunostaining has higher basal levels of immunostaining throughout the granule and dendritic layers of the dentate gyrus. **H,** Quantification of average OD across the dorsal blade of the dentate gyrus in both ipsilateral and contralateral sections for p-ser240/244. Abbreviations: DG, dentate gyrus; GCL, granule cell layer; IML, inner molecular layer; MML, middle molecular layer; OML, outer molecular layer. Scale bars: **A,** 200µm; **C,** 50 µm.

The extent of rpS6 phosphorylation induction depends on the duration of high frequency stimulation

Figure 1 illustrates activation of p-rpS6 with prolonged HFS, but for physiological relevance, it is important to determine how much synaptic activation is required to induce phosphorylation of rpS6. To define the stimulation conditions required to induce maximal p-rpS6, short high frequency trains (10 pulses at 400hz) were delivered at an interval of one-train/10 seconds for 5, 15, 30, 60, or 120 minutes to generate a stimulus dose-rpS6 phosphorylation response curve. Delivery of merely 30 high frequency trains (5 minutes of HFS) led to increases in immunostaining for p-ser235/236 in granule cell bodies and dendritic laminae (Figure 2B). Quantification of OD for immunostaining of p-rpS6 at ser235/236 at two measuring sites across the dorsal blade of the dentate gyrus, GCL and MML, revealed that increases were evident at 5 minutes and became more prominent with longer periods of stimulation (Figure 2M and 2N, respectively). Comparison of levels of immunostaining on the stimulated vs. control sides with different durations of HFS (N=5 animals per time point) by two-way ANOVA yielded an overall $F(4,40)=7.45$, $p=0.0001$ in the GCL and an overall $F(4,40)=9.85$, $p<0.0001$ in the MML. Post-hoc analysis with Bonferroni correction revealed significant differences between stimulated and control sides at all time points for both the GCL and MML for ser235/236 (Figure 2M and 2N, respectively, for details on statistics, see figure legends).

There were also increases in immunostaining for p-ser240/244 after 5 minutes of HFS (Figure 2H) over both cell bodies and dendrites. Quantification of OD of immunostaining for p-ser240/244 at the two measuring sites, GCL and MML, revealed that

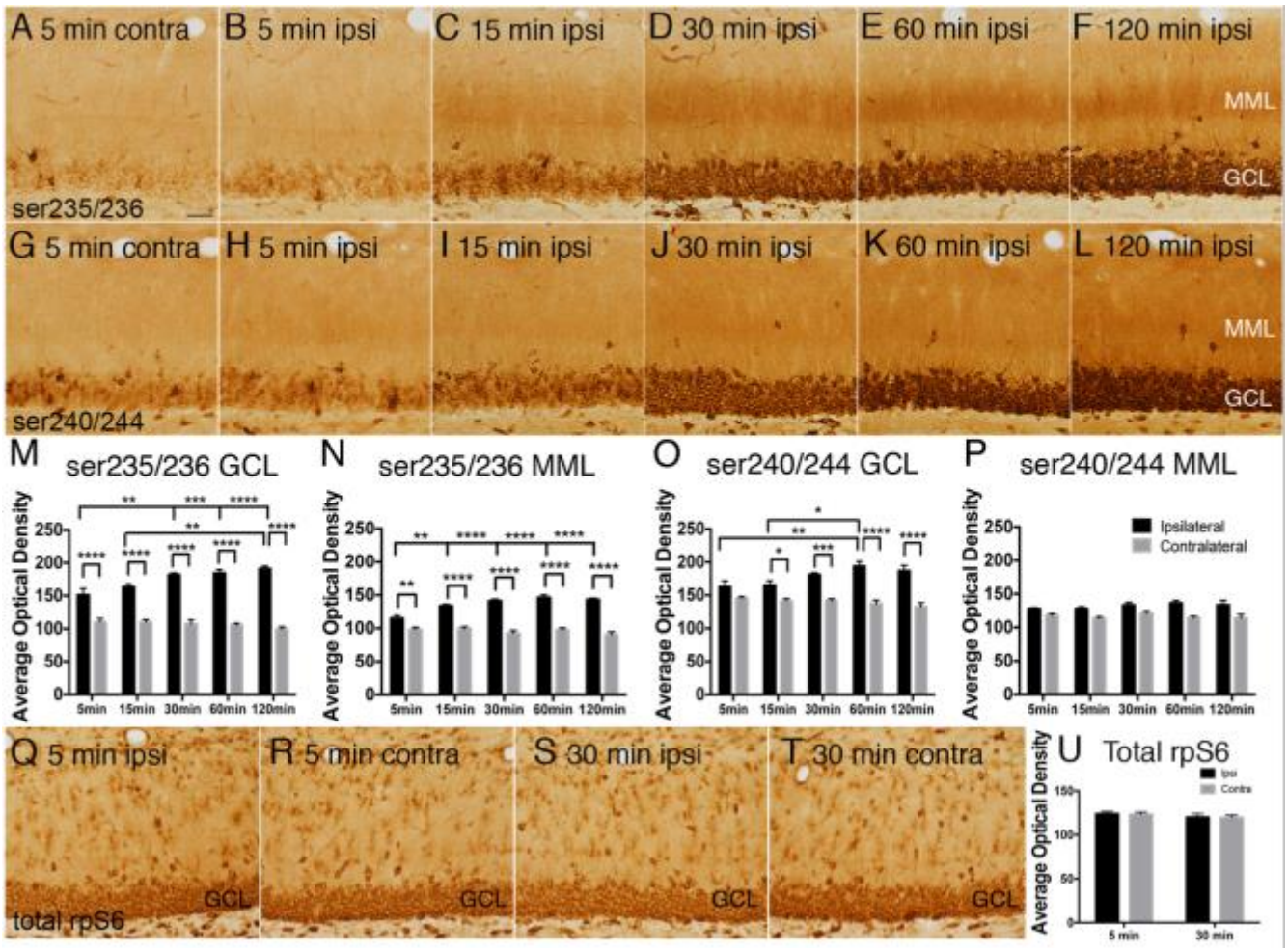

Figure 2. Stimulus dose-rpS6 phosphorylation time course reveals extent of p-rpS6 depends on duration of HFS. A, Immunostaining of p-ser235/236 contralateral to stimulation following 5 minutes (30 trains) of HFS. **B,** Immunostaining of p-ser235/236 ipsilateral to stimulation following 5 minutes (30 trains) of HFS. **C, D, E, F,** Immunostaining of p-ser235/236 ipsilateral to stimulation following 15, 30, 60, and 120 minutes of continuous HFS, respectively. **G,** Immunostaining of p-ser240/244 contralateral to stimulation following 5 minutes (30 trains) of HFS. **H,** Immunostaining of p-ser240/244 ipsilateral to stimulation following 5 minutes (30 trains) of HFS. **I, J, K, L,** Immunostaining of p-ser240/244 ipsilateral to stimulation following 15, 30, 60, and 120 minutes of continuous HFS, respectively. **M,** Quantification of average OD of p-ser235/236 across the dorsal blade of the dentate gyrus in ipsilateral and contralateral sections for each time point along the granule cell layer (GCL. Statistical assessment by two-way ANOVA revealed a significant interaction ($F(4,40)=7.45$, $p=0.0001$), main effect of condition ($F(1,40)=429.84$, $p<0.0001$) and main effect of time ($F(4,40)=3.32$, $p=0.0194$). Post-hoc analysis with Bonferroni's correction revealed significant differences between ipsilateral and contralateral OD at all time points in the GCL (Two-way ANOVA, $p<0.05$, N=5 per time point). Post-hoc analysis also revealed a significant difference between 5min ipsilateral vs. 30, 60, and 120min ipsilateral OD and 15min ipsilateral vs. 120min ipsilateral OD ($p<0.05$, N=5). **N,** Quantification of average OD of p-ser235/236 in the middle molecular layer (MML) of the DG in ipsilateral and contralateral sections for each time point. Statistical assessment by two-way ANOVA revealed a significant interaction ($F(4,40)=9.85$, $p<0.0001$), a significant main effect of condition ($F(1,40)=357.91$, $p<0.0001$), and significant main effect of time ($F(4,40)=5.65$,

p=0.0011). Post-hoc analysis with Bonferroni's correction revealed significant differences between ipsilateral and contralateral average OD at all time points (Two-way ANOVA, $p<0.05$, N=5). Post-hoc analysis also revealed a significant difference between 5min ipsilateral vs. 15, 30, 60, and 120min ipsilateral OD ($p<0.05$). **O,** Quantification of average OD of p-ser240/244 in the GCL. Statistical assessment by two-way ANOVA revealed a significant interaction ($F(4,40)=4.54$, $p=0.0041$), a significant main effect of condition ($F(1,40)=109.78$, $p<0.0001$), but no main effect of time ($F(4,40)=1.62$, $p=0.1893$). Post-hoc analysis with Bonferroni's correction revealed a significant difference between ipsilateral and contralateral OD at all time points in the GCL except for the 5-minute time point (Two-way ANOVA, $p<0.05$, N=5). Post-hoc analysis also revealed a significant difference between the 5 min ipsilateral vs. 60 min ipsilateral OD and 15 min ipsilateral vs. 60 min ipsilateral OD (Two-way ANOVA, $p<0.05$, N=5) in the GCL. **P,** Quantification of average OD of p-ser240/244 in MML for ipsilateral and contralateral sections. Statistical assessment by two-way ANOVA revealed a significant main effect of condition ($F(1,40)=41.97$, $p<0.0001$) but no main effect of time ($F(4,40)=0.5014$, $p=0.5014$) or interaction ($F(4,40)=0.96$, $p=0.4394$). **Q,** Immunostaining for total rpS6 in section ipsilateral to stimulation following 5 minutes (30 trains) of HFS. **R,** Immunostaining for total rpS6 contralateral to stimulation following (30 trains) of HFS. **S,** Immunostaining for total rpS6 ipsilateral to stimulation following 30 minutes of continuous HFS. **T,** Immunostaining for total rpS6 contralateral to stimulation following 30 minutes of continuous HFS. **U,** Quantification of average OD of rpS6 for ipsilateral and contralateral sections following 5 and 30 minutes of HFS (main effect of condition: $F(1,16)=0.04$, $p=0.8451$; main effect of time: $F(1,16)=1.73$, $p=0.2074$); interaction: $F(1,16)=0.00$, $p=0.9870$, one-way ANOVA). Abbreviations: GCL, granule cell layer; MML, middle molecular layer. Scale bar: **A,** 50 μm. Error bars are s.e.m.

the extent of the increase in staining in the dendritic layer was not as great as that observed for p-ser235/236 but became more prominent with longer periods of stimulation (Figure 2O and 2P, respectively). Comparisons of levels of immunostaining on the stimulated vs. control sides with different durations of HFS (N=5 animals per time point) by two-way ANOVA yielded an overall $F(4,40)=4.54$, $p=0.0041$ in the GCL and an overall $F(4,40)=0.96$, $p=0.4394$ in the MML. Post-hoc analysis with Bonferroni correction revealed significant differences between stimulated and control sides at all time points for the granule cell layer for p-ser240/244 except for the 5 min time point (Figure 2O and 2P, for statistics, see figure legend). Although the band of increased immunostaining in the activated dendritic lamina was detected for p-ser240/244, the band was not as prominent as that observed with immunostaining for p-ser235/236. In the MML, the average percent change from contralateral following 30-120minutes of HFS for p-ser235/236 was 45.6% vs. 7.5% for p-ser240/244 (two-way ANOVA, $F(4,40)=3.23$, $p=0.0218$, N=5). Post-hoc analysis with Bonferroni correction revealed significant differences between p-ser235/236 and p-ser240/244 at all time points except the 5-minute time point ($p<0.05$).

To determine if the robust phosphorylation of p-rpS6 observed with prolonged HFS is also accompanied with an increase in the synthesis of rpS6, immunostaining for total rpS6 was done to quantify the changes in the synthesis of rpS6. Immunostaining for total rpS6 revealed no difference between stimulated and non-stimulated (control) sides following 5-120 minutes of continuous HFS. Figure 2Q-2T, shows representative images of stimulated and non-stimulated sides following 5 and 30 minutes of continuous HFS. Comparisons of levels of immunostaining on the stimulated vs. control sides following 5

and 30 minutes of continuous HFS (N=5 animals per time point) by two-way ANOVA yielded an overall $F(1,16)=0.00$, $p=0.9870$ (Figure 2U).

Rapid and prolonged phosphorylation of ribosomal protein S6 following induction of long-term potentiation

Determining when rpS6 phosphorylation initiates, peaks and depletes sets constraints on which mRNAs may be preferentially translated after a bout of synaptic activity, for example as a result of induction of LTP. For instance, newly-synthesized *Arc* mRNA does not reach dendrites in quantity until about 30 minutes after transcription is induced (Wallace et al. 1998). Phosphorylation of rpS6 could affect translation of newly-synthesized *Arc* in dendrites only if activation in dendrites persists until the mRNAs are available for translation. To determine the duration of p-rpS6 post LTP induction, we induced LTP in anesthetized rats (30 trains at 400Hz, 1/10 seconds) and allowed rats to survive for periods ranging from 5 minutes to 6 hours post-LTP induction. Immunostaining for p-ser235/236 and p-ser240/244 of rpS6 revealed similar activation parameters but overall increases in immunostaining for p-ser235/236 were more robust than for p-ser240/244 (Figure 3A-J vs. Figure 3K-T, respectively).

Increases in immunostaining for p-ser235/236 were first evident in the granule cell layer and dendrites 15 minutes post-stimulation (Figure 3C) and peak phosphorylation was observed at 30 minutes (Figure 3D). Levels of p-rpS6 remained enhanced 4 hours post LTP and returned to baseline levels 6 hours post LTP induction (Figure 3I). Similarly, for p-ser240/244, initial increases in immunostaining in both the GCL and MML were first evident 15 minutes post-stimulation (Figure 3M) and peak phosphorylation was observed

at 30 minutes (Figure 3N). Levels of p-rpS6 began to decrease 4 hours post LTP and returned to baseline levels 6 hours post LTP induction (Figure 3S).

To quantitate the changes in p-rpS6 over time, we assessed relative OD in the GCL and MML ipsilateral and contralateral to the stimulation, determined the ratio of ipsilateral to contralateral (I/C) signal, and then expressed values as percent change from contralateral, which provides an internal control for any variability in immunostaining across sections. Figure 3E and 3J illustrate a plot of the changes in immunostaining over time post LTP induction over the GCL and the MML for p-ser235/236. A one-way ANOVA comparing percent change in OD in the GCL revealed an overall $F(6,28)=2.785$, $p=0.0299$ in the GCL and an overall $F(6,28)=7.972$, $p<0.0001$ in the MML (N=5 for each time point). Figure 3O and 3T illustrate a plot of the changes in immunostaining over time post LTP induction over the GCL and the MML for p-ser240/244. A one-way ANOVA comparing the percent change in OD in the GCL revealed an overall $F(6,28)=3.264$, $p=0.0146$ and an overall $F(6,28)=4.078$, $p=0.0046$ in the MML (N=5 for each time point). For statistical comparisons between individual time points, see figure legend. These quantitative results reveal that p-rpS6 after brief HFS to induce LTP actually peaks at a time when newly-transcribed Arc mRNA transcripts are appearing in dendrites.

It was noteworthy that even when HFS was delivered for 2hrs, astrocytes in the activated zone did not stain positively for p-rpS6. P-rpS6-positive astrocytes were seen only near electrode tracks. This is noteworthy because of the striking activation of p-rpS6 in astrocytes by a learning experience (see below).

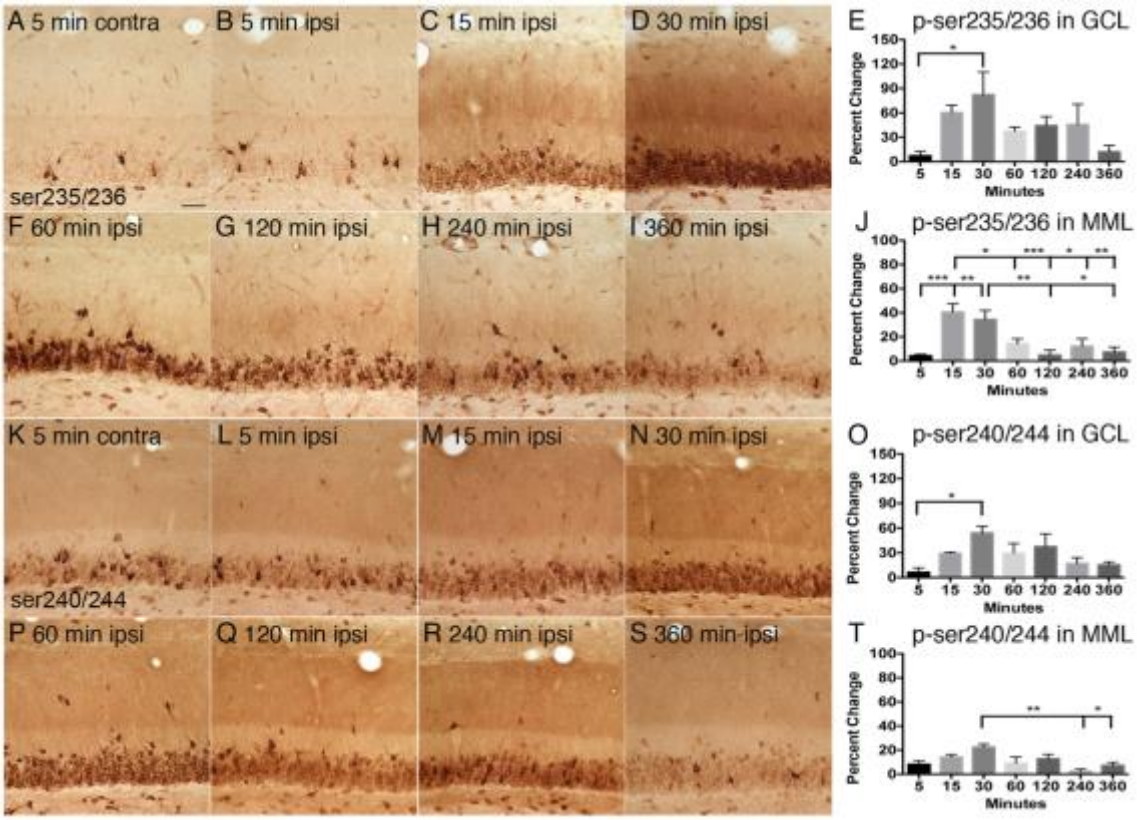

Figure 2.3. LTP induction triggers rapid and prolonged phosphorylation of rpS6. A, Immunostaining of p-ser235/236 contralateral to stimulation 5 minutes (10 trains) post HFS delivery. **B,** Immunostaining of p-ser235/236 ipsilateral to stimulation 5 minutes (10 trains) post HFS delivery. **C, D, E, F, G, H,** Immunostaining of p-ser235/236 ipsilateral to stimulation at a time point 15, 30, 60,120, 240 and 360 minutes post LTP induction (30 trains), respectively. **I,** Quantification of percent change from contralateral for p-ser235/236 in the GCL of the dorsal blade of the DG. Statistical assessment by one-way ANOVA revealed an overall $F(6,28)=2.785$, $p=0.0299$. Post-hoc analysis with Bonferroni's correction revealed a significant difference in percent change between 5 and 30 minutes post LTP. **J,** Quantification of percent change from contralateral for p-ser235/236 in the MML of the dorsal blade of the DG. Statistical assessment by one-way ANOVA revealed an overall $F(6,28)=7.972$, $p<0.001$. Post-hoc analysis with Bonferroni's correction revealed a significant difference in percent change between 5 vs. 15, 30 minutes, 15 vs. 60, 120, 240, 360 minutes, and 30 vs. 120, 360 minutes post LTP. **K,** Immunostaining of p-ser240/244 contralateral to stimulation 5 minutes (10 trains) post HFS delivery. **L,** Immunostaining of p-ser240/244 ipsilateral to stimulation 5 minutes (10 trains) post HFS delivery. **M, N, O, P, Q, R,** Immunostaining of p-ser240/244 ipsilateral to stimulation at a time point 15, 30, 60,120, 240 and 360 minutes post LTP induction (30 trains), respectively. **S,** Quantification of percent change from contralateral for p-ser240/244 in the GCL of the dorsal blade of the DG. Statistical assessment by one-way ANOVA revealed an overall $F(6,28)=3.264$, $p=0.0146$. Post-hoc analysis with Bonferroni's correction revealed a significant difference in percent change between 5 and 30 minutes post LTP. **T,** Quantification of percent change from contralateral for p-ser240/244 in the MML of the dorsal blade of the DG. Statistical assessment by one-way ANOVA revealed an overall $F(6,28)=4.078$, $p=0.0046$. Post-hoc analysis with Bonferroni's correction revealed a significant difference in percent change between 30 vs. 240, and 360 minutes post LTP. Scale bars: **A,** 50 μm. Error bars are s.e.m.

Phosphorylation of rpS6 is dependent on NMDA receptor activation

Because LTP induction requires activation of post-synaptic NMDA receptors (Gustafsson and Wigström 1988), we assessed whether the NMDA receptor antagonist, APV, blocked activation of rpS6 phosphorylation. For this, a micropipette containing APV (10mg/ml in saline) was positioned in the dorsal blade of the dentate gyrus prior to HFS and baseline responses were collected for 10 minutes followed by delivery of continuous HFS (60 minutes). Immediately after stimulation, each animal was perfused and brain sections were immunostained for p-rpS6 as above.

We have previously shown that when APV-filled micropipettes are positioned in the dentate gyrus prior to HFS, IEG induction is blocked in an area several millimeters in diameter around the micropipette (Steward and Worley 2001). Blockade is local, so areas distant from the APV-filled micropipette serve as intra-animal control. APV also blocks LTP of population excitatory postsynaptic potentials (EPSPs) and population spikes recorded from the infusion area, providing an on-line positive control for the effectiveness of NMDA-receptor blockade.

In the presence of APV, there was no increase in population EPSP slope or population spike amplitude following delivery of 30 high frequency trains (our standard paradigm for inducing perforant path LTP). The percent change from baseline recorded via the APV micropipette was -6.13 % ± 15.12 % for population spike amplitude in comparison to 114.15 % ± 17.99 % in control experiments with saline-filled microelectrodes. The percent change from drug baseline for population EPSP slope was 4.49 % ± 11.24 % in comparison to 30.25 % ± 2.22 % in control experiments.

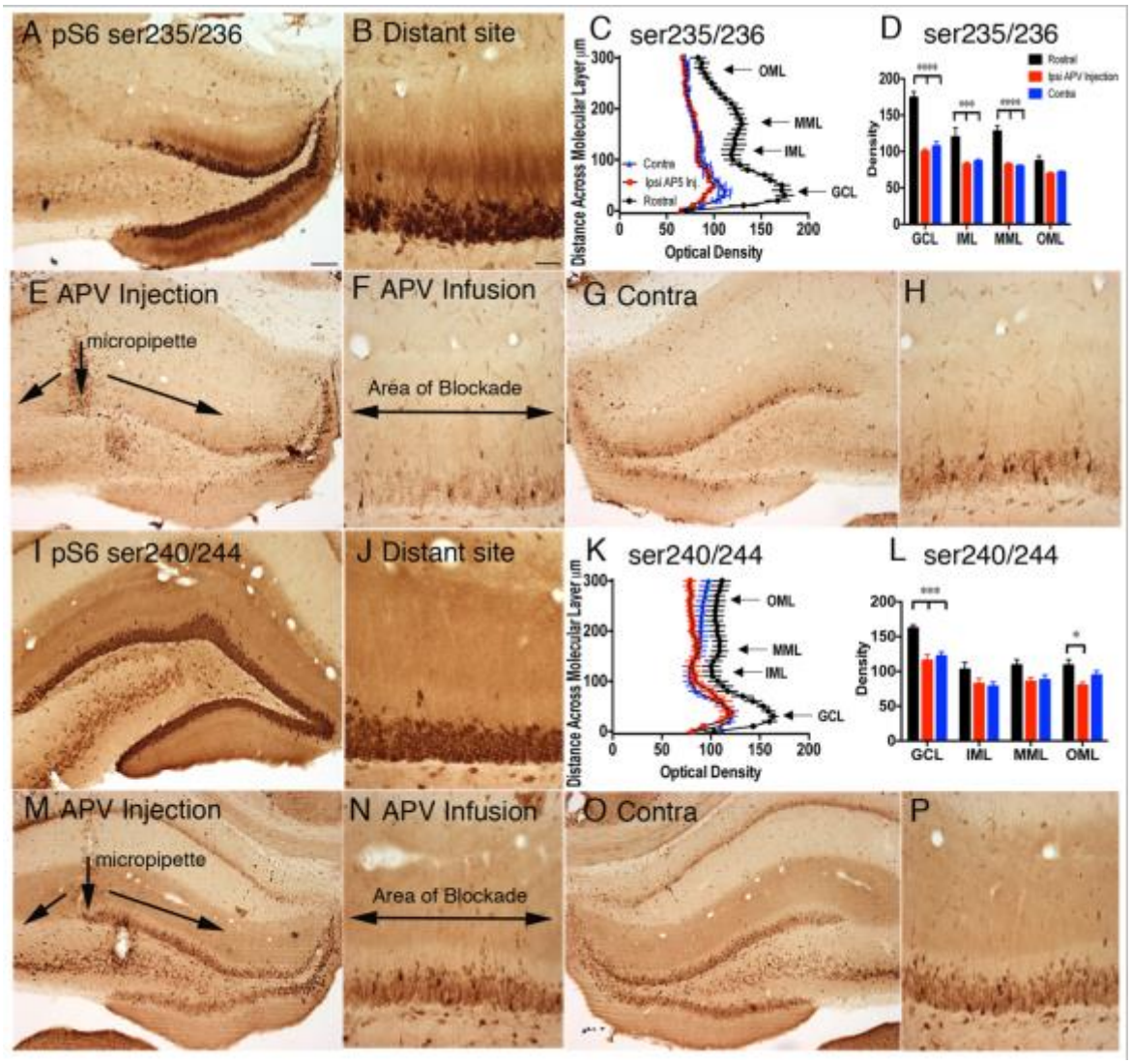

Figure 2.4. Phosphorylation of rpS6 is dependent on NMDA receptor activation. A, Immunostaining of p-ser235/236 ipsilateral to stimulation in rostral section distant from the APV infusion area. **B,** High-magnification image of A. **C,** Quantification of average OD across the dorsal blade of the DG in ipsilateral section distant from the injection site (rostral), ipsilateral section within the infusion area, and contralateral section. **D,** Statistical assessment at four sites along the dorsal blade of the dentate gyrus, GCL, IML, MML, OML (ser235/236, N=4), error bars represent SEM. Statistical assessment by two-way ANOVA revealed a significant interaction ($F(6,27)=9.68$, $p<0.0001$), a significant main effect treatment ($F(2,9)=29.42$, $p=0.0001$), and a significant main effect of region ($F(3,27)=74.58$, $p<0.0001$). Post-hoc analysis with Bonferroni's correction revealed a significant difference between rostral vs. injection site and contralateral OD in the GCL, IML and MML (Two-way ANOVA, N=4, $p<0.05$). **E,** Immunostaining of p-ser235/236 within the injection site in the presence of NMDAR antagonist, APV. **F,** High-magnification image of E. **G,** Immunostaining of p-ser235/236 contralateral to stimulation. **H,** High-magnification image of G. **I,** Immunostaining of p-ser240/244 ipsilateral to stimulation in section distant from the APV injection site. **J,** High-magnification image of I. **K,** Quantification of average OD across the dorsal blade of the dentate gyrus in ipsilateral section distant from the injection site (caudal), ipsilateral section within the infusion area, and contralateral section. **L,** Statistical assessment at four sites along the dentate

gyrus, GCL, IML, MML, OML (ser240/244, N=4), error bars represent SEM. Statistical assessment by two-way ANOVA revealed a significant interaction ($F(6,27)=2.88$, $p=0.0267$) a significant main effect of treatment ($F(2,9)=6.95$, $p=0.0149$), and a significant main effect of region ($F(3, 27)=71.19$, $p<0.0001$). Post-hoc analysis with Bonferroni's correction revealed a significant difference between rostral vs. injection site and contralateral OD in the GCL and a significant difference between rostral vs. injection site OD in the OML. **M,** Immunostaining of p-ser240/244 within the injection site in the presence of NMDAR antagonist, APV. **N,** High-magnification image of M. **O,** Immunostaining of p-ser240/244 contralateral to the stimulation. **P,** High-magnification image of O. Scale bars: **A,** 200μm; **B,** 50 μm.

Immunostaining for p-ser235/236 revealed strong activation of p-rpS6 in areas distant from the APV-filled micropipette (Figure 4A and 4B) and a complete block of p-rpS6 in the area of APV infusion (Figure 4E and 4F). Within the infusion area, immunostaining was comparable to the contralateral control (Figure 4G and 4H). Higher magnification views (Figure 4F) reveal a few individual neurons that are positive for p-rpS6 as on the control side (Figure 4H).

Similarly, immunostaining for p-ser240/244 revealed strong activation of p-rpS6 in areas distant from the APV-filled micropipette (Figure 4I and 4J), whereas immunostaining in the area of APV infusion (Figure 4M and 4N) was comparable to that on the contralateral non-stimulated side (Figure 4O and 4P). Quantitative analyses as above revealed that in the area surrounding the micropipette, levels of immunostaining for both p-ser235/236 and p-ser240/244 were actually somewhat less than on the contralateral (control) values (Figure 4C and 4K, respectively, see legends for statistics). These data indicate that NMDA receptor activation is critical for activation of rpS6 phosphorylation in both cell body and dendritic layers.

Exploration of a novel environment leads to increased numbers of p-rpS6-positive neurons

Learning experiences activate some of the same intracellular cascades as seen with induction of LTP, including activation of IEG expression in select populations of neurons. To further explore linkages between regulation of rpS6 phosphorylation and learning, we assessed rpS6 phosphorylation following exploration of a toy-filled novel environment. We refer to this as an "unsupervised learning" experience.

All rats were handled prior to the experiment. On the day of the experiment, rats were allowed to explore the novel environment for 30 minutes or 60 minutes; home cage controls were euthanized immediately after removal from their home cage. In what follows, we focus on changes in immunostaining in the hippocampus and dentate gyrus, although it was also evident that behavioral experience activated p-rpS6 in populations of neurons throughout the forebrain.

Immunostaining for p-ser235/236 in rats that were anesthetized immediately upon removal from their home cage (Figure 5A) revealed scattered dentate granule cells that exhibited relatively high levels of p-rpS6 immunostaining (Figure 5D). The labeling of a few scattered granule cells, especially in the dorsal blade of the dentate gyrus, is similar to what is seen with immunocytochemistry or *in situ* hybridization for IEGs under basal conditions. There were also a small number of scattered pyramidal neurons in CA1 that exhibited higher levels of immunostaining in cell bodies (Figure 5G). Pyramidal neurons in CA3 exhibited moderate levels of immunostaining predominately in the cell bodies (Figure 5J). It was noteworthy that overall levels of immunostaining over the neuropil layers qualitatively appeared higher than in rats that had been maintained under anesthesia for prolonged periods, consistent with the finding that synaptic activity drives p-rpS6. We did not quantify this directly, however.

Following 30 minutes of exploration (Figure 5B) there were increases in the level of p-rpS6 immunostaining of neuronal cell bodies in the dentate gyrus, CA1 and CA3 (Figure 5E, 5H, and 5K, respectively). The pattern of immunostaining was qualitatively similar after 60 minutes (Figure 5F, 5I, and 5L). Note also the large number of p-rpS6-positive neurons in the neocortex in Figure 5B and 5C. Notably, p-rpS6-positive cells with astrocyte

morphology were also evident in the molecular layer of the dentate gyrus, stratum oriens and stratum radiatum of CA1-CA3 following unsupervised learning (more on this below). As one measure of activation of p-rpS6, p-rpS6-positive granule cells were counted along the length of the granule cell layer of the dorsal blade of the dentate gyrus (~400μm length). The number of p-rpS6-positive granule cells was 2-fold higher after 30 minutes of exploration and increased further after 60 minutes (one-way ANOVA, $F(2,15)=11.43$, $p=0.0010$, N=6). Post-hoc analysis using a Dunnett's multiple comparisons test revealed that differences were significant at both 30- and 60-minute time points (Figure 5M; $p<0.05$).

To measure the extent of p-rpS6 in the densely packed pyramidal layer of CA1 and CA3, fluorescence intensity (FI) was measured within a boxed region centered in the pyramidal cell layer (see Figure 5G and 5J, respectively) and the FI was averaged along the length of the pyramidal cell layer using ImageJ software. For CA1, FI was measured in a 40μm x 40μm box centered along the pyramidal cell layer and statistical assessment by one-way ANOVA revealed an overall $F(2,6)=22.29$, $p=0.0017$ (N=3 rats per time point). Post-hoc analysis using a Dunnett's multiple comparisons test revealed that differences were significant at both 30- and 60-minute time points (Figure 5N; $p<0.05$). For CA3, FI was measured in a 50μm x 50μm box centered along the pyramidal cell layer and statistical assessment by one-way ANOVA of the average IF in the pyramidal cell layer yielded an overall $F(2,6)=2.556$, $p=0.1574$ (Figure 5O; N=3 rats per time point).

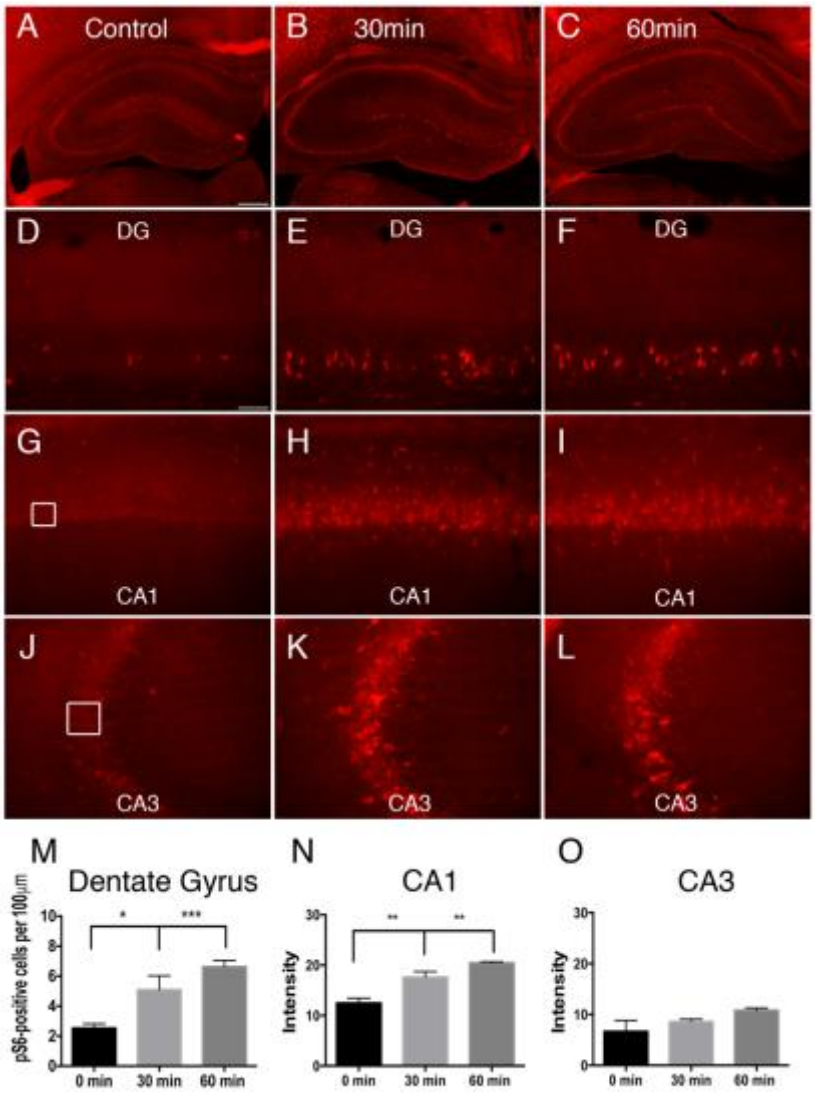

Figure 2.5. Exploration of a novel environment leads to increases in the number of p-ser235/236-positive neurons. A, Immunostaining for p-ser235/236 in the hippocampus of a cage control animal. **B,** Immunostaining for p-ser235/236 in the hippocampus following 30 minutes of unsupervised learning. **C,** Immunostaining of p-ser235/236 in the hippocampus following 60 minutes of unsupervised learning. **D,** High-magnification image of DG in image A. **E,** High-magnification image of DG in image B. **F,** High-magnification image of DG in image C. **G,** High-magnification of CA1 in image A. **H,** High-magnification of CA1 in image B. **I,** High-magnification of CA1 in image C. **J,** High-magnification of CA3 in image A. **K,** High-magnification of CA3 in image B. **L,** High-magnification of CA3 in image C. **M,** Quantification of the number of p-rpS6-positive granule cells in the dorsal blade of the dentate gyrus per 100μm, error bars represent SEM. Statistical assessment of the number of p-rpS6-positive cells in the granule cell layer of the DG by one-way ANOVA revealed an overall $F(2, 15)=11.20$, $p=0.0011$. Post-hoc analysis with Dunnett's for multiple comparisons revealed a significant difference between control animals and animals that experienced 30 minutes and 60 minutes of unsupervised learning (One-way ANOVA, $p<0.05$, $N=6$). **N,** Quantification of average OD in the pyramidal cell layer of CA1, error bars represent SEM. Statistical assessment of the average OD in the pyramidal cell layer of CA1 by one-way ANOVA

revealed an overall $F(2,6)=22.29$, $p=0.0017$. Post-hoc analysis with Dunnett's for multiple comparisons revealed a significant difference between control animals and animals that experienced 30 and 60 minutes of unsupervised learning (One-way ANOVA, $p<0.05$, N=3). **O,** Quantification of average OD in the pyramidal cell layer of CA3, error bars represent SEM. Statistical assessment of the average OD in the pyramidal cell layer of CA3 by one-way ANOVA revealed an overall $F(2,6) = 2.556$, $p=0.1574$, N=3. Scale bars: **A,** 500μm; **D,** 50μm.

Similarly, immunostaining for p-ser240/244 in rats that were anesthetized immediately upon removal from their home cage (Figure 6A) revealed scattered dentate granule cells that exhibited high levels of p-rpS6 immunostaining (Figure 6D) and higher basal level immunostaining in granule cell bodies compared to p-ser235/236 (Figure 5D). There were also a small number of scattered pyramidal neurons in CA1 that exhibited higher levels of immunostaining in cell bodies (Figure 6G). Pyramidal neurons in CA3 exhibited high levels of immunostaining predominately in the cell bodies (Figure 6J).

Following 30 minutes of exploration (Figure 6B) there were increases in the level of p-rpS6 immunostaining of neuronal cell bodies in the dentate gyrus, CA1 and CA3 (Figure 6E, 6H, and 6K, respectively). The pattern of immunostaining was qualitatively similar after 60 minutes (Figure 6F, 6I, and 6L) with a further increase in the number of p-rpS6-positive neuronal cell bodies and increased dendritic immunostaining. p-rpS6-positive cells with astrocyte morphology were also evident in the molecular layer of the dentate gyrus, stratum oriens and stratum radiatum of CA1-CA3 following unsupervised learning. Quantification of the number of p-rpS6-positive granule cells along the length of the granule cell layer of the dorsal blade of the dentate gyrus (~400μm length) revealed a 1.6-fold increase after 30 minutes and a 3-fold increase after 60 minutes of exploration (one-way ANOVA, $F(2,6)=35.52$, $p=0.0005$, $N=3$). Post-hoc analysis using a Dunnett's multiple comparisons test revealed a significant difference at the 60-minute time point (Figure 6M; $p<0.05$).

Quantification of FI in CA1 and statistical assessment by one-way ANOVA revealed an overall $F(2,6)=12.95$, $p=0.0067$ ($N=3$ rats per time point). Post-hoc analysis using a

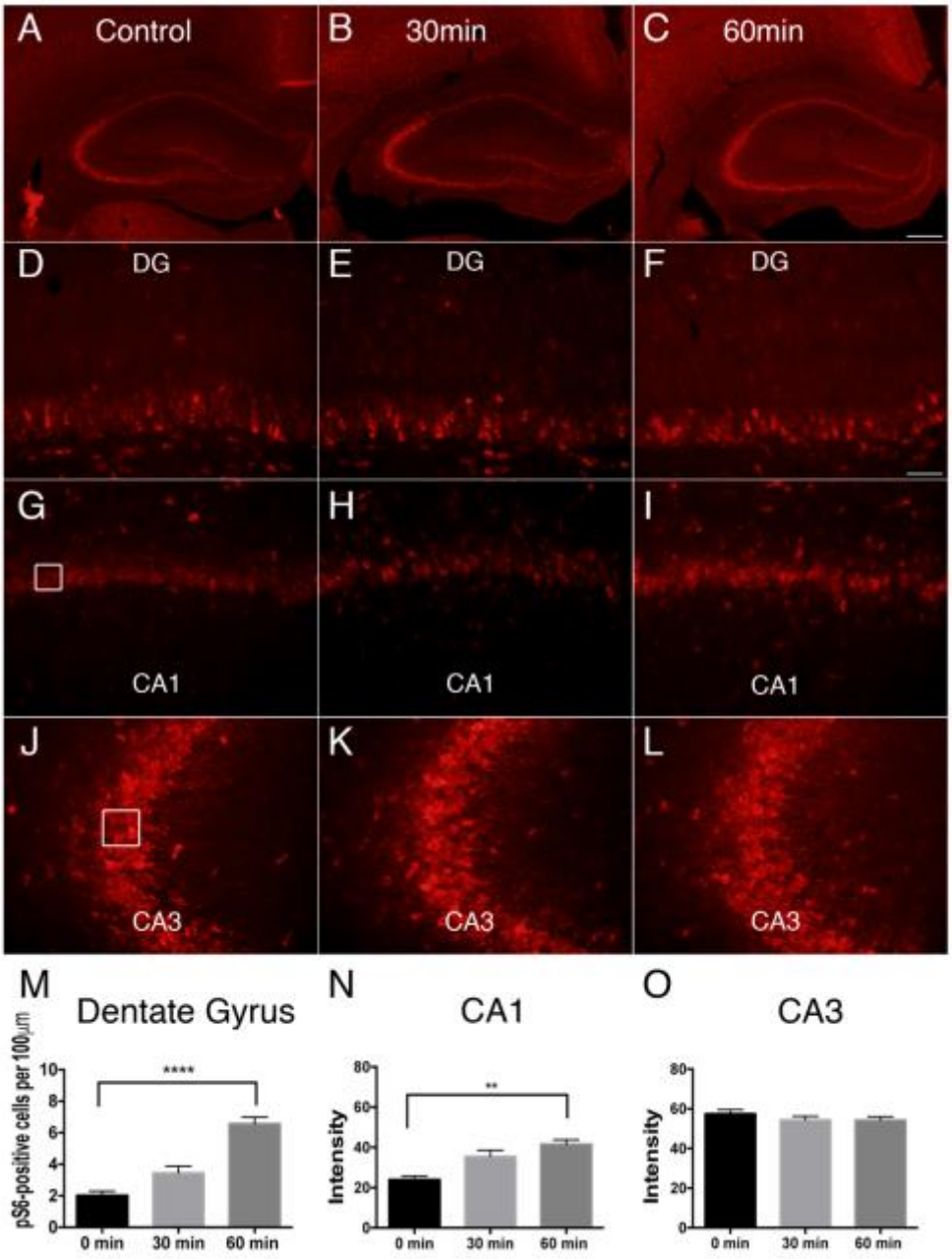

Figure 2.6. Exploration of a novel environment leads to increases in the number of p-ser240/244-positive neurons. A, Immunostaining for p-ser240/244 in the hippocampus of a cage control animal. **B,** Immunostaining for p-ser240/244 in the hippocampus following 30 minutes of unsupervised learning. **C,** Immunostaining of p-ser240/244 in the hippocampus following 60 minutes of unsupervised learning. **D,** High-magnification image of DG in image A. **E,** High-magnification image of DG in image B. **F,** High-magnification image of DG in image C. **G,** High-magnification of CA1 in image A. **H,** High-magnification of CA1 in image B. **I,** High-magnification of CA1 in image C. **J,** High-magnification of CA3 in image A. **K,** High-magnification of CA3 in image B. **L,** High-magnification of CA3 in image C. **M,** Quantification of the number of p-rpS6-positive granule cells in the dorsal blade of the dentate gyrus per 100μm, error bars represent SEM. Statistical

assessment of the number of p-rpS6-positive cells in the granule cell layer of the DG by one-way ANOVA revealed an overall $F(2,6)=35.52$, $p=0.0005$. Post-hoc analysis with Dunnett's for multiple comparisons revealed a significant difference between control animals and animals that experienced 60 minutes of unsupervised learning (One-way ANOVA, $p<0.05$, N=3). **N,** Quantification of average OD in the pyramidal cell layer of CA1, error bars represent SEM. Statistical assessment of the average OD in the pyramidal cell layer of CA1 by one-way ANOVA revealed an overall $F(2,6)=12.95$, $p=0.0067$. Post-hoc analysis with Dunnett's for multiple comparisons revealed a significant difference between control animals and animals that experienced 60 minutes of unsupervised learning (One-way ANOVA, $p<0.05$, N=3). **O,** Quantification of average OD in the pyramidal cell layer of CA3, error bars represent SEM. Statistical assessment of the average OD in the pyramidal cell layer of CA3 by one-way ANOVA revealed an overall $F(2,6) = 0.8796$, $p=0.4624$, N=3. Scale bars: **C,** 500μm; **F,** 50μm.

Dunnett's multiple comparisons test revealed that differences were significant at the 60-minute time point (Figure 6N; $p<0.05$). For CA3, quantification of FI and statistical assessment by one-way ANOVA of the average IF in the pyramidal cell layer yielded an overall $F(2,6)=0.8796$, $p=0.4624$ (Figure 6O; N=3 rats per time point). It is important to note that AF564 was used as a secondary for p-ser235/236 while AF 546 was used as a secondary on p-ser240/244 immunostaining. As a result, intensity values are higher for p-ser240/244 on CA1 and CA3 graphs.

Co-activation of rpS6 phosphorylation and IEG transcription in individual neurons

The activation of p-rpS6 in individual neurons as a result of experience is reminiscent of what is seen with IEG transcription, including *Arc*. To assess whether a learning experience triggers p-rpS6 in the same neurons in which *Arc* is induced, brains were co-immunostained for Arc protein and the p-ser235/236 antibody (Figure 7). We focused on the dentate granule cells because experience-dependent increases in the number of Arc positive neurons have been well characterized (Guzowski et al. 1999; Ramirez-Amaya et al. 2005; Vazdarjanova et al. 2006). In home cage controls, there were only a few p-rpS6-positive or Arc protein-positive granule cells (Figure 7A and 7B, respectively). Many neurons were positive for both p-rpS6 and Arc protein (Figure 7C). Following unsupervised learning, there was a striking increase in the number of p-rpS6-positive and Arc protein-positive granule cells, and again, many individual neurons but not all were positive for both p-rpS6 and Arc protein (Figure 7D-7I).

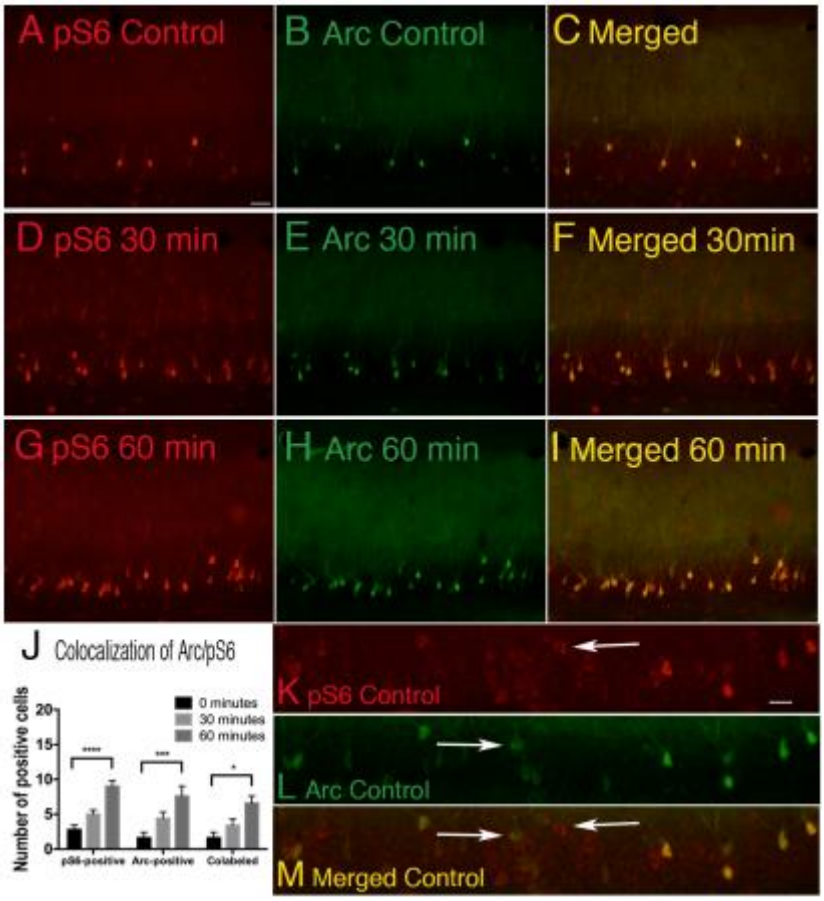

Figure 2.7. Exploration of a novel environment leads to increases in the number of co-activated p-rpS6-positive and Arc protein-positive neurons in the granule cell layer of the dentate gyrus. A. Pattern of immunostaining for p-ser235/236 in cage control animal as revealed by immunofluorescence. **B,** Pattern of immunostaining for Arc protein in cage control animal as revealed by immunofluorescence. **C,** Merged image of A and B. **D,** Pattern of immunostaining for p-ser235/236 following 30 minutes of unsupervised learning as revealed by immunofluorescence. **E,** Pattern of immunostaining for Arc protein following 30 minutes of unsupervised learning as revealed by immunofluorescence. **F,** Merged image of D and E. **G,** Pattern of immunostaining for p-ser235/236 following 60 minutes of unsupervised learning as revealed by immunofluorescence. **H,** Pattern of immunostaining for Arc protein following 60 minutes of unsupervised learning as revealed by immunofluorescence. **I,** Merged image of G and H. **J,** Quantification of the number of p-rpS6-positive, Arc protein-positive and co-labeled cells following an unsupervised learning experience, error bars represent SEM. Statistical assessment of the number of p-rpS6, Arc protein-positive cells and co-labeled cells by two-way ANOVA yielded an overall $F(4,24)=4.04$, $p=0.0120$. Post-hoc analysis with Dunnett's for multiple comparisons revealed a significant difference in the number of activated neurons between control animals and animals that experienced 60 minutes of unsupervised learning for p-rpS6-positive, Arc protein-positive and co-labeled conditions. **K,** Pattern of immunostaining for p-ser235/236 in a cage control animal. Arrow shows a p-rpS6 positive cell that is not Arc protein-positive. **L,** Pattern of immunostaining for Arc protein in cage control animal. Arrow shows Arc protein-positive cell that is not p-rpS6-positive. **M,** Merged image of K and L. Arrows show single p-rpS6-positive and Arc protein-positive cells. Scale bars: **A,** 50 μm; **K,** 20 μm.

Consistent with previous findings on Arc, we noted that the increase in the number of Arc protein-positive and p-rpS6-positive granule cells appeared more pronounced in the septal pole of the hippocampus than in the temporal pole. This, however, was not analyzed in detail.

To quantify the extent of co-labeling, the number of p-rpS6 and Arc protein positive cells were counted within a boxed region (120μm x 200μm) centered in the dentate gyrus cell body layer (Figure 7J). Statistical analysis of the number of p-rpS6, Arc protein-positive cells and co-labeled cells in each group by two-way ANOVA yielded an overall $F(4,24)=3.06$, $p=0.0361$, $N=5$. Post-hoc analysis using a Dunnett's multiple comparisons test revealed a significant difference between control animals and animals that experienced 60 minutes of unsupervised learning for p-rpS6-positive, Arc protein-positive and co-labeled neurons. Overall, in cage controls, 60% of Arc protein positive cells were co-labeled with p-rpS6 and 56% of p-rpS6-positive cells were co-labeled with Arc protein. In animals that explored the novel environment, 90% of Arc protein-positive cells were co-labeled with p-rpS6 and 73% of the p-rpS6-positive cells were co-labeled with Arc protein (Table 1).

Table 1. Percent of co-labeled p-rpS6-positive and Arc protein-positive granule cells

Unsupervised learning	% p-rpS6-positive granule cells co-labeled	% Arc-positive granule cells co-labeled
Cage Control	56	60
30 minutes	64	72
60 minutes	73	90

Percent of co-labeled p-rpS6-positive cells were calculated by dividing the number of co-labeled cells over the total p-rpS6-positive cells. Percent of co-labeled Arc protein-positive cells were calculated by dividing the number of co-labeled cells over the total Arc protein-positive cells.

Learning induced phosphorylation of rpS6 in astrocytes and interneurons

As noted above, there were numerous p-rpS6-positive cells with astrocyte morphology in the dendritic layers of the DG, CA1-CA3 regions following unsupervised learning (Figure 5E, 5F, 5H, 5I, 5K, 5L), which were not evident in home cage controls (Figure 5D, 5G, 5J). Co-immunostaining for p-ser235/236 (Figure 8A) and glial fibrillary acidic protein (GFAP) (Figure 8B) revealed that p-rpS6-positive cells with astrocyte morphology were GFAP-positive (Figure 8C).

The presence of p-rpS6-positive cells with neuronal morphology in the dendritic laminae of the DG, CA1 and CA3 raised the question of whether these might be inhibitory interneurons. Co-immunostaining for parvalbumin (PV), p-rpS6 and Arc protein revealed that some p-rpS6-positive cells in the molecular layer of the dentate gyrus, and stratum oriens and stratum radiatum of CA1-CA3 were also positive for PV (Figure 8F and 8I). In some cases, immunostaining for p-rpS6 was primarily in the cell body whereas immunostaining for PV extended into dendrites (Figure 8D-8F). Some PV-positive cells also immunostained for Arc protein. Figure 8G-8I illustrates two Arc protein-positive cells one of which is also PV-positive. Taken together these results indicate that learning induced p-rpS6 is found in a variety of cell types from principal cells to interneurons to astrocytes.

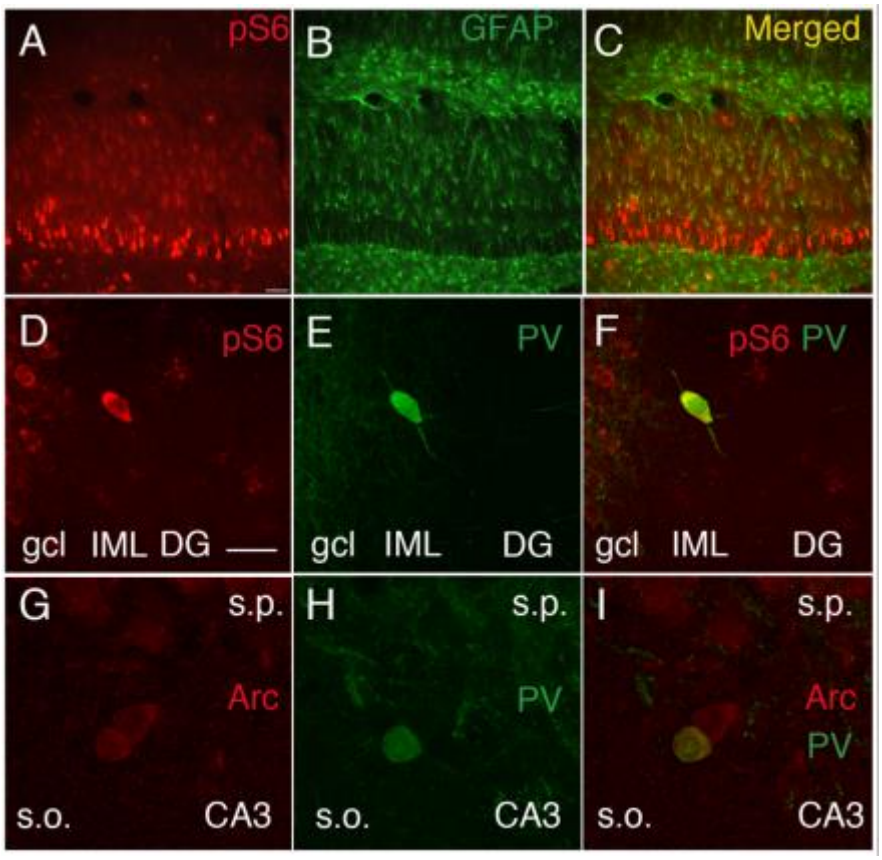

Figure 2.8. Learning induced phosphorylation of rpS6 in astrocytes and interneurons. A, Pattern of immunostaining of p-ser235/236 following 60 minutes of unsupervised learning. **B,** Pattern of immunostaining of GFAP following 60 minutes of unsupervised learning. **C,** Merged image of image A and B. **D,** Immunostaining of p-ser235/236 in the IML of the DG. **E,** Immunostaining of PV-positive cell in the IML of the DG. **F,** Merged image of D and E. Image shows co-labeled interneuron in the IML of the DG in a cage control. **G,** Immunostaining of Arc protein in stratum oriens of CA3. **H,** Immunostaining of PV-positive cell in S.O of CA3. **I,** Merged image of image G and H. Image shows two Arc-positive cells in S.O. of CA3, one of which colocalizes with a PV-positive cell. Scale bars: **A,** 50 μm; **I,** 30 μm. Abbreviations: IML, inner molecular layer; DG, dentate gyrus; s.o., stratum oriens; s.p., stratum pyramidale.

Robust increases in rpS6 phosphorylation are not accompanied by increases in protein synthesis

Increases in p-rpS6 could indicate an increase in overall levels of protein synthesis or a shift in translation from one population of mRNAs to another without altering overall levels of translation. To test the hypothesis that induction of rpS6 phosphorylation leads to an overall increase in protein synthesis, HFS was unilaterally delivered for 30 or 90 minutes to the perforant path to generate maximal p-rpS6, C14-leucine (50-70μCi per 250g of body weight) was administered via tail vein injection at the start of 30-minute HFS or 30 minutes prior to the end of stimulation for 90-minute HFS. Rats were then perfused and prepared for autoradiographic assessment. Surprisingly, there were no differences in labeling on the stimulated side compared to non-stimulated side (Figure 9). To quantify labeling, images of the dentate gyrus were used to measure the average OD over the GCL and dendritic laminae as illustrated in Figure 9C and 9D. OD values were then calculated as an I/C ratio (Figure 9E) and expressed as a percent change (Figure 9F). As illustrated in the bar graphs, average I/C ratios were near 1.0 (Figure 9E and 9F; two-way ANOVA, $F(3,15)=0.96$, $p=0.4358$, $N=3$ for 30min and $N=4$ for 90 min), indicating no change in protein synthesis despite the dramatic increases in p-rpS6.

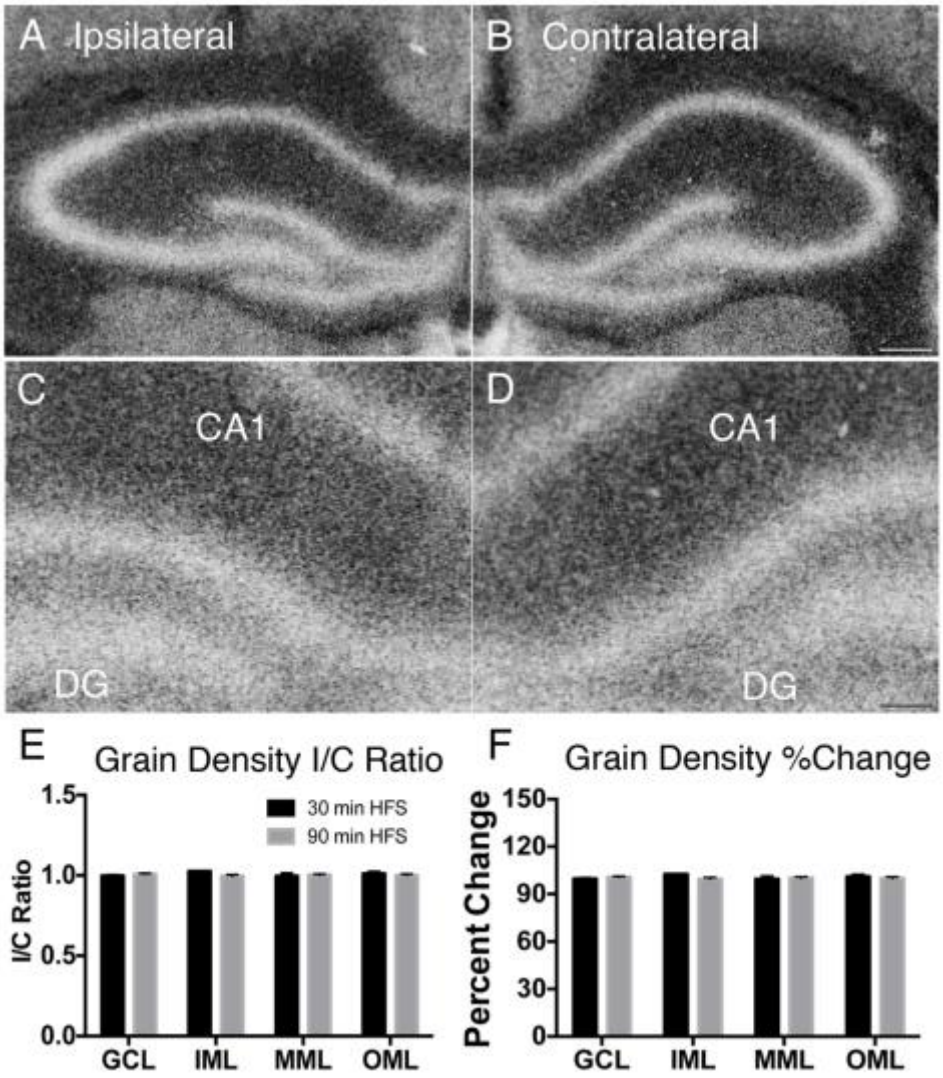

Figure 2.9. Robust increases in S6 phosphorylation does not result in increases in global protein synthesis. A, 4X magnification image of autoradiograph film ipsilateral to stimulation following 90 minutes of HFS. **B,** 4X magnification image of autoradiograph film contralateral to stimulation (non-stimulated) following 90 minutes of HFS. **C,** High-magnification image of A. **D,** High-magnification image of B. **E,** Quantification of ipsilateral/contralateral ratio following 30 minutes or 90 minutes of HFS, error bars represent SEM. **F,** Quantification of percent change from contralateral following 30 minutes or 90 minutes of HFS, error bars represent SEM. Statistical assessment of average grain density were then calculated as an I/C ratio and expressed as a percent change. Statistical analysis of the percent change in average grain density by two-way ANOVA yielded an overall $F(3,20)=1.01$, $p=0.4104$ (N=3, for 30 min and N=4 for 90 min; Two-way ANOVA, $p<0.05$). Scale bars: **B,** 200μm; **D,** 100μm.

DISCUSSION

Our results confirm previous findings that patterns of synaptic activity that induce LTP induce phosphorylation of rpS6 (p-rpS6) in postsynaptic neurons (Panja et al. 2009) and reveal several novel findings including: 1) Activation of p-ser235/236 occurs locally and is especially robust in the region of the activated synapses, whereas this localized activation is less prominent with p-ser240/244; 2) Induction of phosphorylation depends on NMDA receptor activation; 3) Following LTP induction, p-rpS6 peaks 30 minutes post stimulation, a time at which IEG transcripts are available in quantity for translation; 4) Experience activates p-rpS6 in many of the same neurons in which IEG expression is induced; 5) robust p-rpS6 is not associated with global increases in protein synthesis.

Selective activation of rpS6 phosphorylation near active synapses

Strong synaptic activation triggers selective induction of phosphorylation of ser235/236 in activated dendritic domains; this was less evident with p-ser240/244. This differential pattern of activation could reflect differences in the signaling pathways through which phosphorylation is induced. Phosphorylation of rpS6 occurs at five serine residues (Krieg et al. 1988) in sequence starting with ser236, ser235, ser240, ser244 then ser247 (Flotow and Thomas 1992; Wettenhall et al. 1992). It has been reported that ser240/244 is predominately mTOR-dependent being phosphorylated by S6K1 and S6K2 (Pende et al. 2004). In contrast, ser235/236 has been implicated as a target for multiple signaling pathways including MAPK/ERK via RSK (Roux et al. 2007) and PKA (Gobert et al. 2008; Moore et al. 2009; Biever et al. 2015a). Thus, the relatively higher activation in the region

of active synapses for p-ser235/236 could be because it integrates signals from multiple pathways.

The more robust increase in immunostaining in the region of active synapses for p-ser235/236 invites the speculation that induction of p-ser235/236 is especially important for regulating local translation of mRNAs at synapses. In this regard, a recent study has reported transient translocation of rpS6 into spines of dentate granule cells following induction of perforant path LTP (Nihonmatsu et al. 2015), which were seen at 15 minutes but not 35 minutes after LTP induction.

Phosphorylation of rpS6 is driven by NMDA receptor activation

Synaptically-driven phosphorylation of S6 was completely blocked by local infusion of the NMDA receptor antagonist, APV, which is noteworthy because NMDA receptor activation is required for LTP induction (Harris et al. 1984; Wigstrom and Gustafsson 1986). This finding links activation of p-rpS6 with other events that occur during LTP induction including activation of intracellular signaling pathways [reviewed in (Bliss and Collingridge 1993; Cortes-Mendoza et al. 2013)] that involve Ca^{2+}/CaM-dependent protein kinase (Lynch and Baudry 1984; Malenka et al. 1989; Bading et al. 1993), PI3K and S6-kinase (Cammalleri et al. 2003; Lenz and Avruch 2005), and MAPK (Impey et al. 1998; Kelleher et al. 2004b). The fact that LTP-inducing stimuli induces p-rpS6 in an NMDA receptor-dependent fashion documents a molecular correlate of synaptic plasticity, but it remains to be determined whether there is a mechanistic link.

Phosphorylation of rpS6 is activated by behavioral experience

A learning experience (exploration of a novel environment) induced p-rpS6 in individual neurons scattered throughout the forebrain in a pattern that is similar to what is seen with IEG induction. Moreover, co-immunostaining revealed experience-dependent activation of p-rpS6 in many of the same individual neurons in which IEGs are activated. Previous studies have shown that exploration of a novel environment strongly induces Arc expression in neurons in CA1 and CA3 from 30 minutes up to 2 hours post exploration (Ramirez-Amaya et al. 2005). In the dentate gyrus, Arc is induced in scattered granule cells especially in the dorsal blade of the dorsal hippocampus from 30 minutes up to 8 hours post exploration (Ramirez-Amaya et al. 2005). Additional studies also document changes in expression of IEGs following natural synaptic activity (Worley et al. 1991) and increased expression in CA1 and CA3 subfields following spatial memory tasks (Vazdarjanova et al. 2006) with a dominance in CA1 (Hess et al. 1995; Guzowski et al. 1999; Vann et al. 2000). Given the evidence that Arc induction is critical for both LTP and long-term memory (Guzowski et al. 2000; Bramham et al. 2008), the high degree of co-activation suggests that both may play a role in activity-dependent synaptic plasticity.

Our findings that a learning experience induces both p-rpS6 and IEG transcription in individual neurons adds to previous findings implicating mTOR activation and its downstream substrates in learning and memory (Jacinto and Hall 2003; Dash et al. 2006; Antion et al. 2008b; Hoeffer and Klann 2010). For example, radial arm maze training triggers mTOR activation and phosphorylation of its down stream substrates, 4EBP1 and p70S6K, and infusion of rapamycin inhibited mTOR activation and retarded acquisition (Qi et al. 2010). Indeed, S6K is induced in several brain regions following other types of

training (Belelovsky et al. 2005; Dash et al. 2006; Parsons et al. 2006; Bekinschtein et al. 2007).

Surprisingly, experience also induced p-rpS6 in astrocytes in the hippocampus, which was not seen following HFS. This activation of p-rpS6 in astrocytes may indicate events in astrocytes that are activated uniquely under conditions of behavioral learning but not HFS. Alternatively, activation of p-rpS6 in astrocytes may be uniquely sensitive to urethane anesthesia. In either case, the fact behavioral experience strongly regulates p-rpS6 in astrocytes raises the provocative idea of behavioral regulation of mRNA translation in astrocytes.

Robust phosphorylation of rpS6 is not accompanied by increases in global protein synthesis

Induction of p-rpS6 occurs under conditions that lead to increases in protein synthesis (Duncan and McConkey 1982; Thomas et al. 1982; Jefferies and Thomas 1996) including mitogenic stimulation (Gressner and Wool 1974), or treatment with hormones (Smith et al. 1979), growth factors (Thomas et al. 1982), and nutrients (Proud 2002). Nevertheless, our results document that there are no detectable increases in global protein synthesis when rpS6 phosphorylation is strongly activated by synaptic stimulation. If p-rpS6 is regulating translation following induction of perforant path LTP, it is not reflected in overall levels of incorporation of amino acid precursors in dentate granule cells.

The absence of any increase in protein synthesis with perforant path LTP is surprising because of previous studies of LTP correlates in hippocampal slices *in vitro.* Previous studies have reported increases in 35S-methionine incorporation (Kelleher et al.

2004b), induced expression of 5TOP mRNAs (Tsokas 2005; Tsokas et al. 2007; Gobert et al. 2008), and increases in protein synthesis (Kelleher et al. 2004b; Klann and Dever 2004; Antion et al. 2008a) after LTP induction. One possible explanation is that mechanisms of perforant path LTP are different than forms of LTP studies in hippocampal slices in vitro. Differences may also be due to technical variables. For example, in the study of Kelleher et al, the slice medium was artificial cerebral spinal fluid, and it is not reported whether it was supplemented with amino acids. It is possible that their results depended on the fact that the pulse-labeling was under conditions of short-term amino acid starvation. Under these conditions, proteins critical for structural remodeling and consolidation may be depleted (Lynch et al. 2014). In this regard, it is noteworthy that the consequences of protein synthesis inhibitors also depend on the time of application (Kelleher et al. 2004a).

Our finding of no detectable difference in global protein synthesis in the dentate gyrus despite robust induction of p-rpS6 is in line with other reports (Biever et al. 2015a). However, the lack of increase in global protein synthesis does not rule out the possibility that p-rpS6 may be involved in the preferential translation of specific mRNAs (Jefferies 1997). It may be that the population of mRNAs whose translation is regulated by p-rpS6 is so small in number that changes in their translation rate would not be reflected in overall protein synthesis levels. Alternatively, p-rpS6 may initiate translation of a subset of mRNAs at the same time that translation of other mRNAs is decreased, resulting in no overall change. Finally, it is also possible that p-rpS6 may be involved in other roles besides translation (Biever et al. 2015b; Meyuhas 2015). Further studies will be required to assess these possibilities.

REFERENCES

Abraham WC, Williams JM. 2003. Properties and mechanisms of LTP maintenance. *Neuroscientist* **9**: 463-474.

Antion MD, Hou L, Wong H, Hoeffer CA, Klann E. 2008a. mGluR-Dependent Long-Term Depression Is Associated with Increased Phosphorylation of S6 and Synthesis of Elongation Factor 1A but Remains Expressed in S6K-Deficient Mice. *Mol Cell Biol* **28**: 2996-3007.

Antion MD, Merhav M, Hoeffer CA, Reis G, Kozma SC, Thomas G, Schuman EM, Rosenblum K, Klann E. 2008b. Removal of S6K1 and S6K2 leads to divergent alterations in learning, memory, and synaptic plasticity. *Learn Mem* **15**: 29-38.

Bading H, Ginty DD, Greenberg ME. 1993. Regulation of gene expression in hippocampal neurons by distinct calcium signaling pathways. *Science* **260**: 181-186.

Barth-Baus D, Stratton CA, Parrott L, Myerson H, Meyuhas O, Templeton DJ, Landreth GE, Hensold JO. 2002. S6 phosphorylation-independent pathways regulate translation of 5'-terminal oligopyrimidine tract-containing mRNAs in differentiating hematopoietic cells. *Nucleic Acids Res* **30**: 1919-1928.

Bekinschtein P, Katche C, Slipczuk LN, Igaz LM, Cammarota M, Izquierdo I, Medina JH. 2007. mTOR signaling in the hippocampus is necessary for memory formation. *Neurobiology of Learning and Memory* **87**: 303-307.

Belelovsky K, Elkobi A, Kaphzan H, Nairn AC, Rosenblum K. 2005. A molecular switch for translational control in taste memory consolidation. *European Journal of Neuroscience* **22**: 2560-2568.

Biever A, Puighermanal E, Nishi A, David A, Panciatici C, Longueville S, Xirodimas D, Gangarossa G, Meyuhas O, Herve D et al. 2015a. PKA-dependent phosphorylation of ribosomal protein S6 does not correlate with translation efficiency in striatonigral and striatopallidal medium-sized spiny neurons. *J Neurosci* **35**: 4113-4130.

Biever A, Valjent E, Puighermanal E. 2015b. Ribosomal Protein S6 Phosphorylation in the Nervous System: From Regulation to Function. *Front Mol Neurosci* **8**: 75.

Bliss TV, Collingridge GL. 1993. A synaptic model of memory: long-term potentiation in the hippocampus. *Nature* **361**: 31-39.

Bliss TV, Lomo T. 1973. Long-lasting potentiation of synaptic transmission in the dentate area of the anaesthetized rabbit following stimulation of the perforant path. *J Physiol (Lond)* **232**: 331-356.

Bramham CR, Worley PF, Moore MJ, Guzowski JF. 2008. The immediate early gene Arc/Arg3.1: regulation, mechanisms, and function. *J Neurosci* **28**: 11760-11767.

Burgin KE, Waxham MN, Rickling S, Westgate SA, Mobley WC, Kelly PT. 1990. In situ hybridization histochemistry of Ca2+/calmodulin-dependent protein kinase in developing rat brain. *J Neurosci* **10**: 1788-1798.

Cajigas IJ, Tushev G, Will TJ, tom Dieck S, Fuerst N, Schuman EM. 2012. The local transcriptome in the synaptic neuropil revealed by deep sequencing and high-resolution imaging. *Neuron* **74**: 453-466.

Cammalleri M, Lutjens R, Berton F, King AR, Simpson C, Francesconi W, Sanna PP. 2003. Time-restricted role for dendritic activation of the mTOR-p70S6K pathway in the induction of late-phase long-term potentiation in the CA1. *Pro Natl Acad Sci USA* **100**: 14368-14373.

Chotiner JK, Nielson J, Farris S, Lewandowski G, Huang F, Banos K, de Leon R, Steward O. 2010. Assessment of the role of MAP kinase in mediating activity-dependent transcriptional activation of the immediate early gene Arc/Arg3.1 in the dentate gyrus in vivo. *Learn Memory* **17**: 117-129.

Cortes-Mendoza J, Diaz de Leon-Guerrero S, Pedraza-Alva G, Perez-Martinez L. 2013. Shaping synaptic plasticity: the role of activity-mediated epigenetic regulation on gene transcription. *Int J Dev Neurosci* **31**: 359-369.

Dash PK, Orsi SA, Moore AN. 2006. Spatial memory formation and memory-enhancing effect of glucose involves activation of the tuberous sclerosis complex-Mammalian target of rapamycin pathway. *J Neurosci* **26**: 8048-8056.

Davis S, Vanhoutte P, Pagès C, Caboche J, Laroche S. 2000. The MAPK/ERK cascade targets both Elk-1 and cAMP response element-binding protein to control long-term potentiation-dependent gene expression in the dentate gyrus in vivo. *J Neurosci* **20**: 4563-4572.

Desmond NL, Levy WB. 1983. Synaptic correlates of associative potentiation/depression: an ultrastructural study in the hippocampus. *Brain Res* **265**: 21-30.

Douglas RM, Goddard GV. 1975. Long-term potentiation of the perforant path-granule cell synapse in the rat hippocampus. *Brain Res* **86**: 205-215.

Duncan R, McConkey EH. 1982. Preferential utilization of phosphorylated 40-S ribosomal subunits during initiation complex formation. *Eur J Biochem* **123**: 535-538.

Farris S, Lewandowski G, Cox CD, Steward O. 2014. Selective Localization of Arc mRNA in Dendrites Involves Activity- and Translation-Dependent mRNA Degradation. *J Neurosci* **34**: 4481-4493.

Fifková E, Van Harreveld A. 1977. Long-lasting morphological changes in dendritic spines of dentate granular cells following stimulation of the entorhinal area. *J Neurocytol* **6**: 211-230.

Flotow H, Thomas G. 1992. Substrate recognition determinants of the mitogen-activated 70K S6 kinase from rat liver. *J Biol Chem* **267**: 3074-3078.

Fukazawa Y, Saitoh Y, Ozawa F, Ohta Y, Mizuno K, Inokuchi K. 2003. Hippocampal LTP is accompanied by enhanced F-actin content within the dendritic spine that is essential for late LTP maintenance in vivo. *Neuron* **38**: 447-460.

Gobert D, Topolnik L, Azzi M, Huang L, Badeaux F, Desgroseillers L, Sossin WS, Lacaille JC. 2008. Forskolin induction of late-LTP and up-regulation of 5' TOP mRNAs translation via mTOR, ERK, and PI3K in hippocampal pyramidal cells. *J Neurochem* **106**: 1160-1174.

Gressner AM, Wool IG. 1974. The phosphorylation of liver ribosomal proteins in vivo. Evidence that only a single small subunit protein (S6) is phosphorylated. *J Biol Chem* **249**: 6917-6925.

Gustafsson B, Wigström H. 1988. Physiological mechanisms underlying long-term potentiation. *Trends in Neurosciences* **11**: 156-162.

Guzowski JF, Lyford GL, Stevenson GD, Houston FP, McGaugh JL, Worley PF, Barnes CA. 2000. Inhibition of activity-dependent arc protein expression in the rat hippocampus impairs the maintenance of long-term potentiation and the consolidation of long-term memory. *J Neurosci* **20**: 3993-4001.

Guzowski JF, McNaughton BL, Barnes CA, Worley PF. 1999. Environment-specific expression of the immediate-early gene Arc in hippocampal neuronal ensembles. *Nat Neurosci* **2**: 1120-1124.
Harris EW, Ganong AH, Cotman CW. 1984. Long-term potentiation in the hippocampus involves activation of N-methyl-D-aspartate receptors. *Brain Res* **323**: 132-137.
Harris KM, Fiala JC, Ostroff L. 2003. Structural changes at dendritic spine synapses during long-term potentiation. *Philos T R Soc B* **358**: 745-748.
Hess US, Lynch G, Gall CM. 1995. Regional patterns of c-fos mRNA expression in rat hippocampus following exploration of a novel environment versus performance of a well-learned discrimination. *J Neurosci* **15**: 7796-7809.
Hoeffer CA, Klann E. 2010. mTOR signaling: At the crossroads of plasticity, memory and disease. *Trends in Neurosciences* **33**: 67-75.
Huang F, Chotiner JK, Steward O. 2007. Actin polymerization and ERK phosphorylation are required for Arc/Arg3.1 mRNA targeting to activated synaptic sites on dendrites. *J Neurosci* **27**: 9054-9067.
Impey S, Obrietan K, Wong ST, Poser S, Yano S, Wayman G, Deloulme JC, Chan G, Storm DR. 1998. Cross talk between ERK and PKA is required for Ca2+ stimulation of CREB-dependent transcription and ERK nuclear translocation. *Neuron* **21**: 869-883.
Jacinto E, Hall MN. 2003. TOR signalling in bugs, brain and brawn. *Nat Rev Mol Cell Bio* **4**: 117-126.
Jefferies HB, Reinhard C, Kozma SC, Thomas G. 1994. Rapamycin selectively represses translation of the "polypyrimidine tract" mRNA family. *Proc Natl Acad Sci USA* **91**: 4441-4445.
Jefferies HBJ. 1997. Rapamycin suppresses 5'TOP mRNA translation through inhibition of p70s6k. *EMBO J* **16**: 3693-3704.
Jefferies HBJ, Thomas G. 1996. Ribosomal Protein S6 Phosphorylation and Signal Transduction. In *Translational Control* (ed. JW Hershey, MB Mathews, N Sonenberg), pp. 389-409. Cold Spring Harbor Laboratory Press, Cold Spring Harbor, NY
Kandel ER. 2001. The molecular biology of memory storage: a dialogue between genes and synapses. *Science* **294**: 1030-1038.
Kelleher RJ, 3rd, Govindarajan A, Tonegawa S. 2004a. Translational regulatory mechanisms in persistent forms of synaptic plasticity. *Neuron* **44**: 59-73.
Kelleher RJ, Govindarajan A, Jung H-Y, Kang H, Tonegawa S. 2004b. Translational control by MAPK signaling in long-term synaptic plasticity and memory. *Cell* **116**: 467-479.
Klann E, Dever TE. 2004. Biochemical mechanisms for translational regulation in synaptic plasticity. *Nature reviews Neuroscience* **5**: 931-942.
Krieg J, Hofsteenge J, Thomas G. 1988. Identification of the 40 S ribosomal protein S6 phosphorylation sites induced by cycloheximide. *J Biol Chem* **263**: 11473-11477.
Kruppa J, Clemens MJ. 1984. Differential kinetics of changes in the state of phosphorylation of ribosomal protein S6 and in the rate of protein synthesis in MPC 11 cells during tonicity shifts. *EMBO J* **3**: 95-100.
Lenz G, Avruch J. 2005. Glutamatergic regulation of the p70S6 kinase in primary mouse neurons. *J Biol Chem* **280**: 38121-38124.
Levy WB, Steward O. 1979. Synapses as associative memory elements in the hippocampal formation. *Brain research* **175**: 233-245.

Lin B, Kramar EA, Bi X, Brucher FA, Gall CM, Lynch G. 2005. Theta stimulation polymerizes actin in dendritic spines of hippocampus. *J Neurosci* **25**: 2062-2069.

Link W, Konietzko U, Kauselmann G, Krug M, Schwanke B, Frey U, Kuhl D. 1995. Somatodendritic expression of an immediate early gene is regulated by synaptic activity. *Proc Natl Acad Sci USA* **92**: 5734-5738.

Lyford GL, Yamagata K, Kaufmann WE, Barnes CA, Sanders LK, Copeland NG, Gilbert DJ, Jenkins NA, Lanahan AA, Worley PF. 1995. Arc, a growth factor and activity-regulated gene, encodes a novel cytoskeleton-associated protein that is enriched in neuronal dendrites. *Neuron* **14**: 433-445.

Lynch G, Baudry M. 1984. The biochemistry of memory: a new and specific hypothesis. *Science* **224**: 1057-1063.

Lynch G, Kramár EA, Gall CM. 2014. Protein synthesis and consolidation of memory-related synaptic changes. *Brain Research*.

Malenka RC, Kauer JA, Perkel DJ, Mauk MD, Kelly PT, Nicoll RA, Waxham MN. 1989. An essential role for postsynaptic calmodulin and protein kinase activity in long-term potentiation. *Nature* **340**: 554-557.

Medvedev NI, Popov VI, Dallérac G, Davies HA, Laroche S, Kraev IV, Rodriguez Arellano JJ, Doyère V, Stewart MG. 2010. Alterations in synaptic curvature in the dentate gyrus following induction of long-term potentiation, long-term depression, and treatment with the N-methyl-d-aspartate receptor antagonist CPP. *Neuroscience* **171**: 390-397.

Meyuhas O. 2000. Synthesis of the translational apparatus is regulated at the translational level. *Eur J Biochem* **267**: 6321-6330.

Meyuhas O. 2008. Chapter 1 Physiological Roles of Ribosomal Protein S6: One of Its Kind. In *International Review of Cell and Molecular Biology*, Vol 268, pp. 1-37. Elsevier.

Meyuhas O. 2015. Ribosomal Protein S6 Phosphorylation: Four Decades of Research. *Int Rev Cell Mol Biol* **320**: 41-73.

Mieulet V, Roceri M, Espeillac C, Sotiropoulos A, Ohanna M, Oorschot V, Klumperman J, Sandri M, Pende M. 2007. S6 kinase inactivation impairs growth and translational target phosphorylation in muscle cells maintaining proper regulation of protein turnover. *Am J Physiol Cell Physiol* **293**: C712-722.

Moore CE, Xie J, Gomez E, Herbert TP. 2009. Identification of cAMP-dependent kinase as a third in vivo ribosomal protein S6 kinase in pancreatic beta-cells. *J Mol Biol* **389**: 480-494.

Nguyen PV, Abel T, Kandel ER. 1994. Requirement of a critical period of transcription for induction of a late phase of LTP. *Science* **265**: 1104-1107.

Nguyen PV, Kandel ER. 1996. A macromolecular synthesis-dependent late phase of long-term potentiation requiring cAMP in the medial perforant pathway of rat hippocampal slices. *J Neurosci* **16**: 3189-3198.

Nielsen PJ, Duncan R, McConkey EH. 1981. Phosphorylation of Ribosomal Protein S6. Relationship to Protein Synthesis in HeLa Cells. *Eur J Biochem* **120**: 523-527.

Nihonmatsu I, Ohkawa N, Saitoh Y, Inokuchi K. 2015. Targeting of ribosomal protein S6 to dendritic spines by in vivo high frequency stimulation to induce long-term potentiation in the dentate gyrus. *Biol Open* **4**: 1387-1394.

Nygard O, Nilsson L. 1990. Translational dynamics. Interactions between the translational factors, tRNA and ribosomes during eukaryotic protein synthesis. *Eur J Biochem* **191**: 1-17.

Panja D, Dagyte G, Bidinosti M, Wibrand K, Kristiansen AM, Sonenberg N, Bramham CR. 2009. Novel translational control in Arc-dependent long term potentiation consolidation in vivo. *J Biol Chem* **284**: 31498-31511.

Parsons RG, Gafford GM, Helmstetter FJ. 2006. Translational control via the mammalian target of rapamycin pathway is critical for the formation and stability of long-term fear memory in amygdala neurons. *J Neurosci* **26**: 12977-12983.

Pende M, Um SH, Mieulet V, Sticker M, Goss VL, Mestan J, Mueller M, Fumagalli S, Kozma SC, Thomas G. 2004. S6K1-/-/S6K2-/- Mice Exhibit Perinatal Lethality and Rapamycin-Sensitive 5'-Terminal Oligopyrimidine mRNA Translation and Reveal a Mitogen-Activated Protein Kinase-Dependent S6 Kinase Pathway. *Mol Cell Biol* **24**: 3112-3124.

Proud CG. 2002. Regulation of mammalian translation factors by nutrients. *Eur J Biochem* **269**: 5338-5349.

Qi S, Mizuno M, Yonezawa K, Nawa H, Takei N. 2010. Activation of mammalian target of rapamycin signaling in spatial learning. *Neurosci Res* **68**: 88-93.

Ramirez-Amaya V, Vazdarjanova A, Mikhael D, Rosi S, Worley PF, Barnes CA. 2005. Spatial exploration-induced Arc mRNA and protein expression: evidence for selective, network-specific reactivation. *J Neurosci* **25**: 1761-1768.

Roux PP, Shahbazian D, Vu H, Holz MK, Cohen MS, Taunton J, Sonenberg N, Blenis J. 2007. RAS/ERK signaling promotes site-specific ribosomal protein S6 phosphorylation via RSK and stimulates cap-dependent translation. *J Biol Chem* **282**: 14056-14064.

Ryan MM, Mason-Parker SE, Tate WP, Abraham WC, Williams JM. 2011. Rapidly induced gene networks following induction of long-term potentiation at perforant path synapses in vivo. *Hippocampus* **21**: 541-553.

Smith CJ, Wejksnora PJ, Warner JR, Rubin CS, Rosen OM. 1979. Insulin-stimulated protein phosphorylation in 3T3-L1 preadipocytes. *Pro Natl Acad Sci USA* **76**: 2725-2729.

Steward O, Levy WB. 1982. Preferential localization of polyribosomes under the base of dendritic spines in granule cells of the dentate gyrus. *J Neurosci* **2**: 284-291.

Steward O, Schuman EM. 2001. Protein synthesis at synaptic sites on dendrites. *Annu Rev Neurosci* **24**: 299-325.

Steward O, Wallace C, Lyford G, Worley P. 1998. Synaptic activation causes the mRNA for the IEG Arc to localize selectively near activated postsynaptic sites on dendrites. *Neuron* **21**: 741-751.

Steward O, Worley PF. 2001. Selective targeting of newly synthesized Arc mRNA to active synapses requires NMDA receptor activation. *Neuron* **30**: 227-240.

Stolovich M, Tang H, Hornstein E, Levy G, Cohen R, Bae SS, Birnbaum MJ, Meyuhas O. 2002. Transduction of growth or mitogenic signals into translational activation of TOP mRNAs is fully reliant on the phosphatidylinositol 3-kinase-mediated pathway but requires neither S6K1 nor rpS6 phosphorylation. *Mol Cell Biol* **22**: 8101-8113.

Tang H, Hornstein E, Stolovich M, Levy G, Livingstone M, Templeton D, Avruch J, Meyuhas O. 2001. Amino acid-induced translation of TOP mRNAs is fully dependent on phosphatidylinositol 3-kinase-mediated signaling, is partially inhibited by rapamycin, and is independent of S6K1 and rpS6 phosphorylation. *Mol Cell Biol* **21**: 8671-8683.

Thomas G, Martin-Pérez J, Siegmann M, Otto AM. 1982. The effect of serum, EGF, PGF2 alpha and insulin on S6 phosphorylation and the initiation of protein and DNA synthesis. *Cell* **30**: 235-242.

Tiedge H, Brosius J. 1996. Translational machinery in dendrites of hippocampal neurons in culture. *J Neurosci* **16**: 7171-7181.

Tsokas P. 2005. Local Protein Synthesis Mediates a Rapid Increase in Dendritic Elongation Factor 1A after Induction of Late Long-Term Potentiation. *J Neurosci* **25**: 5833-5843.

Tsokas P, Ma T, Iyengar R, Landau EM, Blitzer RD. 2007. Mitogen-Activated Protein Kinase Upregulates the Dendritic Translation Machinery in Long-Term Potentiation by Controlling the Mammalian Target of Rapamycin Pathway. *J Neurosci* **27**: 5885-5894.

Vann SD, Brown MW, Erichsen JT, Aggleton JP. 2000. Fos imaging reveals differential patterns of hippocampal and parahippocampal subfield activation in rats in response to different spatial memory tests. *J Neurosci* **20**: 2711-2718.

Vazdarjanova A, Ramirez-Amaya V, Insel N, Plummer TK, Rosi S, Chowdhury S, Mikhael D, Worley PF, Guzowski JF, Barnes CA. 2006. Spatial exploration induces ARC, a plasticity-related immediate-early gene, only in calcium/calmodulin-dependent protein kinase II-positive principal excitatory and inhibitory neurons of the rat forebrain. *J Comp Neurol* **498**: 317-329.

Wallace CS, Lyford GL, Worley PF, Steward O. 1998. Differential intracellular sorting of immediate early gene mRNAs depends on signals in the mRNA sequence. *J Neurosci* **18**: 26-35.

Wettenhall RE, Erikson E, Maller JL. 1992. Ordered multisite phosphorylation of Xenopus ribosomal protein S6 by S6 kinase II. *J Biol Chem* **267**: 9021-9027.

Wigstrom H, Gustafsson B. 1986. Postsynaptic control of hippocampal long-term potentiation. *J Physiol (Paris)* **81**: 228-236.

Worley PF, Christy BA, Nakabeppu Y, Bhat RV, Cole AJ, Baraban JM. 1991. Constitutive expression of zif268 in neocortex is regulated by synaptic activity. *Pro Natl Acad Sci USA* **88**: 5106-5110.

CHAPTER 3

Synaptic activation of ribosomal protein S6 phosphorylation is differentially regulated by mTOR and MAPK signaling pathways at activated dendritic domains

ABSTRACT

Phosphorylation of ribosomal protein S6 (rpS6) is commonly linked to translational efficiency in response to a wide range of stimuli including growth factors, insulin, and synaptic activity. Multiple signaling pathways including MAPK/ERK, PKA, PKC, and mTOR regulate phosphorylation of rpS6. But insufficient knowledge is known about how these different signaling pathways regulate phosphorylation of rpS6 to accomplish translational control in neurons. Previously, we showed that high-frequency stimulation (HFS) of the medial perforant path triggers robust phosphorylation of rpS6 in granule cell bodies and locally in activated dendritic domains implicating a role in local translational control. Here we test the regulation of rpS6 phosphorylation by mTOR and MAPK/ERK signaling pathways in subcellular compartments (cell bodies vs. dendrites) of the dentate gyrus following synaptic stimulation. To examine how mTOR and MAPK signaling pathways regulate rpS6 phosphorylation, specific pharmacological agents were locally infused into the dentate gyrus *in vivo* during HFS to inhibit fundamental mTOR- and MAPK/ERK-dependent kinases. Local infusion of the PI3-kinase inhibitor, wortmannin, blocked rpS6 phosphorylation in neuronal cell bodies but not in the region of activated synapses, the middle molecular layer. Local infusion of the mTOR inhibitor, rapamycin, completely blocked activation of rpS6 phosphorylation in granule cell bodies and dendrites, while an infusion of a selective S6K1 inhibitor, PF4708671, attenuated phosphorylation of rpS6 in both the granule cell bodies and dendrites. Local infusion of U0126, an MEK inhibitor,

attenuated rpS6 phosphorylation specifically in the dendritic laminae, while a selective RSK inhibitor, SL0101-1, attenuated rpS6 phosphorylation in both granule cell bodies and dendrites. These results indicate that rpS6 phosphorylation in the granule cell bodies is predominately regulated by PI3K/mTOR-dependent signaling, while MAPK/ERK-dependent signaling regulates rpS6 phosphorylation in the dendritic laminae. These results offer a mechanism by which mTOR and MAPK/ERK pathways regulates synaptically-driven rpS6 phosphorylation to regulate translational control of local protein synthesis at specific subcellular compartments, granule cell bodies vs. dendrites.

INTRODUCTION

Long-lasting forms of synaptic plasticity induce mRNA transcription and de novo protein synthesis, processes that contribute to long-term synaptic modifications including changes in synaptic strength or structural alterations (Kandel, 2001). Long-term potentiation (LTP) is a key candidate for the molecular and cellular mechanism underlying learning and memory (Frey, 2001). But the mechanisms regulating LTP-induced synaptic plasticity remain elusive. Stimulation of the medial perforant path (MPP) is commonly used as a model to investigate signaling events at synapses as it contains well-characterized projections originating from the medial entorhinal cortex that terminates in a precisely defined lamina, the middle molecular layer of the dentate gyrus (Steward, 1976). We have previously shown that high-frequency stimulation (HFS) of the MPP triggers robust phosphorylation of ribosomal protein S6 (rpS6) in granule cell bodies and selectively at activated dendritic domains (Pirbhoy et al., 2016). Furthermore, activation of rpS6 phosphorylation was also shown to be dependent on NMDA receptor activation implicating a role for rpS6 phosphorylation in LTP-induced synaptic plasticity (Pirbhoy et al., 2016).

LTP induction involves the activation of NMDA receptors (Harris et al., 1984) and an influx of calcium into the postsynaptic cell (Lynch et al., 1983), initiating signal transduction cascades that activate a broad range of downstream signaling molecules (Collingridge and Bliss, 1987). But precise mechanism on how NMDA receptor-dependent LTP induction activates mTOR and MAPK/ERK-dependent pathways to regulate the activation of rpS6 phosphorylation in dentate granule cells is not well-established.

Phosphorylation of rpS6 occurs in an ordered fashion beginning with serine 236, 235, 240, 244, and 247 (Flotow and Thomas, 1992; Wettenhall et al., 1992). Phosphorylation of rpS6 at ser240/244 is predominantly mTOR-dependent, while phosphorylation at ser235/236 is regulated by multiple signaling pathways including PKC, MAPK/ERK (Gangarossa and Valjent, 2012), PKA (Biever et al., 2015), mTOR (Roux et al., 2007; Gobert et al., 2008). Phosphorylation of rpS6 is implicated in recruiting mRNAs to polysomes (Nielsen et al., 1981), regulating translation of mRNAs containing a 5' terminal oligopyrimidine (5TOP) motif (Jefferies et al., 1994; Terada et al., 1994), and mTOR-dependent protein synthesis (Dufner and Thomas, 1999; Klann and Dever, 2004). Phosphorylation of rpS6 is also used as a read-out of increased neuronal activity (Knight et al., 2012). In this study, the authors immunoprecipitated rpS6 phosphorylated ribosomes to identify activity-induced genes in activated neurons in the hypothalamus affected by changes in salt balance or food availability (Knight et al., 2012). The vast presence of rpS6 in different neuronal types, suggests that specific regulation of rpS6 phosphorylation by signaling pathways is critical to accomplishing specific functional processes.

Accumulating evidence suggest that mTOR regulates processes related to cell growth, protein synthesis, and translation of mRNAs with long and complex 5' untranslated

regions (UTR) (Hay and Sonenberg, 2004) and mRNAs with a 5' terminal oligopyrimidines (TOP) motif (Thoreen et al., 2012). Studies involving hippocampal slices have demonstrated that mTOR also contributes to the expression of late-phase LTP (L-LTP) (Tang et al., 2002). The MAPK/ERK signaling pathway has also been shown to be required for activation of translation factors in response to neural activity, L-LTP and hippocampal memory formation (Kelleher et al., 2004). The potential role of MAPK/ERK in translational control has prompted the hypothesis that cross-talk between mTOR and the MAPK/ERK signaling pathways cooperate to coordinate regulation of cap-dependent and 5TOP mRNA translation (Wang, 2001; Kelleher et al., 2004; Shahbazian et al., 2006). Here we propose that phosphorylation of rpS6 may function as a mechanism to regulate activity-dependent translational control. To investigate the contribution of mTOR and MAPK/ERK signaling to induction of rpS6 phosphorylation, selective pharmacological inhibitors were locally infused into the dorsal blade of the dentate gyrus during perforant path stimulation. The effect of each inhibitor on basic synaptic transmission was assessed by recording field excitatory postsynaptic potentials (fEPSPs) during drug delivery and synaptic stimulation. The effects of each pharmacological inhibitor were determined using phospho-specific antibodies that recognize phosphorylation of rpS6 at subsets of serine residues, ser235/236, and ser240/244.

Results of this study reveal that local infusion of the PI3-kinase inhibitor, wortmannin, blocked rpS6 phosphorylation in the granule cell bodies leaving the band of increased rpS6 phosphorylation in the MML intact. Local delivery of the mTOR inhibitor, rapamycin, blocked phosphorylation of rpS6 at both ser235/236 and ser240/244. Local infusion of the selective S6K1 inhibitor, PF4708671, attenuated immunostaining of rpS6

phosphorylation in both granule cell bodies and dendrites. Local infusion of the MEK inhibitor, U0126, attenuated rpS6 phosphorylation specifically in the dendritic laminae, while a local infusion of the selective RSK inhibitor, SL0101-1, attenuated rpS6 phosphorylation in both the granule cell bodies and dendrites. These results indicate that rpS6 phosphorylation in activated dendritic domains is primarily regulated by MAPK/ERK signaling, whereas PI3-kinase/mTOR-dependent signaling predominately regulates activation of rpS6 phosphorylation in granule cell bodies. This differential regulation of rpS6 phosphorylation may serve as a mechanism for activity-dependent translational control.

MATERIALS AND METHODS

Animals: Experimental animals were adult female (150-300g) Sprague-Dawley rats from Harlan laboratories. Rats were anesthetized with 20% urethane and positioned in a stereotaxic apparatus as described previously (Steward et al., 1998). All experimental procedures were approved by the Institutional Animal Care and Use Committee (IACUC) of the University of California, Irvine.

Acute neurophysiology preparation: Acute neurophysiological techniques were used to stimulate the medial perforant path projections to the dentate gyrus unilaterally. Projections from the entorhinal cortex to the dentate gyrus are predominately unilateral, so the contralateral side serves as an intra-animal control. A stimulating electrode, an insulated tungsten microelectrode, was stereotaxically positioned in the medial entorhinal cortex (4.0mm lateral, 1.0mm anterior to lambda within a 3.0-4.0mm range below the

cortical surface). Electrode depth was adjusted to obtain a maximal evoked response in the dentate gyrus with minimal stimulus intensity. Stimulus intensity was set to evoke an approximately 1.5mV population spike. The recording electrode, a glass micropipette filled with 0.9% saline, was positioned in the cell body layer of the dentate gyrus (3.5mm posterior, 1.5-1.7mm lateral to bregma and approximately 3.0mm below the cortical surface). The depth of the recording electrode was adjusted to record the positive-going field potential generated by perforant path stimulation.

Experimental Procedure: After positioning electrodes, test stimulation was delivered at a rate of 1/10sec to determine baseline response amplitude. Then high-frequency stimulation was initiated as described below.

High-Frequency Stimulation (HFS): All cases received 60 minutes of continuous HFS, which is the standard paradigm used to cause Arc mRNA to localize selectively in activated dendritic domains (Steward et al., 1998). Delivery of HFS involved three bouts of 10 400Hz trains followed by test stimulation to determine the extent of LTP, then continuing HFS at a rate of 1/10sec for the remaining 60 minutes.

Immediately after the end of stimulation, rats received a lethal dose of Euthasol (0.5ml) or Fatal-plus (0.5ml) and were perfused with 4% paraformaldehyde within 5 minutes of the last stimulus train.

Local Drug Infusions: Stimulating and recording electrodes were positioned as described above, and baseline response amplitude was assessed using a saline-filled recording electrode. The saline filled microelectrode was then replaced with a microelectrode filled with the designated pharmacological agent (see below), and response amplitude was monitored to confirm placement. Once drug electrode was positioned, no test responses were taken for a 15-20-minute period. Response amplitude with drug electrode was then taken for 15-20 minutes. After recording response amplitude post-drug delivery, HFS was delivered as described above. For U0126, evoked potentials were recorded by connecting leads directly to the metal barrel of the Hamilton microsyringe. A total volume of 0.1-0.2µl (20µM U0126) was injected via Hamilton syringe into the dorsal blade of the dentate gyrus before HFS delivery. Post infusion, no test responses were taken for a 30-minute period, then a 15-minute post infusion baseline was recorded. HFS was then delivered as mentioned above. Of note, in all experiments, stimulus intensity was set to evoke a population spike of approximately 1.5mV. In some cases, when the saline electrode was switched to place the drug-filled electrode, the population spike dropped below 1.5mV. As a result, values for all drugs are reported for the total number of cases and as a separate value where cases under 1.5mV are excluded.

Pharmacological Agents: PI3 kinase inhibitor, Wortmannin, (4.7mM (2mg/ml) in 10% DMSO in saline; RBI, Cat. W107). Akt inhibitor, LY294002, (1mM (343.8µg/ml) in 10% DNMSO in saline; Sigma, Cat. L9908). Rapamycin, mTOR inhibitor, (0.1mM (91.417µg/ml) in 10%DMSO in saline; LC Laboratories, Cat. R5000). S6K1 inhibitor, PF4708671, (100µM (39.0µg/ml) in 10%DMSO in saline; Tocris, Cat. 4032). MEK inhibitor, U0126, (20µM

(8.53μg/ml) in 10%DMSO in saline; Promega, Cat. V112A). RSK inhibitor, SL0101-1, (10μM (15.5μg/ml) in 10% DMSO in saline; AdooQ bioscience, Cat. A1160).

Immunohistochemistry: Brains were sectioned in the coronal plane on a Vibratome at 40μm and sections were stored in phosphate buffer (pH 7.4) before staining. Prior to immunostaining, free-floating sections were placed in microfuge tubes with nano-pure water and then the microfuge tubes were placed in boiling water for 5min for antigen retrieval. Sections were then treated with H_2O_2 to block endogenous peroxidase activity, transferred to 0.01% Tween in PBS for 15min, blocked for 1-2hrs at RT in TSA blocking buffer and then incubated for 18-20hrs in a 1:100 dilution of S6 phospho-specific antibodies that recognize phosphorylated ser235/236 (Cell Signaling, catalog #4858) or ser240/244 (Cell Signaling, catalog #2215). Sections were then incubated in a 1:250 dilution of biotinylated donkey anti-rabbit IgG for 2hrs (Jackson Laboratories, 711-065-152), treated with ABC for 1hr and stained for 5min in DAB. Sections were mounted on 0.5% gelatin subbed slides. Slides were dehydrated through washes of graded ethanol, cleared in 3 changes of xylene and coverslipped with DPX mountant for histology. For pERK immunostaining, free-floating sections were placed in microfuge tubes with nano-pure water and heated to 95C for 5 minutes. Sections were then washed with TBS and placed in blocking buffer for 2hrs (10% normal goat serum in TBS) and then incubated for 30-34hrs in a 1:200 dilution of polyclonal phosphorylated ERK antibody (Cell Signaling, catalog 9101). Sections were then incubated in a 1:200 dilution of biotin conjugated goat anti-rabbit IgG secondary in 10% NGS for 2hrs, treated with ABC for 1hr and stained for 3min in DAB.

Image Quantification: Optical density (OD) across the granule cell layer and molecular layers of the dentate gyrus was quantified using NIH imageJ as described in detail previously (Farris et al., 2014). Images were taken at 20X at the same exposure. A line region of interest (ROI) was aligned perpendicular to the cell body layer extending through the dendritic laminae, and OD was measured at 20μm intervals. The OD at each level was averaged across the total number of line measurements per image to obtain an average value along the line ROI for each section (~19 measurements). Overall, the average line ROI values per case were then averaged across rats to generate an "average optical density vs. distance" graph where *N*=number of rats. Values are presented as mean ± SEM. For the assessment of changes in immunostaining per region (granule cell layer (GCL), inner molecular layer (IML), middle molecular layer (MML), outer molecular layer OML), values were obtained as described above except that OD values were taken from each corresponding region.

Synaptic Plasma Membrane Fractionation: SPM fractionation protocol was adapted from Perez-Otano (2004) (Blackstone et al., 1992). Briefly, two hours of continuous HFS (as detailed above) was delivered unilaterally to the medial perforant path of adult female rats. Immediately after stimulation, animals were sacrificed and ipsilateral and contralateral hippocampi dissected and homogenized separately. The hippocampi were suspended in 10 mL of 0.32M sucrose, 4mM HEPES pH 7.4. Homogenized solution was centrifuged at 3000 rpm for 5 min at 4C to remove the pelleted nuclear fraction (P1). Supernatant was collected and spun at 13,000 rpm for 15min. Supernatant was then tossed and the pellet was

resuspended in 0.32M sucrose, 4mM HEPES pH 7.4. Homogenized pellet was then spun at 13000 rpm for 15min. The resulting pellet was then lysed by hypo-osmotic shock using 9mL of ice cold ddH20 and pH adjusted to 7.4 using 1.0M HEPES solution pH7.4. Lysate was then spun for 30 min to yield a supernatant (S3), crude synaptic vesicle fraction, and a pellet (P3), lysed synaptosomal membrane fraction. Pellet was resuspended in 3mL of 0.32M sucrose, 4mM HEPES pH 7.4. Resuspended membranes were layered on top of a discontinuous sucrose gradient containing 0.8 to 1.0 to 1.2M sucrose. Gradient was spun at 30,000rpm for 2hrs at 4C in a SW41 rotor. Synaptic plasma membrane layer, between 1.0 and 1.2M sucrose was recovered and diluted to 0.16M sucrose by adding 50uM calcium chloride and spun at 21,500rpm in a SW41 rotor. Pellet was then resuspended in 200uL of lysis buffer (50mM Tris-HCL pH 7.4, 150mM NaCl, 5mM EDTA, 1% Triton X-100, 1mM PMSF, and 1% protease inhibitor cocktail and phosphatase inhibitor cocktail). Samples were then frozen at -80C.

Western Blot: Protein concentrations were determined with Pierce BCA protein assay kit. 5μg of total protein were loaded onto 4-20% Mini-Protean TGX gels (cat. 456-1095) and transferred to Immobilon-FL polyvinylidene fluoride (PVDF) membranes (cat. IPFL00010). Membranes were then blocked in Odyssey Blocking Buffer (LI-COR, cat. 927-40000) for 1hr and incubated overnight in primary dilution buffer (Odyssey blocking buffer with 0.2% Tween-20) with p-rpS6 235/236 at a dilution of 1:1000 or total rpS6 at a dilution of 1:1000 at 4C. Membranes were then incubated in a 1:15,000 dilution of goat anti-rabbit IR Dye 800CW (LI-COR, cat. 926-32211) for 1 hour and imaged using Odyssey Fc imagining

system. For detection of total protein, membranes were stripped by incubating membranes in Newblot IR Strip Buffer for 15 minutes (LI-COR, cat. 928-40028).

Western Blot Analysis: Quantification of signal band intensity was done using LI-COR Image Studio ver. 3.1. Phosphoproteins were normalized to total protein.

Statistical Analysis: All statistical analyses were done using Prism (GraphPad Software, San Diego, USA). For all analyses, "N"= number of animals.

RESULTS

Phosphorylation of ribosomal protein S6 is differentially regulated in granule cell bodies and dendrites

Both mTOR- and MAPK/ERK-dependent signaling pathways regulate phosphorylation of rpS6 at ser235/236, while phosphorylation at ser240, ser244, ser247 is predominately mTOR-dependent (Roux et al., 2007). Phosphorylation of rpS6 has been shown to occur in granule cell bodies and dendrites following HFS (Panja et al., 2009; Pirbhoy et al., 2016), but little is known about the role of rpS6 phosphorylation in synaptic plasticity of dentate granule cells. PI3-kinase activation is one of the initial signaling events elicited by LTP induction and increased phosphorylation levels are observed in tetanized-tissue compared to untetanized tissue (Kelly et al., 2000). In addition, inhibitors of PI3-kinase block the expression of LTP in the perforant path indicating a critical role for PI3-kinase in the expression of LTP in the dentate gyrus (Kelly et al., 2000). To define the contribution of PI3-kinase signaling in regulating rpS6 phosphorylation in dentate granule

cells, the PI3-kinase inhibitor, wortmannin, was locally infused into the dorsal blade of the dentate gyrus during continuous HFS. Delivery of wortmannin was administered via a glass pulled micropipette filled with wortmannin, a technique that allows the local diffusion of the drug within an area several millimeters in diameter (Steward and Worley, 2001).

Positive-going field excitatory postsynaptic potentials (EPSPs) were recorded during local delivery of wortmannin via a glass pulled microelectrode. Analysis of the strength of an fEPSP was evaluated from the slope of the EPSP and amplitude of the population spike. Local infusion of the PI3-kinase inhibitor, wortmannin, did not alter basic synaptic transmission or LTP. Following replacement of the saline-filled micropipette with the wortmannin-filled micropipette, there was a small decrease in response amplitude from the saline baseline that remained stable at 83.02 ± 9.789% (mean ± SEM, N=8) of baseline for the population spike and 86.05 ± 3.17% (N=8) for EPSP slope. A population spike below 1.5mV was recorded for one case (0.66mV) when recording synaptic responses. The baseline with the excluded case was 85.59 ± 10.91% of baseline (N=7) for population spike amplitude and 87.27 ± 3.38% of baseline for EPSP slope (N=7). Following delivery of 30 high-frequency trains (a standard paradigm for inducing perforant path LTP), there was an increase in population EPSP slope and population spike amplitude similar to control cases in the presence of a saline-filled microelectrode. The percent change from baseline recorded via the wortmannin micropipette was 24.88 ± 4.88% (Mean ± SEM, N=7) for EPSP slope compared to 28.32 ± 3.34% (N=6) in control experiments with saline-filled microelectrodes ($p=0.5618$; $t(11)=0.5855$; student's t-test for unpaired samples; percent change from baseline for EPSP slope with all cases was 25.46 ± 4.27%, N=8).

Immunostaining of rpS6 phosphorylation using phospho-specific antibodies that detect phosphorylation at ser235/236 and ser240/244 revealed different patterns of rpS6 phosphorylation. Immunostaining with the phospho-specific antibody ser235/236 revealed the surprising result that phosphorylation at ser235/236 (p-ser235/236) is differentially regulated in cell bodies vs. dendrites. In distant areas from the wortmannin-filled micropipette (Figure 1A and 1B), immunostaining for p-ser235/236 revealed the expected robust induction of rpS6 phosphorylation. In the area surrounding the wortmannin-filled micropipette (Figure 1E and 1F), the distinct band of increased immunostaining in the molecular layer was reduced, but not to the level of control, non-stimulated sections (Figure 1G and 1H). Levels of immunostaining for p-ser235/236 in the granule cells of sections within the infusion area were comparable to control sections (Figure 1G and 1H). Immunostaining for p-ser240/244 revealed the expected induction of rpS6 phosphorylation in areas distant from the wortmannin-filled micropipette (Figure 1I and 1J). In the area surrounding the wortmannin micropipette (Figure 1M and 1N), immunostaining of rpS6 phosphorylation was attenuated in both the granule cell layer and the molecular layer exposing a pattern similar to control sections (Figure 1O and 1P).

To quantify effects of wortmannin blockade, levels of immunostaining were assessed by determining average optical density (OD) across the dorsal blade of the dentate gyrus. OD values in the region of the blockade (Infusion) were compared with distant areas outside the sphere of inhibition (Ipsilateral) and to the contralateral, non-stimulated side (Contra). Graphs show representative cases for each condition plotted as average OD values measured across the dorsal blade of the dentate gyrus from the granule cell layer to the outer molecular layer (approx. 300 μm; Figure 1C and 1K). To provide a

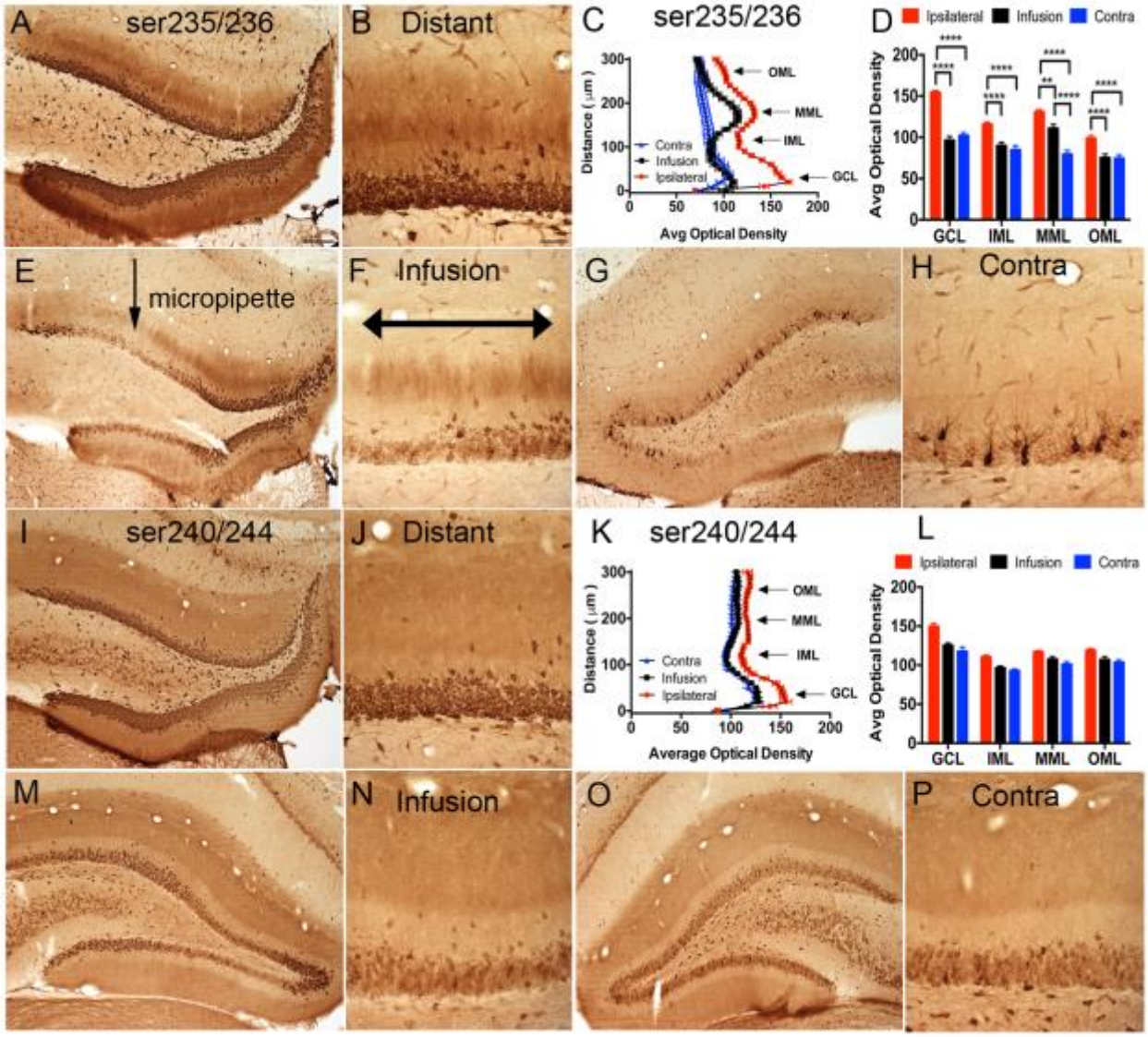

Figure 3.1. Local infusion of the PI3-kinase inhibitor, wortmannin, blocks phosphorylation of rpS6 in the granule cell bodies not in dendrites. A, Immunostaining for p-ser235/236 ipsilateral to stimulation in a section distant from the infusion area. **B,** High-magnification image of A. **C,** Quantification of average OD across the dorsal blade of the dentate gyrus in ipsilateral sections distant from the injection site, ipsilateral sections within the infusion area, and contralateral, non-stimulated sections. **D,** Statistical assessment at four sites along the dentate gyrus (denoted by the arrows), GCL, IML, MML, OML (ser235/236, N=8), error bars represent SEM. Statistical assessment by two-way ANOVA revealed a significant interaction ($F(6,84)=8.44$, $p<0.0001$), a significant main effect of treatment ($F(2,84)=114.30$, $p<0.0001$) and a significant main effect of region ($F(3,84)=42.36$, $p<0.0001$). Post-hoc analysis with Bonferroni's multiple comparisons tests revealed that ipsilateral sections were statistically different than sections within the infusion area and contralateral sections in all regions. Notably, in the MML, sections within the infusion area were significantly different than contralateral sections (Two-way ANOVA, N=8, $p<0.05$). **E,** Immunostaining of p-ser235/236 ipsilateral to the stimulation in a section within the infusion area in the presence of wortmannin (arrow denotes injection site). **F,** High-magnification image of E (arrow denotes infusion area). Note the blockade of p-rpS6 specifically in the GCL and robust

phosphorylation of rpS6 in the MML of dentate gyrus. **G,** Immunostaining of p-ser235/236 contralateral to the stimulation. **H,** High-magnification image of G. **I,** Immunostaining of p-ser240/244 in a section distant from the infusion area. **J,** High-magnification image of I. **K,** Quantification of average OD across the dorsal blade of the dentate gyrus in ipsilateral sections distant from the injection site, ipsilateral sections within the infusion area, and contralateral sections. **L,** Statistical assessment at four sites along the dentate gyrus (denoted by the arrows), GCL, IML, MML, OML (ser240/244, N=5), error bars represent SEM. Statistical assessment by two-way ANOVA revealed a main effect of treatment ($F(2,48)=41.26$, $p<0.0001$) and a main effect of region ($F(3,48)=48.69$, $p<0.0001$), but no significant interaction ($F(6,48)=1.72$, $p=0.137$). **M,** Immunostaining of p-ser240/244 ipsilateral to stimulation within the infusion area in the presence of wortmannin. **N,** High-magnification image of M. **O,** Immunostaining of p-ser240/244 contralateral to the stimulation. **P,** High-magnification image of O. Scale bars: **A,** 200μm; **B,** 50 μm.

statistical analysis of the blockade, average OD values at four measuring sites were compared: the granule cell layer (GCL), the trough of the inner molecular (IML), the peak immunostaining in the middle molecular layer (MML), and a distance of 280μm from the GCL to represent the outer molecular layer (OML) (denoted by arrows in Figure 1C and 1K). Quantitative comparisons of levels of immunostaining for ipsilateral, infusion and contralateral sections (N=8 animals for ser235/236 and N=5 animals for ser240/244) in each of the four measuring sites by two-way ANOVA yielded an overall $F(6,84) = 8.44$, $p<0.0001$ (N=8, Figure 1D) for ser235/236 and an overall $F(6,48) = 1.72$, $p=0.1377$ (N=5, Figure 1L) for ser240/244. Post-hoc analysis with Bonferroni's multiple comparisons tests revealed that ipsilateral sections were statistically different than sections within the infusion area and contralateral sections in all regions for ser235/236. Notably, in the MML, sections within the infusion area were significantly different than contralateral sections (Figure 1D) (N=8, Two-way ANOVA, $p<0.05$). Collectively, these data suggest the surprising conclusion that PI3-kinase activation is critical for rpS6 phosphorylation at ser235/236 in granule cell bodies but has a minimal role in the local activation of rpS6 phosphorylation in the portion of the dendrite contacted by active synapses.

Local infusion of reversible PI3-kinase inhibitor attenuates phosphorylation of rpS6 at cell bodies and dendrites

The PI3-kinase inhibitor, wortmannin is an irreversible, selective, cell-permeable fungal metabolite that acts as a potent inhibitor of PI3-kinase with an I_C50 of 5nM (Arcaro and Wymann, 1993). Another commonly used PI3-kinase inhibitor is LY294002, a selective PI3-kinase inhibitor (Vlahos et al., 1994). Unlike wortmannin that abolishes PI3-kinase activity, LY294002 is a reversible inhibitor that acts on the ATP binding site of PI3-kinase

(Vlahos et al., 1994). Both wortmannin and LY294002 have been shown to be required for the expression of LTP in hippocampal slices (Sanna et al., 2002). To test how reversible inhibition of PI3-kianse affects regulation of rpS6 phosphorylation in granule cells, LY294002 was locally infused into the dentate gyrus. Local infusion of LY294002 did not alter basic synaptic transmission. Following replacement of the saline-filled micropipette with the LY294002-filled micropipette, the response amplitude remained stable at 91.55 ± 17.44% of baseline (mean ± SEM, N=6) for the population spike and 86.09 ± 10.13% (N=6) of baseline for EPSP slope. A population spike below 1.5mV was recorded for one case (0.57mV) when recording synaptic responses. The baseline with the excluded case was 106.5 ± 10.96% (N=5) of baseline for the population spike and 90.97 ± 10.87% of baseline for EPSP slope (N=5). Following delivery of 30 high-frequency trains, there was an increase in population EPSP slope and population spike amplitude similar to control cases in the presence of a saline-filled microelectrode. The percent change from baseline recorded via the LY294002 micropipette was 16.20 ± 11.12% (N=5) compared to 28.32 ± 3.34% in control experiments with saline-filled micropipettes ($p=0.2865$; $t(9)=1.133$; student's t-test for unpaired samples; percent change from baseline for EPSP slope with all cases was 8.47 ± 11.12%, N=6).

Immunostaining for p-ser235/236 revealed the expected robust activation of rpS6 phosphorylation in areas distant from the LY294002-filled micropipette (Figure 2A and 2B). In the area surrounding the LY294002-filled micropipette (Figure 2E and 2F), there was an attenuation in the intensity of immunostaining for rpS6 phosphorylation observed in granule cells. Dentate granule cells within the infusion area (Figure 2F) had a more scattered pattern of phosphorylated rpS6-positive cells compared to the densely packed

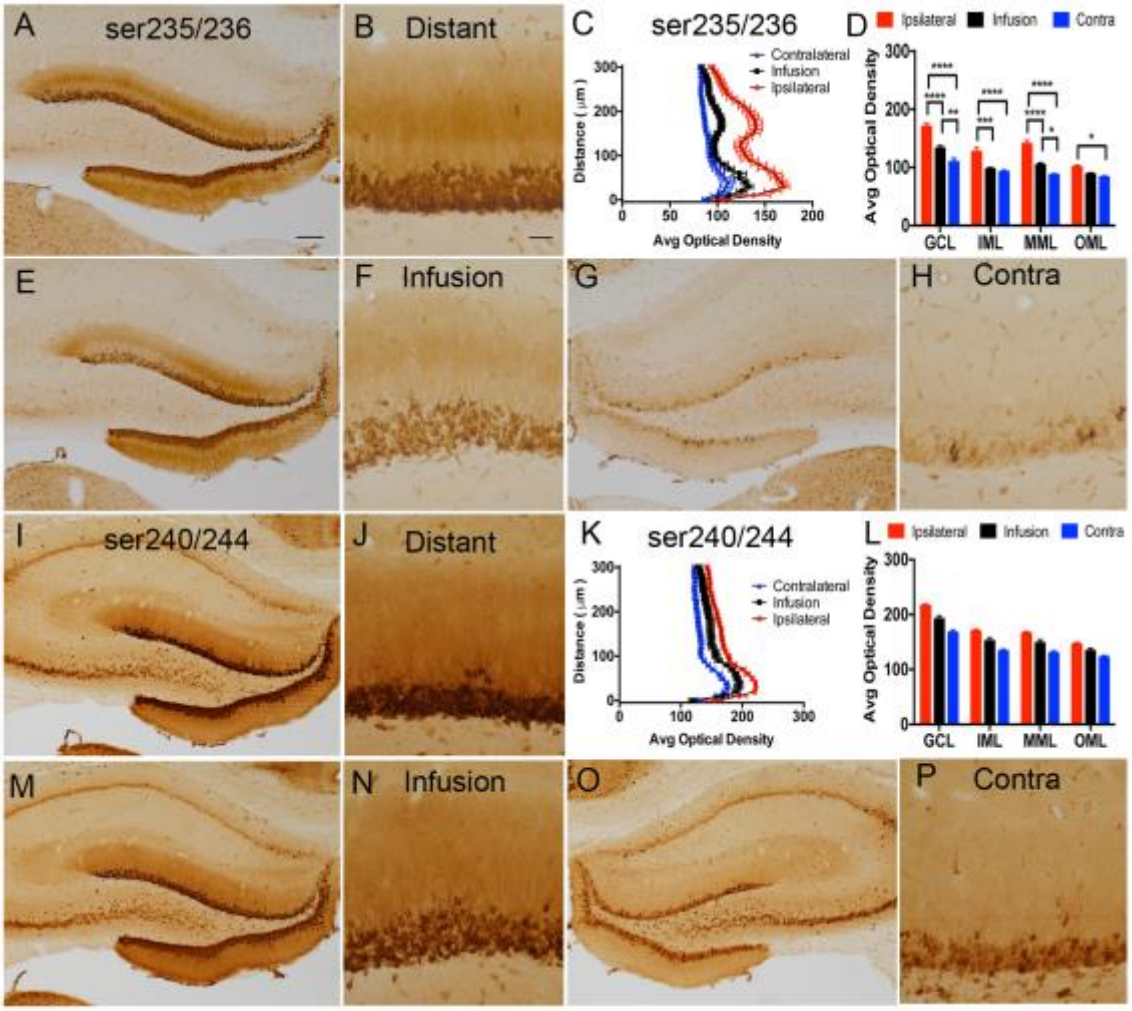

Figure 3.2. Local infusion of the reversible PI3-kinase inhibitor, LY294002, attenuates phosphorylation of rpS6 in cell bodies and dendrites A, Immunostaining for p-ser235/236 ipsilateral to stimulation in a section distant from the infusion area. **B,** High-magnification image of A. **C,** Quantification of average OD across the dorsal blade of the dentate gyrus in ipsilateral sections distant from the injection site, ipsilateral sections within the infusion area, and contralateral, non-stimulated sections. **D,** Statistical assessment at four sites along the dentate gyrus, GCL, IML, MML, OML (ser235/236, N=6), error bars represent SEM. Statistical assessment by two-way ANOVA revealed a significant interaction ($F(6,60)=4.41$, $p=0.0009$), a significant main effect of treatment ($F(2,60)=82.00$, $p<0.0001$) and a significant main effect of region ($F(3,60)=51.62$, $p<0.0001$). Post-hoc analysis with Bonferroni's multiple comparisons tests revealed that ipsilateral sections were statistically different than sections within the infusion area and contralateral sections in the GCL, IML and MML. Ipsilateral sections were also significantly different than contralateral sections in the OML. Notably, sections within the infusion area were also statistically different than contralateral sections in the GCL and MML (Two-way ANOVA, N=6, $p<0.05$). **E,** Immunostaining of p-ser235/236 ipsilateral to the stimulation in a section within the infusion area in the presence of LY294002. **F,** High-magnification image of E. Note the reduction p-rpS6 in the GCL and throughout the molecular layer of dentate gyrus. The distinct band of rpS6 phosphorylation remains in sections within the infusion area. **G,** Immunostaining of p-ser235/236 contralateral to the stimulation. **H,** High-magnification image of G. **I,** Immunostaining of p-ser240/244 in a section distant from the

infusion area. **J,** High-magnification image of I. **K,** Quantification of average OD across the dorsal blade of the dentate gyrus in ipsilateral sections distant from the injection site, ipsilateral sections within the infusion area, and contralateral sections. **L,** Statistical assessment at four sites along the dentate gyrus, GCL, IML, MML, OML (ser240/244, N=6), error bars represent SEM. Statistical assessment by two-way ANOVA revealed a main effect of treatment ($F(2,60)=67.23$, $p<0.0001$) and a main effect of region ($F(3,60)=94.19$, $p<0.0001$), but no significant interaction ($F(6,60)=1.37$, $p=0.2402$). **M,** Immunostaining of p-ser240/244 ipsilateral to stimulation within the infusion area in the presence of LY294002. **N,** High-magnification image of M. **O,** Immunostaining of p-ser240/244 contralateral to the stimulation. **P,** High-magnification image of O. Scale bars: **A,** 200μm; **B,** 50 μm.

granule cell body activation observed in distant areas (Figure 2B). There was also a reduction in the intensity of immunostaining throughout the molecular layer. The discernable band of rpS6 phosphorylation was also attenuated but remained discernable (Figure 2F). Immunostaining for p-ser240/244 also revealed the expected robust activation of rpS6 phosphorylation in distant sections from the infusion area (Figure 2I and 2J). Within the infusion area (Figure 2M and 2N), a similar pattern was observed in the granule cell bodies as seen with p-ser235/236. Immunostaining revealed a scattered pattern of phosphorylated rpS6-positive cells with some granule cells showing robust activation and others showing partial activation (Figure 2N). In the dendritic layers, there was a small reduction in the intensity level of immunostaining throughout the molecular layer.

To quantify the effects of LY294002 on induction of rpS6 phosphorylation, the graphs show representative cases for each condition (Ipsilateral, Infusion, Contra) plotted as average OD values measured across the dorsal blade of the dentate gyrus from the GCL to the OML (Figure 2C and 2K). To provide a statistical analysis of the blockade, we calculated the average OD at four measuring sites for comparison: (GCL, IML, MML, OML). Quantitative comparisons of levels of immunostaining for ipsilateral, infusion and contralateral sections in each of the four measuring sites by two-way ANOVA yielded an overall $F(6,60)=4.42$, $p=0.0009$ (N=6, Figure 2D) for p-ser235/236 and $F(6,60)=1.37$, $p=0.2404$ (N=6, Figure 2L) for p-ser240/244. Post-hoc analysis with Bonferroni's multiple comparisons tests revealed that ipsilateral sections were statistically different than sections within the infusion area and contralateral sections in the GCL, IML and MML for ser235/236. Ipsilateral sections were also significantly different than contralateral

sections in the OML. Notably, sections within the infusion area were also statistically different than contralateral sections in the GCL and MML (Figure 2D; N=6, Two-way ANOVA, $p<0.05$). Collectively, these data suggest that PI3-kinase activation contributes to the induction of rpS6 phosphorylation at ser235/236 in both cell bodies and dendrites, but in contrast to treatment with wortmannin, inhibition of PI3-kinase with a reversible inhibitor does not abolish phosphorylation of rpS6 in the granule cell bodies.

Local infusion of mTOR inhibitor, rapamycin, blocks rpS6 phosphorylation in both cell bodies and dendrites

Defined mechanisms detailing molecular connections between synaptic activity and mTOR-dependent translational control are obscure. Previous studies have shown that inhibition of mTOR with rapamycin treatment results in a reduction in the magnitude of late-phase LTP (L-LTP). Furthermore, it has been demonstrated that mTOR, along with translation factors, eIF4E and 4EBP1 and 4EBP2, are present at postsynaptic sites indicating a role in long-term plasticity (Tang et al., 2002). To define mTOR-dependent regulation of rpS6 phosphorylation in dentate granule cells, the mTOR inhibitor, rapamycin, was locally infused into the dentate gyrus. Local delivery of rapamycin into the hippocampus did not alter basic synaptic transmission. Following replacement of the saline-filled micropipette with the rapamycin-filled micropipette, the response amplitude remained stable at 78.17 ± 18.58% (mean ± SEM, N=5) of baseline for the population spike and 139.4 ± 51.89% (N=5) of baseline for EPSP slope. A population spike below1.5mV was recorded for 2 cases (0.52-1.40mV) when recording synaptic responses. The baseline with the excluded cases was 106.4 ± 11.89% of baseline (N=3) for population spike and 87.26 ± 12.38% of baseline (N=3) for EPSP slope. Following the delivery of HFS, there was an

increase in population EPSP slope and population spike amplitude similar to control cases in the presence of a saline-filled microelectrode. The percent change from baseline recorded via the rapamycin micropipette was 33.95 ± 28.9% (mean ± SEM, N=3) compared to 28.32 ± 3.34% (N=6) in control experiments with saline-filled micropipettes ($p=0.7814$; $t(7)=0.2884$; student's t-test for unpaired samples; percent change from baseline for all cases was 261.1 ± 224.1%, N=5).

Induction of rpS6 phosphorylation is considered to be a marker for mTOR activation, so immunostaining for rpS6 phosphorylation is the best positive control for the effectiveness of rapamycin. Immunostaining for p-ser235/236 revealed the expected robust activation of rpS6 phosphorylation in areas distant from the rapamycin-filled micropipette (Figure 3A and 3B). Within the infusion area, phosphorylation of rpS6 was completely blocked in the area surrounding the rapamycin micropipette (Figure 3E and 3F) in both the granule cell bodies and dendrites. In the granule cell layer, phosphorylation of rpS6 was completely abolished to levels comparable to contralateral non-stimulated sections (Figure 3G and 3H). In the molecular layer, phosphorylation of rpS6 was completely abolished in the IML, and OML; residual phosphorylation remained in some instances in the MML (Figure 3F). Similarly, immunostaining for p-ser240/244 revealed the expected induction of rpS6 phosphorylation in areas distant from the rapamycin-filled micropipette (Figure 3I and 3J) and complete blockade of granule cell bodies and dendrites in the area surrounding the rapamycin micropipette (Figure 3M and 3N) comparable to contralateral non-stimulated sections (Figure 3O and 3P). For p-ser240/244, rapamycin completely blocked all dendritic layers leaving no residual activation of rpS6 phosphorylation in the MML (Figure 3N).

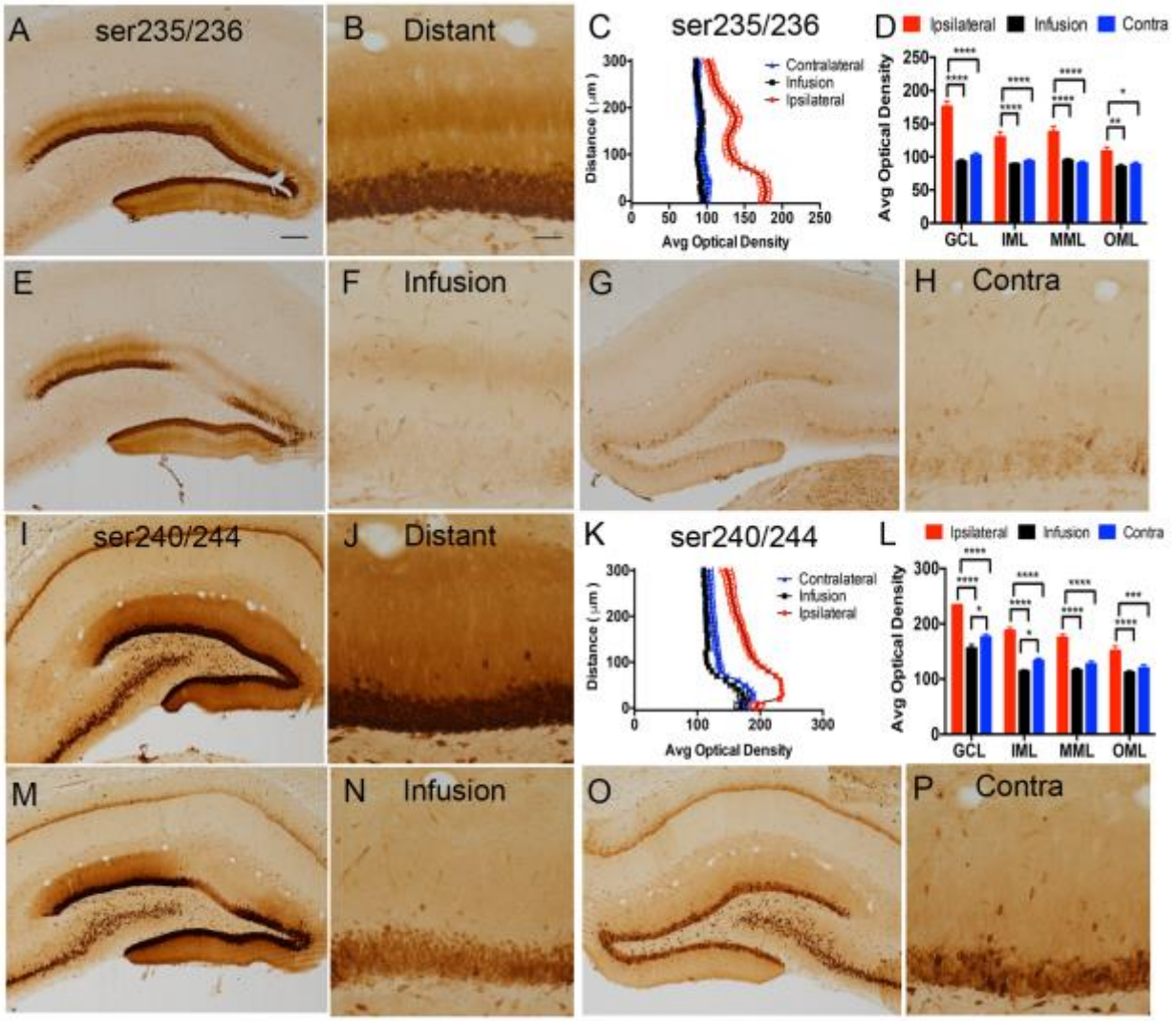

Figure 3.3. Local infusion of mTOR inhibitor, rapamycin, completely blocks phosphorylation of rpS6. A, Immunostaining for p-ser235/236 ipsilateral to stimulation in a section distant from the infusion area. **B,** High-magnification image of A. **C,** Quantification of average OD across the dorsal blade of the dentate gyrus in ipsilateral sections distant from the injection site, ipsilateral sections within the infusion area, and contralateral, non-stimulated sections. **D,** Statistical assessment at four sites along the dentate gyrus, GCL, IML, MML, OML (ser235/236, N=5), error bars represent SEM. Statistical assessment by two-way ANOVA revealed a significant interaction ($F(6,48)=7.29$, $p<0.0001$), a significant main effect of treatment ($F(2,48)=105.62$, $p<0.0001$) and a significant main effect of region ($F(3,48)=17.00$, $p<0.0001$). Post-hoc analysis with Bonferroni's multiple comparisons tests revealed that ipsilateral sections were statistically different than sections within the infusion area and contralateral sections in all regions (Two-way ANOVA, N=5, $p<0.05$). **E,** Immunostaining of p-ser235/236 ipsilateral to the stimulation in a section within the infusion area in the presence of rapamycin. **F,** High-magnification image of E. Note rapamycin infusion completely blocks phosphorylation of rpS6 in the GCL and throughout the molecular layer of dentate gyrus. The distinct band of rpS6 phosphorylation remained in some instances in sections within the infusion area. **G,** Immunostaining of p-ser235/236 contralateral to the stimulation. **H,** High-magnification image of G. **I,** Immunostaining of p-ser240/244 in a section distant from the

infusion area. **J,** High-magnification image of I. **K,** Quantification of average OD across the dorsal blade of the dentate gyrus in ipsilateral sections distant from the injection site, ipsilateral sections within the infusion area, and contralateral sections. **L,** Statistical assessment at four sites along the dentate gyrus, GCL, IML, MML, OML (ser240/244, N=5), error bars represent SEM. Statistical assessment by two-way ANOVA revealed a significant interaction ($F(6,48)=3.05$, $p=0.0131$, a significant main effect of treatment ($F(2,48)=162.19$, $p<0.0001$) and a significant main effect of region ($F(3,48)=80.86$, $p<0.0001$). Post-hoc analysis with Bonferroni's multiple comparisons tests revealed that ipsilateral sections were statistically different than sections within the infusion area and contralateral sections in all regions. Notably, sections within the infusion area were statistically different than contralateral sections in the GCL and IML (Two-way ANOVA, N=5, $p<0.05$). **M,** Immunostaining of p-ser240/244 ipsilateral to stimulation within the infusion area in the presence of rapamycin. **N,** High-magnification image of M. **O,** Immunostaining of p-ser240/244 contralateral to the stimulation. **P,** High-magnification image of O. Scale bars: **A,** 200μm; **B,** 50 μm.

To quantify the effects of rapamycin, the graphs show representative cases for each condition (Ipsilateral, Infusion, Contra) plotted as average OD values measured across the dorsal blade of the dentate gyrus from the GCL to the OML (Figure 3C and 3K). To provide a statistical analysis of the blockade, we calculated the average OD at four measuring sites for comparison: (GCL, IML, MML, OML). Quantitative comparisons of levels of immunostaining for ipsilateral, infusion and contralateral sections in each of the four measuring sites by two-way ANOVA yielded an overall $F(6,48)=7.29$, $p<0.0001$ for p-ser235/236 (N=5, Figure 3D) and an overall $F(6,48)=3.05$, $p=0.0131$ for p-ser240/244 (N=5, Figure 3L). Post-hoc analysis with Bonferroni's multiple comparisons tests revealed that ipsilateral sections were statistically different than sections within the infusion area and contralateral sections in all regions for p-ser235/236 and p-ser240/244 (Figure 3D and 3L, respectively). Notably, for p-ser240/244, sections within the infusion area were statistically different than contralateral sections in the GCL and IML (Figure 3L; N=5, Two-way ANOVA, $p<0.05$). Taken together, these results indicate that mTOR activation is critical for induction of rpS6 phosphorylation in both the granule cell bodies and dendrites for p-ser235/236 and p-ser240/244.

Local infusion of the S6K1 inhibitor attenuates rpS6 phosphorylation in the granule cell bodies and dendritic laminae

S6K1 and S6K2 are downstream targets of mTOR that are associated with enhanced protein synthesis (Dufner and Thomas, 1999), 5TOP mRNA translation (Jefferies, 1997) and are attributed roles in promoting ribosome biogenesis (Ferrari and Thomas, 1994). S6K1 has been shown to localize in the nucleus and cytosol of cells, while S6K2 is highly restricted to the nucleus of cells (Lee-Fruman et al., 1999; Park et al., 2002). While

activation of S6K1 is reported to be primarily by mTOR (Thoreen et al., 2012), studies indicate that S6K2 may also be regulated by the downstream substrate of ERK, p90 ribosomal protein S6 kinase (RSK) (Wang et al., 2001). To determine the involvement of the mTOR-dependent kinase, S6K1, on induction of rpS6 phosphorylation the selective S6K1 inhibitor, PF4708671, was locally infused into the dentate gyrus. PF4708671 is a specific inhibitor for S6K1 and does not target S6K2 (Pearce et al., 2010). Local delivery of PF4708671 did not alter basic synaptic transmission. Following replacement of the saline-filled micropipette with the PF4708671-filled micropipette, there was a decrease in response amplitude and slope. The response amplitude remained stable at 93.84 ± 45.03% (mean ± SEM, N=7) of baseline for the population spike and 88.13 ± 39.23% (N=7) of baseline for EPSP slope. A population spike below 1.5mV was recorded for four cases (0.16-1.3mV) when recording synaptic responses. The baseline with the excluded cases was 83.53 ± 20.56% of baseline (N=3) for population spike amplitude and 81.64 ± 5.47% of baseline (N=3) for EPSP slope. Following the delivery of 30 trains of HFS, the percent change from baseline recorded via the PF4708671 micropipette was -6.34 ± 8.98% (N=3) compared to 28.32 ± 3.34% (N=6) in control experiments with saline-filled micropipettes ($p=0.0027$; $t(7)=4.533$; student's t-test for unpaired samples; percent change from baseline with all cases was -10.25 ± 31.14%, N=7).

Immunostaining for p-ser235/236 revealed the expected robust activation of rpS6 phosphorylation in areas distant from the PF4708671-filled microelectrode (Figure 4A and 4B). In areas near the PF4708671-filled microelectrode, there was reduction in the intensity level of immunostaining for rpS6 phosphorylation in the granule cell layer (Figure 4E and 4F). The pattern of immunostaining for phosphorylated rpS6-positive granule cells

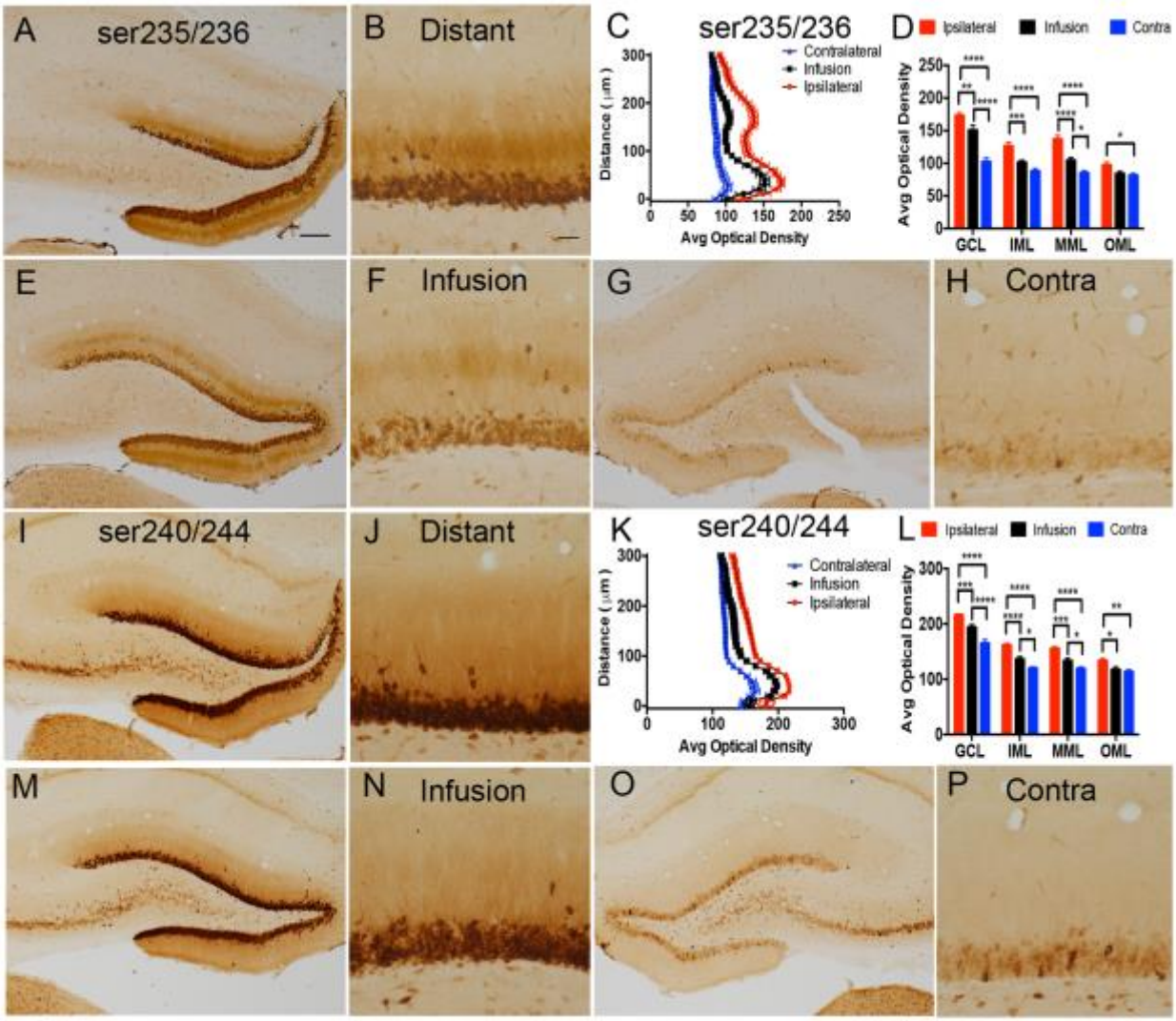

Figure 3.4. Local infusion of the S6K1 inhibitor, PF4708671, attenuates phosphorylation of rpS6 in cell bodies and dendrites. A, Immunostaining for p-ser235/236 ipsilateral to stimulation in a section distant from the infusion area. **B,** High-magnification image of A. **C,** Quantification of average OD across the dorsal blade of the dentate gyrus in ipsilateral sections distant from the injection site, ipsilateral sections within the infusion area, and contralateral, non-stimulated sections. **D,** Statistical assessment at four sites along the dentate gyrus, GCL, IML, MML, OML (ser235/236, N=7), error bars represent SEM. Statistical assessment by two-way ANOVA revealed a significant interaction ($F(6,72)=7.89$, $p<0.0001$), a significant main effect of treatment ($F(2,72)=94.99$, $p<0.0001$) and a significant main effect of region ($F(3,72)=75.68$, $p<0.0001$). Post-hoc analysis with Bonferroni's multiple comparisons tests revealed that ipsilateral sections were statistically different than sections within the infusion area and contralateral sections in the GCL, IML, and MML. Ipsilateral sections were also significantly different than contralateral sections in the OML. Notably, sections within the infusion area were also statistically different than contralateral sections in the GCL and MML (Two-way ANOVA, N=7, $p<0.05$). **E,** Immunostaining of p-ser235/236 ipsilateral to the stimulation in a section within the infusion area in the presence of PF4708671. **F,** High-magnification image of E. Note local infusion of PF4708671 attenuates phosphorylation of rpS6 in the GCL and throughout the molecular layer of dentate gyrus. The

distinct band of rpS6 phosphorylation remained discernable. **G,** Immunostaining of p-ser235/236 contralateral to the stimulation. **H,** High-magnification image of G. **I,** Immunostaining of p-ser240/244 in a section distant from the infusion area. **J,** High-magnification image of I. **K,** Quantification of average OD across the dorsal blade of the dentate gyrus in ipsilateral sections distant from the injection site, ipsilateral sections within the infusion area, and contralateral sections. **L,** Statistical assessment at four sites along the dentate gyrus, GCL, IML, MML, OML (ser240/244, N=7), error bars represent SEM. Statistical assessment by two-way ANOVA revealed a significant interaction ($F(6,72)=3.04$, $p=0.0105$, a significant main effect of treatment ($F(2,72)=87.07$, $p<0.0001$) and a significant main effect of region ($F(3,72)=174.83$, $p<0.0001$). Post-hoc analysis with Bonferroni's multiple comparisons tests revealed that ipsilateral sections were statistically different than sections within the infusion area and contralateral sections in all regions. Notably, sections within the infusion area were also statistically different than contralateral sections in the GCL, IML, and MML (Two-way ANOVA, N=7, $p<0.05$). **M,** Immunostaining of p-ser240/244 ipsilateral to stimulation within the infusion area in the presence of PF4708671. **N,** High-magnification image of M. **O,** Immunostaining of p-ser240/244 contralateral to the stimulation. **P,** High-magnification image of O. Scale bars: **A,** 200μm; **B,** 50 μm.

was more scattered with very few fully activated rpS6-positive cells and a larger number of moderate to low level of phosphorylated rpS6-positive cells (Figure 4F). In the dendritic layers, there was also an attenuation in the intensity level of rpS6 immunostaining throughout the dendritic laminae that remained elevated compared to controls (Figure 4G and 4H). The distinct band of rpS6 phosphorylation in the MML remained discernable (Figure 4F) but not to the same intensity level as observed in areas distant from the infusion area (Figure 4B). For p-ser240/244, immunostaining of sections distant from the infusion area revealed the expected robust phosphorylation of rpS6 (Figure 4I and 4J). In sections within the infusion area, there was a reduction in the intensity level of phosphorylated rpS6-positive cells the granule cell layer (Figure 4N) compared to the densely packed activation of granule cells observed in distant regions (Figure 4J). In the dendritic layers, there was a reduction in the intensity level of immunostaining for rpS6 phosphorylation throughout the molecular layer of the dentate gyrus, but not to the same level observed in controls (Figure 4O and 4P).

To quantify the effects of PF4708671, the graphs show representative cases for each condition (Ipsilateral, Infusion, Contra) plotted as average OD values measured across the dorsal blade of the dentate gyrus from the GCL to the OML (Figure 4C and 4K). To provide a statistical analysis of the blockade, we calculated the average OD at four measuring sites for comparison: (GCL, IML, MML, OML). Quantitative comparisons of levels of immunostaining for ipsilateral, infusion and contralateral sections in each of the four measuring sites by two-way ANOVA yielded an overall $F(6,72)=7.89$, $p<0.0001$ (N=7, Figure 4D) for p-ser235/236 and $F(6,72)=3.04$, $p=0.0105$ (N=7, Figure 4L) for p-ser240/244. Post-hoc analysis with Bonferroni's multiple comparisons tests revealed that ipsilateral sections

were statistically different than sections within the infusion area and contralateral sections in the GCL, IML, and MML. Ipsilateral sections were also significantly different than contralateral sections in the OML. Notably, sections within the infusion area were also statistically different than contralateral sections in the GCL and MML for p-ser235/236 (Figure 4D; N=7, Two-way ANOVA, $p<0.05$). For p-ser240/244, post-hoc analysis with Bonferroni's multiple comparisons tests revealed that ipsilateral sections were statistically different than sections within the infusion area and contralateral sections in all regions. Notably, sections within the infusion area were also statistically different than contralateral sections in the GCL, IML, and MML (Figure 4L; N=7, Two-way ANOVA, $p<0.05$). Taken together these results reveal that S6K1 contributes to p-ser235/236 predominately in the IML, but also contributes to phosphorylation in the GCL and MML. Moreover, S6K1 contributes to phosphorylation of ser240/244 in the granule cell layer and molecular layer of the dentate gyrus.

MAPK/ERK-dependent signaling regulates dendritic phosphorylation of rpS6

Accumulating evidence suggests that activation of ERK is involved in synaptic plasticity and learning and memory (Impey et al., 1999; Mazzucchelli and Brambilla, 2000; Sweatt, 2001). Studies show that ERK activation is required for inducible phosphorylation of translation initiation factors including rpS6, eIF4E, and 4EBP (Kelleher et al., 2004). As a result, it is proposed that mTOR and MAPK/ERK signaling interact to regulate activity-dependent translational control (Kelleher et al., 2004). To determine the involvement of the MAPK signaling pathway in induction of rpS6 phosphorylation, the MEK inhibitor, U0126, was locally infused into the dentate gyrus. U0126 inhibits activation of ERK1/2 by inhibiting the kinase activity of MEK1/2 (Favata et al., 1998). Local delivery of U0126 into

the dentate gyrus was done using a Hamilton syringe. Evoked potentials were recorded by connecting leads directly to the metal barrel of the Hamilton microsyringe. A total volume of 0.1-0.2µl was injected via Hamilton syringe into the dorsal blade of the dentate gyrus before HFS. Post infusion, no test responses were taken for a 30-minute period, then a 15-minute post infusion baseline was recorded. For U0126 experiments, placement of the Hamilton syringe in the granule cell layer resulted in a rapid decrease in response amplitude and EPSP slope. Following delivery of the drug, there was a further decrease in response amplitude of the population spike that remained stable at 50.49 ± 6.16% (mean ± SEM, N=7) of baseline and EPSP slope stabilized at 57.83 ± 10.15% (N=7) of baseline. A population spike below 1.5mV was recorded for five cases (0.28-0.96mV) when recording synaptic responses. The baseline with the excluded cases was 53.18 ± 17.54% of baseline (N=2) for population spike amplitude and 40.17 ± 20.31% of baseline for EPSP slope (N=2). Following delivery of HFS trains, the percent change from baseline recorded via the U0126 Hamilton syringe was -72.31 ± 4.35% (N=2) compared to 28.32 ± 3.34% (N=6) in control experiments with saline-filled micropipettes ($p<0.0001$; $t(6)=15.63$; student's t-test for unpaired samples; the percent change from baseline for all cases was -43.29 ± 9.85%, N=7).

To confirm the effect of U0126, immunostaining of phosphorylated ERK1/2 (p-ERK) was used as a positive control (Huang et al., 2007). In areas within the U0126 infusion site, p-ERK activation was completely blocked (Figure 5A and 5B). In sections outside of the infusion area, there was increased p-ERK immunostaining in the granule cell layer and the dendritic laminae (Figure 5C and 5D). Immunostaining for p-ser235/236 in areas distant from the infusion site revealed the expected robust induction of rpS6 phosphorylation (Figure 5E and 5F). In areas within the U0126 infusion site, there was a reduction in the

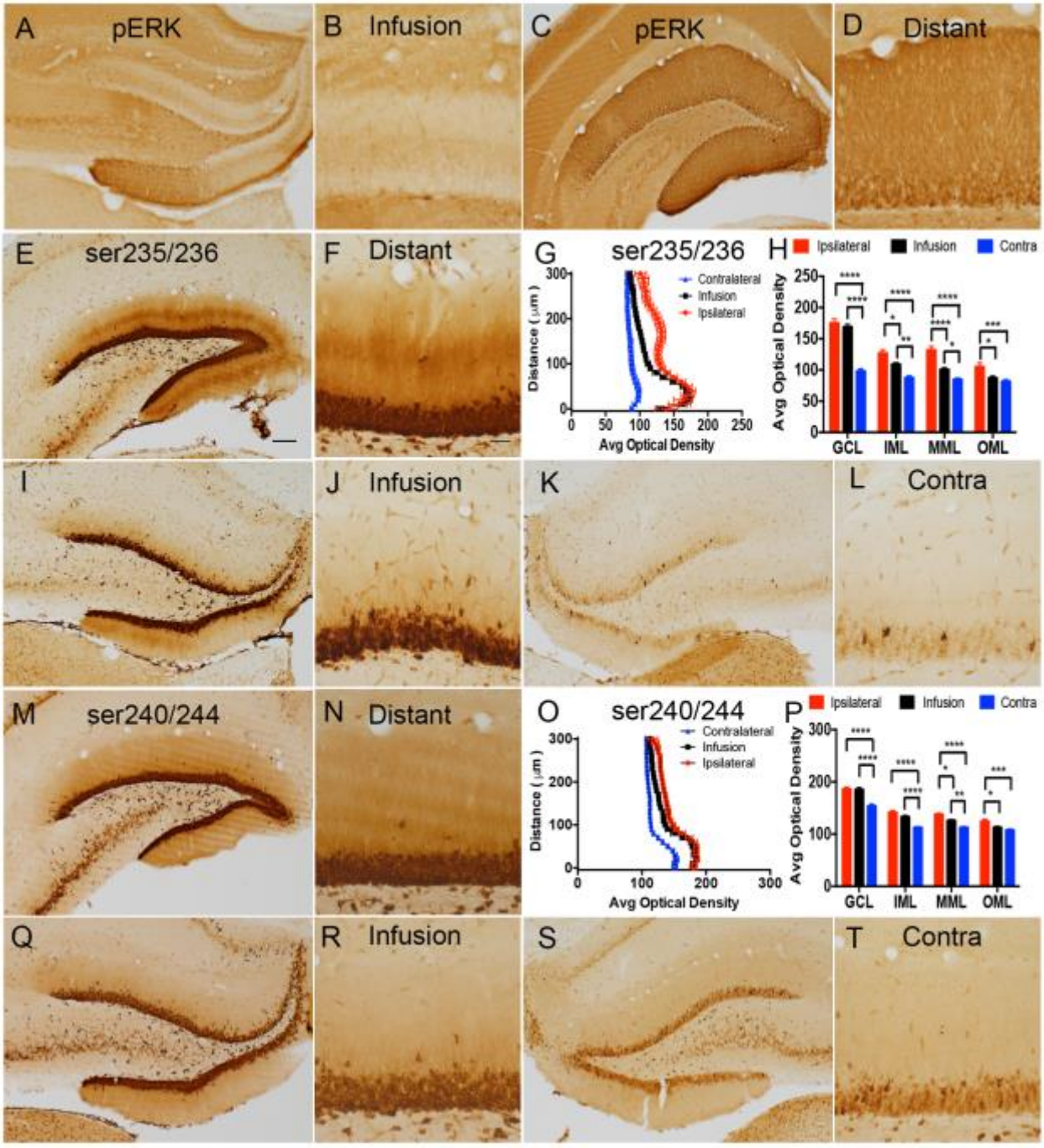

Figure 3.5. Local infusion of the MEK inhibitor, U0126, attenuates dendritic phosphorylation of rpS6. A, Immunostaining of phospho-ERK in section within the infusion area. **B,** High-magnification image of A. **C,** Immunostaining of phospho-ERK in section outside of the infusion area. **D,** High-magnification image of C. **E,** Immunostaining for p-ser235/236 ipsilateral to stimulation in a section distant from the infusion area. **F,** High-magnification image of E. **G,** Quantification of average OD across the dorsal blade of the dentate gyrus in ipsilateral sections distant from the injection site, ipsilateral sections within the infusion area, and contralateral, non-stimulated sections. **H,** Statistical assessment at four sites along the dentate gyrus, GCL, IML, MML, OML (ser235/236, N=7), error bars represent SEM. Statistical assessment by two-way ANOVA

revealed a significant interaction ($F(6,72)=13.02$, $p<0.0001$), a significant main effect of treatment ($F(2,72)=121.41$, $p<0.0001$) and a significant main effect of region ($F(3,72)=94.30$, $p<0.0001$). Post-hoc analysis with Bonferroni's multiple comparisons tests revealed a significant difference between ipsilateral sections and contralateral sections at all measuring sites. There was also a significant difference between sections within the infusion area and contralateral sections in the GCL, IML, and MML. Notably, there was a significant difference between ipsilateral sections and sections within the infusion area in the IML, MML, and OML (Two-way ANOVA, N=7, $p<0.05$). **I,** Immunostaining of p-ser235/236 ipsilateral to the stimulation in a section within the infusion area in the presence of U0126. **J,** High-magnification image of I. Note local infusion of U0126 reduces phosphorylation of rpS6 throughout the molecular layer of dentate gyrus. The distinct band of rpS6 phosphorylation is not discernable. **K,** Immunostaining of p-ser235/236 contralateral to the stimulation. **L,** High-magnification image of K. **M,** Immunostaining of p-ser240/244 in a section distant from the infusion area. **N,** High-magnification image of M. **O,** Quantification of average OD across the dorsal blade of the dentate gyrus in ipsilateral sections distant from the injection site, ipsilateral sections within the infusion area, and contralateral sections. **P,** Statistical assessment at four sites along the dentate gyrus, GCL, IML, MML, OML (ser240/244, N=7), error bars represent SEM. Statistical assessment by two-way ANOVA revealed a significant interaction ($F(6,72)=3.89$, $p=0.0020$, a significant main effect of treatment ($F(2,72)=83.75$, $p<0.0001$) and a significant main effect of region ($F(3,72)=254.91$, $p<0.0001$). Post-hoc analysis with Bonferroni's multiple comparisons tests revealed a significant difference between ipsilateral sections and contralateral sections at all measuring sites. There was also a significant difference between sections within the infusion area and contralateral sections in the GCL, IML, and MML. Notably, there was also a significant difference between ipsilateral sections and sections within the infusion area in the MML and OML (Two-way ANOVA, N=7, $p<0.05$). **Q,** Immunostaining of p-ser240/244 ipsilateral to stimulation within the infusion area in the presence of U0126. **R,** High-magnification image of Q. Note the reduction of rpS6 phosphorylation in the dendritic laminae. **S,** Immunostaining of p-ser240/244 contralateral to the stimulation. **T,** High-magnification image of S. Scale bars: **A,** 200μm; **B,** 50 μm.

intensity level of immunostaining for rpS6 phosphorylation predominately in the dendritic laminae (Figure 5I and 5J). In the granule cell layer, there was robust rpS6 phosphorylation (Figure 5J) similar to areas outside of the infusion site (Figure 5F). In the dendritic laminae, activation of rpS6 phosphorylation resembled a gradient-effect where the IML had the greatest levels of rpS6 phosphorylation; the MML had intermediate levels of rpS6 phosphorylation, and the OML had the lowest levels of rpS6 phosphorylation similar to control non-stimulated sections (Figure 5K and 5L). The discernable band of rpS6 phosphorylation in the MML was not discernable. Immunostaining for p-ser240/244 in areas distant from the infusion site revealed the expected robust induction of rpS6 phosphorylation (Figure 5M and 5N). Within the infusion area, the granule cell layer showed robust rpS6 phosphorylation (Figure 5Q and 5R). In the dendritic laminae, immunostaining of rpS6 phosphorylation was reduced to levels comparable to control non-stimulated sections in the OML (Figure 5S and 5T), while MML and IML remained elevated above control levels.

To quantify effects of the U0126 blockade, levels of immunostaining were assessed by determining average OD across the dorsal blade of the dentate gyrus. The graphs show representative cases for each condition (Ipsilateral, Infusion, Contra) plotted as average OD values measured across the dorsal blade of the dentate gyrus from the GCL to the OML (Figure 5G and 5O). To provide a statistical analysis of the blockade, we calculated the average OD at four measuring sites for comparison: (GCL, IML, MML, OML). Quantitative comparisons of levels of immunostaining for ipsilateral, infusion and contralateral sections in each of the four measuring sites by two-way ANOVA yielded an overall $F(6, 72) = 13.02$, $p<0.0001$ (N=7, Figure 5H) for p-ser235/236 and an overall $F(6, 72) = 3.89$, $p=0.002$ (N=7,

Figure 5P) for p-ser240/244. Post-hoc analysis with Bonferroni's multiple comparisons tests revealed a significant difference between ipsilateral sections and contralateral sections at all measuring sites. There was also a significant difference between sections within the infusion area and contralateral sections in the GCL, IML, and MML. Notably, there was a significant difference between ipsilateral sections and sections within the infusion area in the IML, MML, and OML (Figure 5H; N=7, Two-way ANOVA, $p<0.05$) for p-ser235/236. For p-ser240/244, post-hoc analysis with Bonferroni's multiple comparisons tests revealed a significant difference between ipsilateral sections and contralateral sections at all measuring sites. There was also a significant difference between sections within the infusion area and contralateral sections in the GCL, IML, and MML. Notably, there was also a significant difference between ipsilateral sections and sections within the infusion area in the MML and OML (Figure 5P; N=7, Two-way ANOVA, $p<0.05$). In summary, delivery of U0126 did not affect granule cell immunostaining of rpS6 phosphorylation for either ser235/236 or ser240/244. For p-ser235/236, there was decreased immunostaining in the IML and MML, and complete blockade in the OML. For p-ser240/244, there was reduced immunostaining predominately in the MML and complete blockade in the OML. Collectively, these data indicate that MAPK/ERK plays a minimal role in granule cell activation of rpS6 phosphorylation and contributes predominately to dendritic phosphorylation of rpS6 at both p-ser235/236 and p-ser240/244.

Local inhibition of RSK attenuates rpS6 phosphorylation in dendrites and cell bodies

Phosphorylation of rpS6 at ser235/236 is regulated by S6K1 and S6K2 and the p90 ribosomal protein S6 kinase (RSK) (Roux et al., 2007). There is evidence that S6K2 is activated by both mTOR and MAPK/ERK (Wang et al., 2001; Holz et al., 2005), but RSK

activation is believed to be exclusively targeted by the MAPK/ERK signaling pathway [reviewed in (Anjum and Blenis, 2008)]. The degree to which these kinases contribute to the regulation of rpS6 phosphorylation in granule cell bodies vs. dendrites in response to synaptic activity remains unclear. To determine the contribution of RSK in regulating rpS6 phosphorylation in response to synaptic activity, the selective RSK inhibitor, SL0101-1 was locally infused into the dentate gyrus during HFS. Following replacement of a saline-filled micropipette, with an SL0101-1-filled micropipette, there was a small decrease in response amplitude that stabilized at 83.77 ± 9.46 % (mean ± SEM, N=7) of baseline and 83.86 ± 7.60% of baseline for EPSP slope (N=7). A population spike below 1.5mV was recorded from one case (1.3mV) when recording synaptic responses. The baseline with the excluded cases was 91.21 ± 6.91% of baseline (N=6) for population spike amplitude and 83.59 ± 8.99% of baseline (N=6) for EPSP slope. Following delivery of HFS trains, the percent change from baseline recorded via the SL0101-1 micropipette was 24.01 ± 14.33% (N=6) compared to 28.32 ± 3.34% (N=6) in control experiments with saline-filled micropipettes ($p=0.7757$; $t(10)=0.2927$; student's t-test for unpaired samples; the percent change from baseline for all cases was 24.1 ± 12.11%, N=7).

Immunostaining for p-ser235/236 revealed the expected induction of rpS6 phosphorylation in areas distant from the SL0101-1 infusion area (Figure 6A and 6B). In the infusion area, there was an overall reduction in rpS6 phosphorylation in both the granule cell layer and the dendritic layers (Figure 6E and 6F). In the granule cell layer, there was reduction in the level of intensity of immunostaining for rpS6 phosphorylation and a scattered pattern of granule cell activation. In the dendritic laminae, there was an attenuation of rpS6 phosphorylation throughout the molecular layers that remained

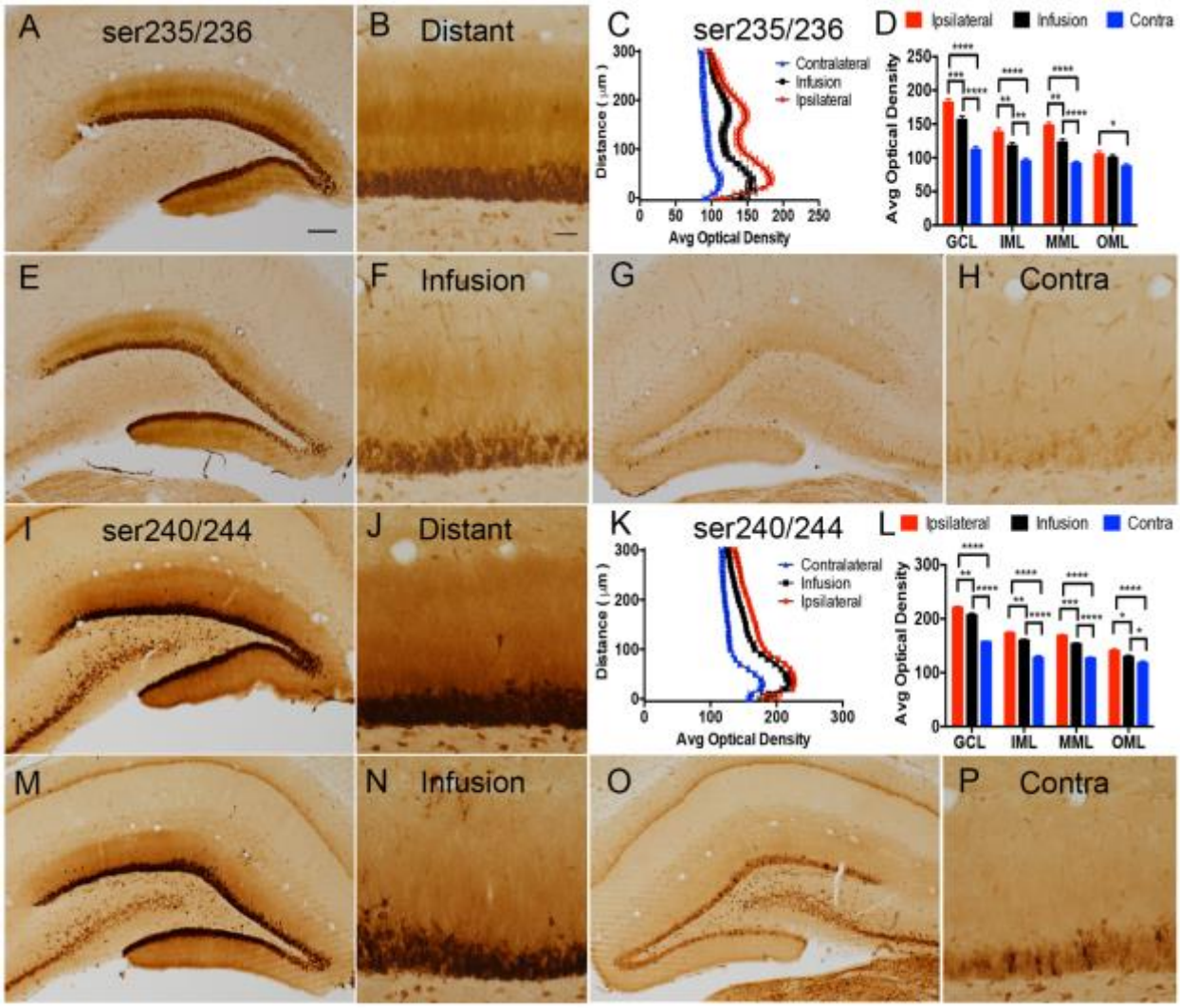

Figure 3.6. Local infusion of RSK inhibitor, SL0101-1, attenuates phosphorylation of rpS6 in granule cell bodies and dendrites. A, Immunostaining for p-ser235/236 ipsilateral to stimulation in a section distant from the infusion area. **B,** High-magnification image of A. **C,** Quantification of average OD across the dorsal blade of the dentate gyrus in ipsilateral sections distant from the injection site, ipsilateral sections within the infusion area, and contralateral, non-stimulated sections. **D,** Statistical assessment at four sites along the dentate gyrus, GCL, IML, MML, OML (ser235/236, N=7), error bars represent SEM. Statistical assessment by two-way ANOVA revealed a significant interaction ($F(6,72)=5.74$, $p<0.0001$), a significant main effect of treatment ($F(2,72)=97.02$, $p<0.0001$) and a significant main effect of region ($F(3,72)=62.56$, $p<0.0001$). Post-hoc analysis with Bonferroni's multiple comparisons tests revealed a significant difference between ipsilateral sections and contralateral sections in all regions. There was also a significant difference between ipsilateral sections and sections within the infusion area in the GCL, IML, and MML. Notably, there was a significant difference between sections within the infusion area and contralateral sections in the GCL, IML, and MML (Two-way ANOVA, N=7, $p<0.05$). **E,** Immunostaining of p-ser235/236 ipsilateral to the stimulation in a section within the infusion area in the presence of SL0101-1. **F,** High-magnification image of E. Note local infusion of SL0101-1

attenuates phosphorylation of rpS6 in the GCL and throughout the molecular layer of dentate gyrus. The distinct band of rpS6 phosphorylation remained elevated above control levels. **G,** Immunostaining of p-ser235/236 contralateral to the stimulation. **H,** High-magnification image of G. **I,** Immunostaining of p-ser240/244 in a section distant from the infusion area. **J,** High-magnification image of I. **K,** Quantification of average OD across the dorsal blade of the dentate gyrus in ipsilateral sections distant from the injection site, ipsilateral sections within the infusion area, and contralateral sections. **L,** Statistical assessment at four sites along the dentate gyrus, GCL, IML, MML, OML (ser240/244, N=7), error bars represent SEM. Statistical assessment by two-way ANOVA revealed a significant interaction ($F(6,72)=11.75$, $p<0.0001$, a significant main effect of treatment ($F(2,72)=258.42$, $p<0.0001$) and a significant main effect of region ($F(3,72)=295.49$, $p<0.0001$). Post-hoc analysis with Bonferroni's multiple comparisons tests revealed that ipsilateral sections were statistically different than sections within the infusion area and contralateral sections in all regions. There was also a significant difference between sections within the infusion area and contralateral sections in all regions (Two-way ANOVA, N=7, $p<0.05$). **M,** Immunostaining of p-ser240/244 ipsilateral to stimulation within the infusion area in the presence of SL0101-1. Note the reduction of rpS6 phosphorylation throughout the molecular layers of the dentate gyrus. **N,** High-magnification image of M. **O,** Immunostaining of p-ser240/244 contralateral to the stimulation. **P,** High-magnification image of O. Scale bars: **A,** 200μm; **B,** 50 μm.

elevated compared to control non-stimulated sections (Figure 6G and 6H). The band of rpS6 phosphorylation in the MML remained discernable (Figure 6F). Immunostaining for p-ser240/244 also revealed the expected robust induction of rpS6 phosphorylation in areas distant from the SL101-1 infusion site (Figure 6I and 6J). In sections within the infusion area, there was a decrease in immunostaining for rpS6 phosphorylation predominately in the dendritic regions (Figure 6M and 6N). The granule cell bodies within the infusion region (Figure 6N) revealed robust rpS6 phosphorylation similar to the densely packed granule cells of sections distant from the infusion area (Figure 6J). In the dendritic layers, there was a reduction in the level of intensity of immunostaining for rpS6 phosphorylation throughout the molecular layer that remained elevated compared to control, non-stimulated sections (Figure 6O and 6P).

Average OD values in ipsilateral, infusion and contralateral sections were measured to quantify the effects RSK inhibition on induction of rpS6 phosphorylation. The graphs show representative cases for each condition (Ipsilateral, Infusion, Contra) plotted as average OD values measured across the dorsal blade of the dentate gyrus from the GCL to the OML (Figure 6C and 6K). To provide a statistical analysis of the blockade, average OD was calculated at four measuring sites for comparison: (GCL, IML, MML, OML). Quantitative comparisons of levels of immunostaining for ipsilateral, infusion and contralateral sections in each of the four measuring sites by two-way ANOVA yielded an overall $F(6,72)=5.74$, $p<0.0001$ for p-ser235/236 (N=7, Figure 6D) and an overall $F(6,72)=11.75$, $p<0.0001$ for p-ser240/244 (N=7, Figure 6L). Post-hoc analysis with Bonferroni's multiple comparisons tests revealed a significant difference between ipsilateral sections and contralateral sections in all regions for p-ser235/236. There was also a significant difference between

ipsilateral sections and sections within the infusion area in the GCL, IML, and MML. Notably, there was a significant difference between sections within the infusion area and contralateral sections in the GCL, IML, and MML (Figure 6D; Two-way ANOVA, N=7, $p<0.05$). For p-ser240/244, post-hoc analysis with Bonferroni's multiple comparisons tests revealed that ipsilateral sections were statistically different than sections within the infusion area and contralateral sections in all regions. There was also a significant difference between sections within the infusion area and contralateral sections in all regions (Figure 6L; Two-way ANOVA, N=7, $p<0.05$). Together these data indicate that RSK contributes to the regulation of rpS6 in both cell bodies and dendrites, which is in contrast to U0126 treatment that does not target granule cell activation.

Phosphorylation of rpS6 at ser235/236 detected in synaptic plasma membrane fraction

Glutamatergic synapses are well-known for their ability to undergo synaptic modifications during development and in the adult mature brain (Feldman and Knudsen, 1998). These synaptic modifications play a role in modifying properties of neural circuits and meeting cellular requirements in response to changes in the local environment. Studies have demonstrated that LTP induction alters dendritic morphology and results in the growth of new spines (Engert and Bonhoeffer, 1999; Maletic-Savatic et al., 1999). Thus, we asked if synaptic activity regulated trafficking of phosphorylated rpS6 to and from synaptic sites, indicating a role for rpS6 phosphorylation in activity-dependent synaptic modifications at the postsynaptic density. Subcellular fractionation studies revealed that phosphorylated rpS6 at ser235/236 was abundant in synaptic plasma membrane fractions (Figure 7A). Phosphorylated rpS6 was normalized to the total rpS6 protein (Figure 7B).

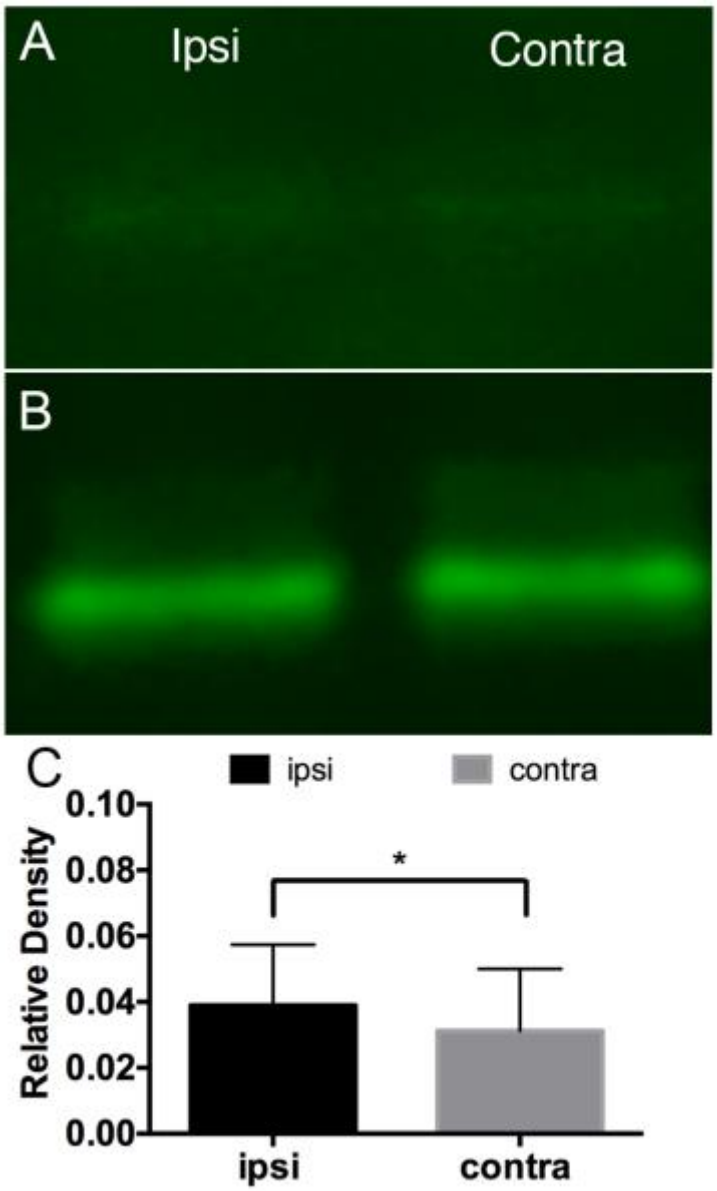

Figure 3.7. Phosphorylated rpS6 is present in synaptic plasma membrane fractions. A, Representative immunoblots showing phosphorylation of rpS6 at ser235/236 post 1 hour HFS for ipsilateral (stimulated) and contralateral (non-stimulated) hippocampi following SPM fractionation. B, Total rpS6 in same samples. C, Quantification of western blot assay for SPM fractions. Phosphoprotein levels were normalized to total protein levels. Bar graphs show average relative density (±SEM). N=2.

Quantification of band signal intensity using Image Studio (LI-COR) revealed a significant difference between stimulated (ipsi) and non-stimulated (contra) SPM fractions (Figure 7C; p=0.0281; t(1)=22.68; student's t-test).

DISCUSSION

This study demonstrates that rpS6 phosphorylation sites, ser235/236, and ser240/244, are differentially activated in the dentate gyrus by mTOR- and MAPK/ERK-dependent signaling pathways following perforant path stimulation. Results show novel findings that indicate PI3-Kinase/mTOR-dependent activation of rpS6 phosphorylation at ser235/236 predominantly in the granule cell bodies, while MAPK/ERK signaling regulates activation in the dendritic laminae. This study also shows the novel finding that phosphorylation of ser240/244 is also regulated by MAPK/ERK-dependent signaling in dentate granule cells. This differential regulation of rpS6 phosphorylation by mTOR and MAPK/ERK signaling pathways points to a potential mechanism by which induction of rpS6 phosphorylation may regulate local translation selectively at activated synapses.

mTOR- and MAPK-dependent signaling pathways differentially regulate rpS6 phosphorylation in cell bodies and dendrites

mTOR is a serine/threonine protein kinase that plays a critical role in protein synthesis in response to nutritional and growth stimuli. Activation of mTOR has been shown to be critical for the acquisition spatial learning tasks (Qi et al., 2010) and LTP induction (Tang et al., 2002). MAPKs are a family of serine/threonine protein kinases that regulate cell proliferation and differentiation. Activation of MAPK/ERK is reported to play a role in L-LTP and memory consolidation (Kelleher et al., 2004). Independently, mTOR and

MAPK have been demonstrated to be critical for synaptic function, plasticity and cognition (Tang et al., 2002; Kelleher et al., 2004; Sweatt, 2004; Qi et al., 2010). Yet, how these pathways interact to regulate synaptic plasticity remains unclear. Here we show that local infusion of the PI3-kinase inhibitor, wortmannin, selectively blocked phosphorylation of rpS6 in the granule cell bodies, while leaving the band of rpS6 phosphorylation in the activated region, the MML, intact. Surprisingly, phosphorylation of rpS6 at ser240/244 revealed a distinct pattern showing an attenuation of immunostaining for rpS6 phosphorylation in both granule cell bodies and dendritic layers. These results point to the surprising conclusion that PI3-kinase regulates induction of rpS6 phosphorylation predominantly in the granule cell bodies, particularly at p-ser235/236. PI3-kinase contributes to phosphorylation of rpS6 at ser240/244 in both cell bodies and dendrites. These results illustrate how mTOR and MAPK signaling pathways can differentially target subcellular compartments in dentate granule cells to achieve translational control in response to synaptic activity.

Local inhibition of mTOR by local delivery of rapamycin reveals mTOR-dependent phosphorylation of rpS6 in cell bodies

Several studies demonstrate that treatment with rapamycin inhibits learning-induced and LTP-induced phosphorylation of translation-related factors and protein synthesis (Tang et al., 2002; Kelleher et al., 2004; Qi et al., 2010). Phosphorylation events that regulate activity or availability of translation-related factors are critical in the control of protein synthesis and growth (Raught et al., 2000). Thus, it is essential to understand mechanisms linking molecular signal transduction pathways to substrates involved in translational control. Here we show that local delivery of the mTOR inhibitor, rapamycin,

abolished induction of rpS6 phosphorylation in both granule cell bodies and dendrites for ser235/236 and ser240/244. Interestingly, when a specific S6K1 inhibitor was locally infused, there was only an attenuation of rpS6 phosphorylation indicating that mTOR may be a critical player in coordinating signaling inputs from signal transduction pathways. With the selective inhibition of S6K1 other kinases remain available to activate phosphorylation of rpS6, for example, S6K2 and RSK. Also, in contrast to local inhibition of PI3-kinase that selectively abolished phosphorylation of rpS6 in cell bodies, inhibition of mTOR results in a complete blockade of rpS6 phosphorylation. Here, it is possible that PI3-kinase activation inhibits downstream signaling from mTOR, but the dendritic layers may receive input from MAPK/ERK-dependent signaling as it has been shown to feed into the PI3-kinase pathway by phosphorylating S6K2 (Wang et al., 2001; Holz et al., 2005). These findings reveal mTOR as a critical regulator of rpS6 phosphorylation indicating a role in coordinating input from various signal transduction pathways to activate phosphorylation of rpS6.

MAPK/ERK regulates phosphorylation of rpS6 in dendrites

Accumulating evidence implicates a role for MAPK/ERK in synaptic plasticity and learning and memory (Impey et al., 1999; Sweatt, 2004). MAPK/ERK has been implicated to play a role in spatial memory, LTP, and as a regulator of translation (Kelleher et al., 2004). In fact, studies have shown that MAPK/ERK activation is critical for the induction of translation-related factors, including rpS6, eIF4E, and 4EBP (Kelleher et al., 2004). But these studies report results from hippocampal homogenates or synaptoneurosomes, so mechanisms detailing the precise localization of translation-related factors in response to synaptic activity remains obscure. Here we show that local infusion of the MEK inhibitor,

U0126, attenuated rpS6 phosphorylation predominately in the dendritic laminae, leaving phosphorylation of rpS6 in the granule cell bodies intact. A gradient-like effect was observed with higher levels of immunostaining present in the IML, intermediate levels present in the MML, and low levels of immunostaining comparable to controls were observed in the OML. Notably, the distinct band of rpS6 phosphorylation in the activated region was not apparent. These results suggest that MAPK/ERK predominantly regulates rpS6 phosphorylation in the dendritic laminae. Interestingly, when the selective RSK inhibitor, SL0101-1 was locally infused there was only an attenuation of rpS6 phosphorylation throughout the granule cell layer and molecular layers. These results indicate that similar to inhibition of mTOR, key substrates are required for the induction of rpS6 phosphorylation. Here the results show that activation of MAPK/ERK is critical for induction of rpS6 phosphorylation in the dendritic laminae. Furthermore, with the selective inhibition of RSK, compensatory signaling from the mTOR-dependent kinases, remain available to phosphorylate rpS6.

Phosphorylation of rpS6 as a mechanism to regulate activity-dependent synaptic modifications via mTOR and MAPK/ERK signaling

Our results show that both mTOR and MAPK/ERK regulate phosphorylation of rpS6 differentially in the granule cell bodies vs. the dendrites. These results support hypotheses implicating mTOR and MAPK/ERK in activity-dependent translational control. Here we show a mechanism by which, mTOR and MAPK/ERK may regulate activity-dependent translation by targeting specific phosphorylation sites on rpS6. Furthermore, we show that phosphorylated rpS6 is abundant in SPM fractions, implicating that phosphorylated rpS6 is transported out synapses where it may regulate local translation. Overall, these findings

suggest that induction of rpS6 phosphorylation via MAPK/ERK-dependent signaling may regulate phosphorylation at activated dendritic domains implicating a role in dendritic protein synthesis, while PI3-kinase/mTOR regulate general translation in the granule cell bodies. Most importantly, we show that activation of mTOR is critical for the induction of rpS6 phosphorylation in both granule cell bodies and dendrites, and MAPK/ERK is critical for the induction of rpS6 in activated dendritic domains. Future studies investigating the translational efficiency achieved by the interaction of mTOR and MAPK/ERK signaling in response to neuronal activity will provide further insights on the contribution of signal transduction pathways in synaptic plasticity and learning and memory.

REFERENCES

Anjum R, Blenis J (2008) The RSK family of kinases: emerging roles in cellular signalling. Nat Rev Mol Cell Biol 9:747-758.

Arcaro A, Wymann MP (1993) Wortmannin is a potent phosphatidylinositol 3-kinase inhibitor: the role of phosphatidylinositol 3,4,5-trisphosphate in neutrophil responses. Biochem J 296 (Pt 2):297-301.

Biever A, Puighermanal E, Nishi A, David A, Panciatici C, Longueville S, Xirodimas D, Gangarossa G, Meyuhas O, Herve D, Girault JA, Valjent E (2015) PKA-dependent phosphorylation of ribosomal protein S6 does not correlate with translation efficiency in striatonigral and striatopallidal medium-sized spiny neurons. J Neurosci 35:4113-4130.

Blackstone CD, Moss SJ, Martin LJ, Levey AI, Price DL, Huganir RL (1992) Biochemical characterization and localization of a non-N-methyl-D-aspartate glutamate receptor in rat brain. J Neurochem 58:1118-1126.

Collingridge GL, Bliss TVP (1987) NMDA receptors - their role in long-term potentiation. Trends in Neurosciences 10:288-293.

Dufner A, Thomas G (1999) Ribosomal S6 kinase signaling and the control of translation. Exp Cell Res 253:100-109.

Engert F, Bonhoeffer T (1999) Dendritic spine changes associated with hippocampal long-term synaptic plasticity. Nature 399:66-70.

Farris S, Lewandowski G, Cox CD, Steward O (2014) Selective Localization of Arc mRNA in Dendrites Involves Activity- and Translation-Dependent mRNA Degradation. J Neurosci 34:4481-4493.

Favata MF, Horiuchi KY, Manos EJ, Daulerio AJ, Stradley DA, Feeser WS, Van Dyk DE, Pitts WJ, Earl RA, Hobbs F, Copeland RA, Magolda RL, Scherle PA, Trzaskos JM (1998)

Identification of a novel inhibitor of mitogen-activated protein kinase kinase. J Biol Chem 273:18623-18632.
Feldman DE, Knudsen EI (1998) Experience-dependent plasticity and the maturation of glutamatergic synapses. Neuron 20:1067-1071.
Ferrari S, Thomas G (1994) S6 Phosphorylation and the p70s6k /p85s6k. Critical Reviews in Biochemistry and Molecular Biology 29:385-413.
Flotow H, Thomas G (1992) Substrate recognition determinants of the mitogen-activated 70K S6 kinase from rat liver. J Biol Chem 267:3074-3078.
Frey JU (2001) Long-lasting hippocampal plasticity: cellular model for memory consolidation? Results Probl Cell Differ 34:27-40.
Gangarossa G, Valjent E (2012) Regulation of the ERK pathway in the dentate gyrus by in vivo dopamine D1 receptor stimulation requires glutamatergic transmission. Neuropharmacology 63:1107-1117.
Gobert D, Topolnik L, Azzi M, Huang L, Badeaux F, Desgroseillers L, Sossin WS, Lacaille JC (2008) Forskolin induction of late-LTP and up-regulation of 5' TOP mRNAs translation via mTOR, ERK, and PI3K in hippocampal pyramidal cells. J Neurochem 106:1160-1174.
Harris EW, Ganong AH, Cotman CW (1984) Long-term potentiation in the hippocampus involves activation of N-methyl-D-aspartate receptors. Brain Res 323:132-137.
Hay N, Sonenberg N (2004) Upstream and downstream of mTOR. Genes Dev 18:1926-1945.
Holz MK, Ballif BA, Gygi SP, Blenis J (2005) mTOR and S6K1 mediate assembly of the translation preinitiation complex through dynamic protein interchange and ordered phosphorylation events. Cell 123:569-580.
Huang F, Chotiner JK, Steward O (2007) Actin polymerization and ERK phosphorylation are required for Arc/Arg3.1 mRNA targeting to activated synaptic sites on dendrites. J Neurosci 27:9054-9067.
Impey S, Obrietan K, Storm DR (1999) Making new connections: role of ERK/MAP kinase signaling in neuronal plasticity. Neuron 23:11-14.
Jefferies HB, Reinhard C, Kozma SC, Thomas G (1994) Rapamycin selectively represses translation of the "polypyrimidine tract" mRNA family. Proc Natl Acad Sci USA 91:4441-4445.
Jefferies HBJ (1997) Rapamycin suppresses 5'TOP mRNA translation through inhibition of p70s6k. EMBO J 16:3693-3704.
Kandel ER (2001) The molecular biology of memory storage: a dialogue between genes and synapses. Science 294:1030-1038.
Kelleher RJ, Govindarajan A, Jung H-Y, Kang H, Tonegawa S (2004) Translational control by MAPK signaling in long-term synaptic plasticity and memory. Cell 116:467-479.
Kelly, Mullany PM, Lynch MA (2000) Protein synthesis in entorhinal cortex and long-term potentiation in dentate gyrus. Hippocampus 10:431-437.
Klann E, Dever TE (2004) Biochemical mechanisms for translational regulation in synaptic plasticity. Nature reviews Neuroscience 5:931-942.
Knight Zachary A, Tan K, Birsoy K, Schmidt S, Garrison Jennifer L, Wysocki Robert W, Emiliano A, Ekstrand Mats I, Friedman Jeffrey M (2012) Molecular Profiling of Activated Neurons by Phosphorylated Ribosome Capture. Cell 151:1126-1137.
Lee-Fruman KK, Kuo CJ, Lippincott J, Terada N, Blenis J (1999) Characterization of S6K2, a novel kinase homologous to S6K1. Oncogene 18:5108-5114.

Lynch G, Larson J, Kelso S, Barrionuevo G, Schottler F (1983) Intracellular injections of EGTA block induction of hippocampal long-term potentiation. Nature 305:719-721.
Maletic-Savatic M, Malinow R, Svoboda K (1999) Rapid dendritic morphogenesis in CA1 hippocampal dendrites induced by synaptic activity. Science 283:1923-1927.
Mazzucchelli C, Brambilla R (2000) Ras-related and MAPK signalling in neuronal plasticity and memory formation. Cell Mol Life Sci 57:604-611.
Nielsen PJ, Duncan R, McConkey EH (1981) Phosphorylation of Ribosomal Protein S6. Relationship to Protein Synthesis in HeLa Cells. Eur J Biochem 120:523-527.
Panja D, Dagyte G, Bidinosti M, Wibrand K, Kristiansen AM, Sonenberg N, Bramham CR (2009) Novel translational control in Arc-dependent long term potentiation consolidation in vivo. J Biol Chem 284:31498-31511.
Park IH, Bachmann R, Shirazi H, Chen J (2002) Regulation of ribosomal S6 kinase 2 by mammalian target of rapamycin. J Biol Chem 277:31423-31429.
Pearce LR, Alton GR, Richter DT, Kath JC, Lingardo L, Chapman J, Hwang C, Alessi DR (2010) Characterization of PF-4708671, a novel and highly specific inhibitor of p70 ribosomal S6 kinase (S6K1). Biochem J 431:245-255.
Pirbhoy PS, Farris S, Steward O (2016) Synaptic activation of ribosomal protein S6 phosphorylation occurs locally in activated dendritic domains. Learn Mem 23:255-269.
Qi S, Mizuno M, Yonezawa K, Nawa H, Takei N (2010) Activation of mammalian target of rapamycin signaling in spatial learning. Neurosci Res 68:88-93.
Raught B, Gingras AC, Gygi SP, Imataka H, Morino S, Gradi A, Aebersold R, Sonenberg N (2000) Serum-stimulated, rapamycin-sensitive phosphorylation sites in the eukaryotic translation initiation factor 4GI. EMBO J 19:434-444.
Roux PP, Shahbazian D, Vu H, Holz MK, Cohen MS, Taunton J, Sonenberg N, Blenis J (2007) RAS/ERK signaling promotes site-specific ribosomal protein S6 phosphorylation via RSK and stimulates cap-dependent translation. J Biol Chem 282:14056-14064.
Sanna PP, Cammalleri M, Berton F, Simpson C, Lutjens R, Bloom FE, Francesconi W (2002) Phosphatidylinositol 3-kinase is required for the expression but not for the induction or the maintenance of long-term potentiation in the hippocampal CA1 region. J Neurosci 22:3359-3365.
Shahbazian D, Roux PP, Mieulet V, Cohen MS, Raught B, Taunton J, Hershey JWB, Blenis J, Pende M, Sonenberg N (2006) The mTOR/PI3K and MAPK pathways converge on eIF4B to control its phosphorylation and activity. EMBO J 25:2781-2791.
Steward O (1976) Topographic organization of the projections from the entorhinal area to the hippocampal formation of the rat. J Comp Neurol 167:285-314.
Steward O, Worley PF (2001) Selective targeting of newly synthesized Arc mRNA to active synapses requires NMDA receptor activation. Neuron 30:227-240.
Steward O, Wallace C, Lyford G, Worley P (1998) Synaptic activation causes the mRNA for the IEG Arc to localize selectively near activated postsynaptic sites on dendrites. Neuron 21:741-751.
Sweatt JD (2001) The neuronal MAP kinase cascade: a biochemical signal integration system subserving synaptic plasticity and memory. J Neurochem 76:1-10.
Sweatt JD (2004) Mitogen-activated protein kinases in synaptic plasticity and memory. Curr Opin Neurbiol 14:311-317.

Tang SJ, Reis G, Kang H, Gingras AC, Sonenberg N, Schuman EM (2002) A rapamycin-sensitive signaling pathway contributes to long-term synaptic plasticity in the hippocampus. Pro Natl Acad Sci USA 99:467-472.
Terada N, Patel HR, Takase K, Kohno K, Nairn AC, Gelfand EW (1994) Rapamycin selectively inhibits translation of mRNAs encoding elongation factors and ribosomal proteins. Proc Natl Acad Sci USA 91:11477-11481.
Thoreen CC, Chantranupong L, Keys HR, Wang T, Gray NS, Sabatini DM (2012) A unifying model for mTORC1-mediated regulation of mRNA translation. Nature 485:109-113.
Vlahos CJ, Matter WF, Hui KY, Brown RF (1994) A specific inhibitor of phosphatidylinositol 3-kinase, 2-(4-morpholinyl)-8-phenyl-4H-1-benzopyran-4-one (LY294002). J Biol Chem 269:5241-5248.
Wang L, Gout I, Proud CG (2001) Cross-talk between the ERK and p70 S6 kinase (S6K) signaling pathways. MEK-dependent activation of S6K2 in cardiomyocytes. J Biol Chem 276:32670-32677.
Wang X (2001) Regulation of elongation factor 2 kinase by p90RSK1 and p70 S6 kinase. EMBO J 20:4370-4379.
Wettenhall RE, Erikson E, Maller JL (1992) Ordered multisite phosphorylation of Xenopus ribosomal protein S6 by S6 kinase II. J Biol Chem 267:9021-9027.

CHAPTER 4

Optogenetic stimulation of the medial perforant path

Abstract

To study activity-dependent trafficking of mRNAs, it is desirable to selectively activate synapses terminating on discrete dendritic domains. *In vivo*, this can be accomplished by stimulating the entorhinal cortex (EC) to activate medial perforant path (MPP) projections to the dentate gyrus (DG). Such selective activation is impractical in slice preparations, however, because current spread makes it difficult to be certain that only perforant path (PP) synapses are activated. Here, we document selective activation of MPP synapses in hippocampal slices using an optogenetic approach. Adult female Sprague-Dawley rats received injections of AAV8-CAG-ChR2-GFP into the medial EC and were allowed to survive for 6-8 weeks to allow for orthograde transport of channelrhodopsin-2 (ChR2) to PP synapses on dentate granule cells. Immunocytochemistry for GFP revealed robust labeling of PP projections to both the DG and hippocampus proper. Other rats were used to prepare transverse horizontal hippocampal slices for *in vitro* neurophysiology. Recording electrodes were positioned in the granule cell layer of the DG to record field excitatory postsynaptic potentials (fEPSPs) as a positive potential or in the synaptic layer to record fEPSPs as a negative potential. Stimulating electrodes, a twisted nichrome wire (65μm) for electrical stimulation or a fiber optic attached to a micromanipulator for optical stimulation, were positioned in the middle molecular layer (MML) of the DG (inner leaf), immediately next to each other. Optical stimulation was delivered using a 473nm blue light to illuminate a spot of approximately 80μm in diameter. Optical stimulation triggered fEPSPs with onset latencies of approximately 4.5ms and peak amplitude at 11ms. Field

EPSPs evoked by electrical stimulation had onset latencies of 2ms and peak amplitude at 5ms. Varying light intensity of the laser from 0-100% resulted in progressive increases in fEPSP amplitude to a maximum of 0.91mV. Delivery of 2x100Hz trains of electrical pulses via the stimulating electrode led to increases in fEPSP amplitude for both electrically-induced and optically-induced responses, indicating that the two modes of stimulation activated overlapping populations of synapses. To characterize currents generated by optical stimulation, patch clamp techniques were used to record from individual granule cells. Optical stimulation with 2Hz trains, 150 pulses led to a 305% increase in EPSC amplitude that remained stable for up to 80 minutes. Our results demonstrate the feasibility of combining orthograde transport of ChR2 and optogenetic stimulation to activate diverse subsets of synapses in hippocampal slices *in vitro*.

Introduction

Synaptic plasticity is viewed as the ability of neurons to alter the strength of synaptic connections in response to experience. The induction of long-term potentiation (LTP) following high-frequency stimulation (HFS) has been shown to result in a persistent increase in synaptic strength between activated synapses and is viewed as a synaptic mechanism underlying certain forms of learning and memory (Bliss and Lomo, 1973; Morris et al., 1986). Identifying molecular substrates that are present at activated synapses is a high priority to identify how LTP-induced processes mediate synaptic plasticity. Furthermore, being able to activate a selective population of synapses would allow for precise examination of LTP-induced changes that occur at activated synapses versus inactive synapses.

The medial perforant path is commonly used as a model to study synaptic plasticity at activated synapses as projections from the medial entorhinal cortex terminate in a precisely defined lamina in the middle molecular layer of the dentate gyrus (Steward, 1976). The selective localization of mRNAs to activated synapses implicate a role for local protein synthesis in activity-dependent synaptic modifications. For example, delivery of HFS to the medial perforant path *in vivo* results in the selective localization of newly synthesized *Arc* mRNA at activated dendrites (Steward et al., 1998). Also, the induction of LTP has also been shown to result in increased accumulation of calcium/calmodulin-dependent protein kinase II (CaMKII) (Ouyang et al., 1999; Steward and Halpain, 1999) and the elongation factor 1 alpha (EF1α) in dendrites (Huang et al., 2005; Tsokas, 2005). But defined mechanisms of how these mRNAs and other translation-dependent factors that localize at dendrites interact and contribute to synaptic modifications remains obscure. Selective activation of the medial perforant path *in vitro* is difficult because current spread makes it difficult to be confident that only perforant path synapses are activated and due to the proximity of medial and lateral projections, but the use of optogenetic stimulation allows for more specificity in the selective activation of the perforant path. Furthermore, using an *in vitro* model permits the characterization of distinct subpopulations of cells and the use of a combination of experimental techniques to explore mechanisms involved in activity-dependent synaptic modifications.

To selectively activate medial perforant path synapses, one needs to be able to label and isolate their activation. To accomplish this, the present set of experiments takes advantage of channelrhodopsin-2 (ChR2), a light-sensitive channel that allows the influx of cations when illuminated by ~470nm blue light (Nagel et al., 2003), resulting in the

activation of synapses expressing ChR2. In the present set of experiments, we demonstrate that delivery of AAV8-CAG-ChR2-GFP into the medial entorhinal cortex results in orthograde transport of ChR2 to medial perforant path synapses. We also show that optogenetic stimulation evokes field excitatory postsynaptic potentials (fEPSPs) in extracellular field recordings and the induction of excitatory postsynaptic currents (EPSCs) following optogenetic stimulation. Together, these findings demonstrate the feasibility of combining orthograde transport of ChR2 and optogenetic stimulation to activate subsets of synapses in hippocampal slices *in vitro*.

Materials and Methods

Animals: Experimental animals were female Sprague-Dawley rats 6-8wks of age from Harlan Laboratories (HSD). Animals were anesthetized using Isoflurane for medial entorhinal injections of AAV8-CAG-ChR2-GFP (UNC Vector Core services, Ed Boyden Neuroactivators Serotype 8, $2x10^{12}$ genome copies). A series of 4 unilateral injections ranging from 3-6 mm below the cortical surface were administered with a total volume of 1.5μL per infusion site. The Hamilton syringe was angled 10 degrees away from the midline. Coordinates for medial entorhinal injections were +0.5mm from lambda suture and 4.0mm lateral. Following surgeries animals received post-operative care and were allowed to survive 8-12wks before experimental procedures. All experimental procedures were approved by the Institutional Animal Care and Use Committee (IACUC) of the University of California, Irvine.

Extracellular field recordings: Hippocampal extracellular field recordings were performed by Brian Trieu. Experiments were performed similarly to extracellular field recordings performed in the laboratory of Dr. Gary Lynch (Trieu et al., 2015). Briefly, rats were decapitated, and the brain quickly removed and submerged in oxygenated, ice-cold, high magnesium artificial cerebral spinal fluid (ACSF) containing (in mM) 124 NaCl, 3 KCl, 1.25 KH_2PO_4, 5 $MgSO_4$, 26 $NaHCO_3$, and 10 dextrose. Transverse horizontal hippocampal slices were prepared using a McIlwain tissue chopper and transferred to an interface recording chamber. Slices were continuously perfused with preheated oxygenated ACSF containing (in mM): 124 NaCl, 3 KCl, 1.25KH_2PO_4, 1.5 $MgSO_4$, 26 $NaHCO_3$, 2.5 $CaCl_2$, and 10 dextrose at a rate of 60-70ml/hr. Recordings began 1.5 hours after transfer to the chamber. Recording electrodes were positioned in the granule cell layer of the dentate gyrus to record field excitatory postsynaptic potentials (fEPSPs) as a positive potential or in the synaptic layer to record fEPSPs as a negative potential. Stimulating electrodes, a twisted nichrome wire (65μm) for electrical stimulation or a fiber optic attached to a micromanipulator for optical stimulation, were positioned in the middle molecular layer (MML) of the dentate gyrus (inner leaf), immediately next to each other. Optical stimulation was delivered using a 473nm blue light to illuminate a spot of approximately 80 μm in diameter.

Whole-Cell Recordings: Whole-cell recordings were performed by Dr. Yousheng Jia, in the laboratory of Dr. Gary Lynch (Trieu et al., 2015). Briefly, hippocampal slices were placed in a submerged recording chamber continuously perfused at 2-3ml/min with oxygenated (95% O_2/5%CO_2) normal ACSF at 32°C. Whole-cell recordings (Axopatch 200A amplifier: Molecular Devices) were made with 4-7MΩ recording pipettes filled with a solution

containing (in mM): 130 $CsMeSO_4$, 10 CsCl, 8 NaCl, 10 HEPES, 0.2 EGTA, 5 QX-314, 2 Mg-ATP, 0.3 Na-GTP. Osmolarity was adjusted to 290-295 mOsm, and pH buffered at 7.25. Excitatory postsynaptic currents (EPSCs) recorded from dentate granule cells were clamped at -70mV in the presence of 50μM picrotoxin.

Immunohistochemistry: Following recording, slices were fixed in 4% paraformaldehyde in 0.1M sodium phosphate buffer (PB), pH 7.2 for 12-16hrs. Sections were then cryoprotected in 20% sucrose/4% paraformaldehyde for 2hrs at 4C. Hippocampal slices were then sectioned on a cryostat at 20μm, mounted on Fisher Super frost plus slides. For immunostaining, slides were washed in Tris-buffered saline (TBS), blocked in 0.1% Triton X-100 with 5% natural goat serum for 1hr and then incubated overnight with a polyclonal Green Fluorescent Protein (GFP) Tag antibody (GFP isolated directly from the jellyfish Aequorea Victoria) made in rabbit/IgG at a dilution of 1:15000 (Invitrogen, cat. A11122). Slides were then incubated using goat anti-rabbit AF488 at a dilution of 1:250 (Invitrogen, cat. A11034).

Results

Transport of ChR2 to Medial perforant path synapses

To selectively activate medial perforant path synapses using optogenetic stimulation, ChR2 must be present at perforant path synapses. To determine optimal delivery of the vector to the perforant path synapses a series of injection parameters were performed in the medial entorhinal cortex. These initial experiments were to determine the optimal concentration and time necessary for the delivery of ChR2 to perforant path

synapses. Delivery of AAV8-CAG-ChR2-GFP was performed using a Hamilton syringe angled 10 degrees away from the midline. Optimal coordinates that led to the robust expression of ChR2-GFP at perforant path synapses was +0.5mm from lambda suture and 4.0mm lateral. A series of 4 unilateral injections ranging from 3-6 mm below the cortical surface were administered with a total volume of 1.5μL per infusion site. Volumes of 1μL resulted in low levels of expression that were not optimal for extracellular field recordings. Volumes of 2μL also produced robust expression at perforant path synapses that were optimal for extracellular recordings. Delivery of ChR2 to perforant path synapses was observed as early as two weeks post injection. Expression of ChR2 was also observed four weeks post injection. At this time point, optogenetic stimulation evoked EPSPs. Eight weeks post injection produced robust expression of ChR2 at perforant path synapses and optogenetic stimulation evoked EPSPs. Figure 1 illustrates one case eight-weeks post-injection. Panels 1A-1C illustrate the native AAV-CAG-ChR2-GFP fluorescence. Panels 1D-1F illustrate the same case following immunostaining for AAV-CAG-ChR2-GFP using a GFP-tag antibody and detection with AF 488.

Optogenetic stimulation elicits field EPSPs

Once ChR2 expression was observed at perforant path synapses and in sufficient quantities to elicit evoked EPSPs, we set out to determine optimal conditions in which optogenetic stimulation elicited field EPSPs (fEPSPs). Extracellular recordings in which 3μM picrotoxin was included in the ACSF produced evoked EPSPs. For extracellular field recordings with a single stimulating and recording electrode (Figure 2A), opto-induced fEPSPs increased in amplitude with increasing light intensities (Figure 2B). An fEPSP with an amplitude of approximately 0.3mV was observed with optical stimulation of 10% light

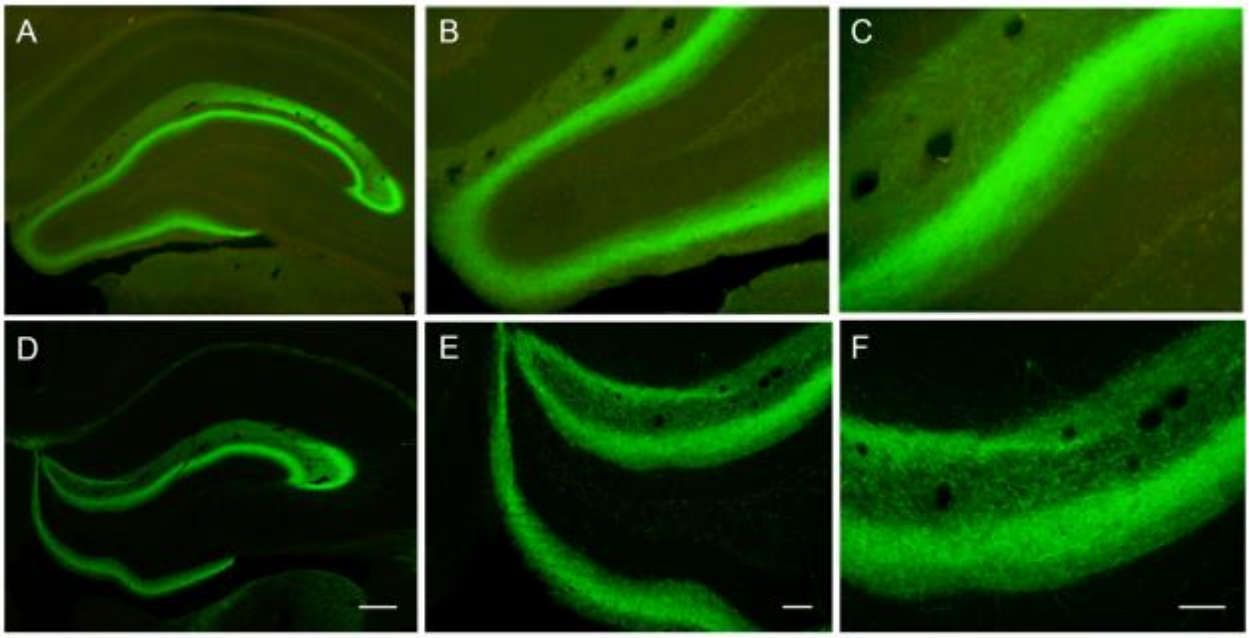

Figure 4.1. ChR2-GFP native Fluorescence and Immunostaining with Alexa Fluor 488. A) Image of native AAV-CAG-ChR2-GFP fluorescence at 4x magnification. **B)** Magnified image of A (10x). **C)** High-magnification image of A (20x). **D)** Image of immunostaining for AAV-CAG-ChR2-GFP using Alexa Fluor 488 at 4x magnification. **E)** Magnified image of D (10x). **F)** High-magnification image of D (20x). Scale bars: **D,** 200μm; **E,** 100μm; **F,** 50μm.

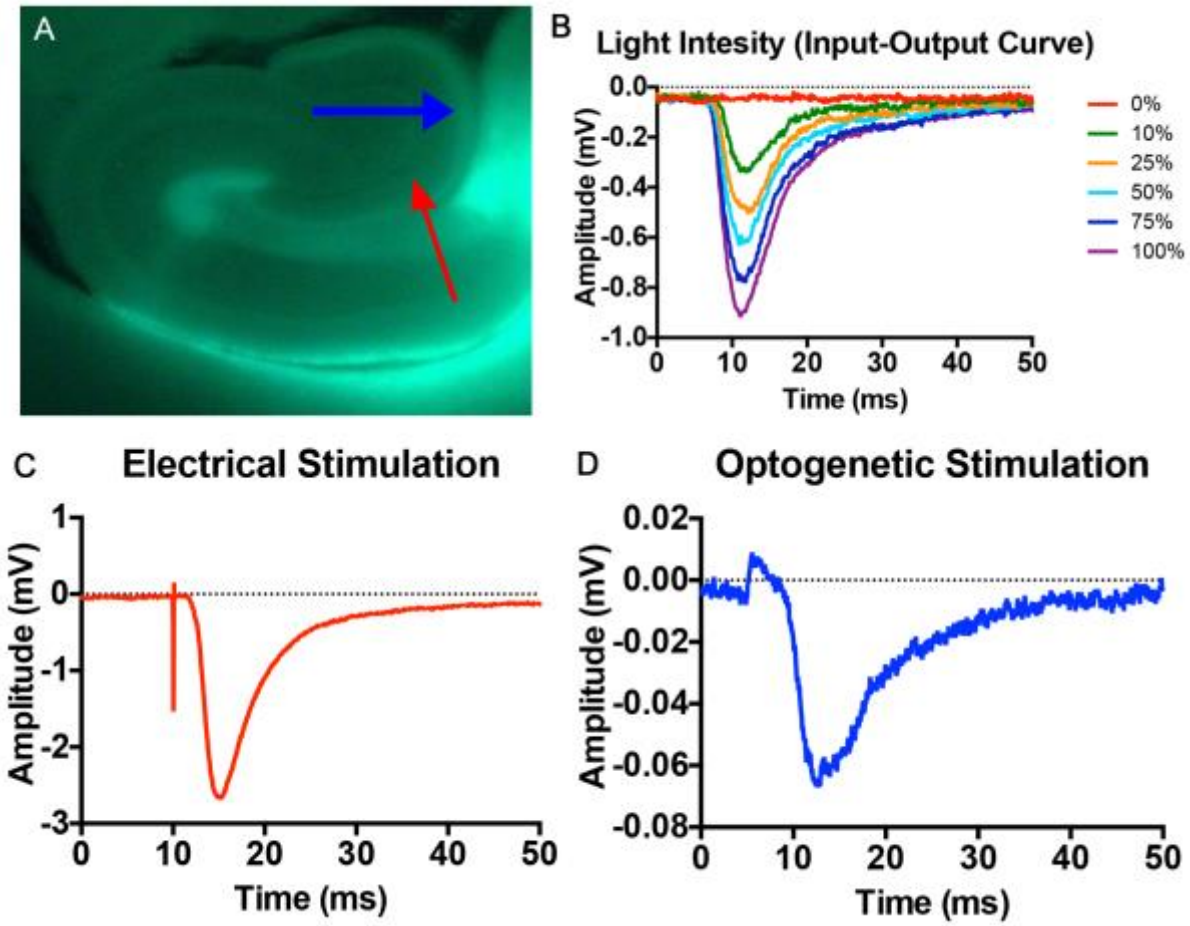

Figure 4.2. Optogenetic stimulation elicits field excitatory postsynaptic potentials (fEPSPs). **A,** Image of recording (blue) and stimulating electrode (red) placement in hippocampal slice. **B,** Opto-induced fEPSP following varying light intensities ranging from 0-100% intensity. **C,** fEPSP following electrical stimulation. **D,** fEPSP following optical stimulation.

intensity. With 100% light intensity, an amplitude of approximately 0.9-1mV was observed. Field EPSPs evoked by electrical stimulation had onset latencies of 2ms and peak amplitude at 5ms (Figure 2C). Optical stimulation triggered fEPSPs with onset latencies of approximately 4.5ms and peak amplitude at 11ms (Figure 2D).

When two stimulating electrodes were placed in the middle molecular layer of the dentate gyrus (Figure 3A), Ch1 and Ch2, potentiation of both Ch1 and Ch2 was observed following delivery of HFS (Figure 3B and 3C). Interestingly, potentiation of the optical response was also observed following delivery of HFS to Ch1 and Ch2 (Figure 3D and 3E). It was also observed that potentiation of the opto-induced fEPSP was greatest following delivery of HFS to Ch2 (Figure 3F). A larger increase in amplitude was observed when optical stimulation was paired with the delivery of HFS to Ch2, suggesting that synapses activated by optical stimulation shared overlapping synapses with those activated by delivery of HFS to Ch2. Collectively, these findings show that induction of LTP by electrical stimulation induces potentiation of optically-induced responses.

Induction of LTP with Optogenetic stimulation

To determine if induction of LTP could be accomplished with optogenetic stimulation, we used whole-cell recordings. EPSCs were recorded at -70mV from dentate granule cells. Figure 4A and 4B illustrate granule cells labeled with AF 594 that were used for whole-cell recordings. Induction of LTP following optogenetic stimulation resulted in a 305% increase in EPSC amplitude (Figure 4C). This effect was replicated in at least five separate whole-cell recordings (Figure 4D).

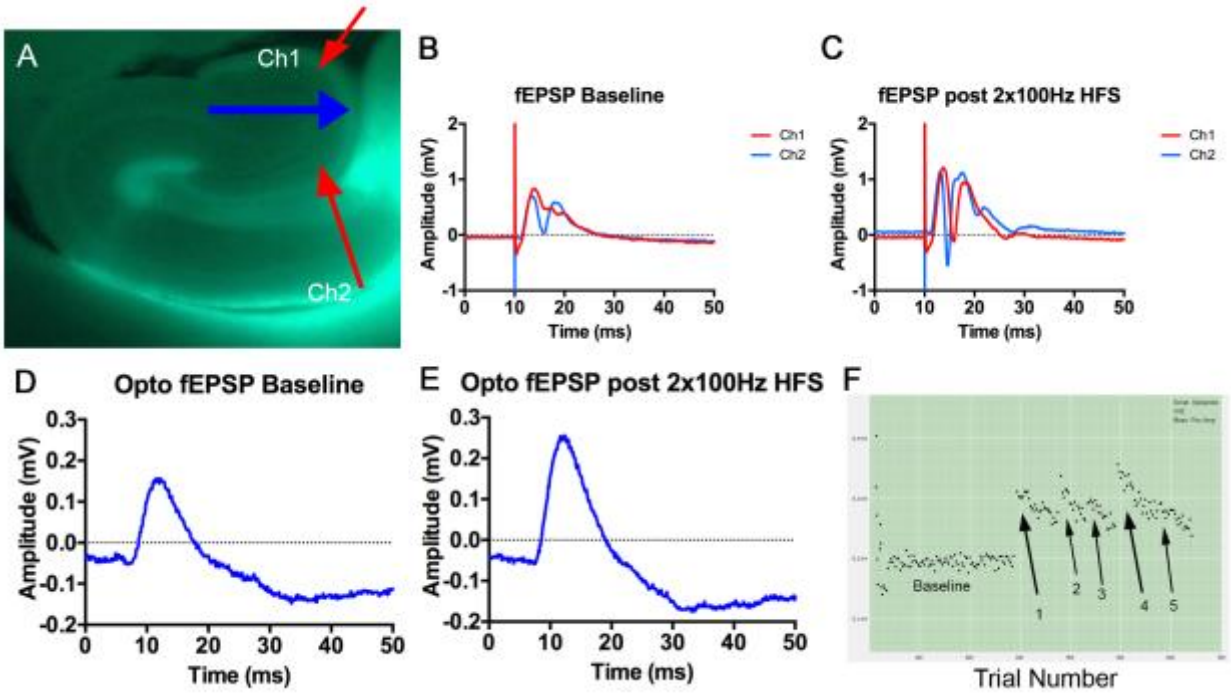

Figure 4.3. Stimulation of perforant path synapses using two stimulating electrodes. A, Image showing recording (red, ch1 and ch2) and stimulating electrode (blue) placement in hippocampal slice. **B,** Channel 1 and 2 baseline fEPSP. **C,** Channel 1 and 2 fEPSP following 2x100Hz of HFS. **D,** Opto fEPSP during baseline. **E,** Opto fEPSP following 2x100Hz to Ch1 and Ch2. Note potentiation of opto fEPSP following HFS stimulation to Ch1 and Ch2. Optical and electrical stimulation activate overlapping populations of synapses. **F)** Positive amplitude of opto fEPSP following HFS and paired HFS/Opto stimulation. Numbers represent: 1, HFS delivered to Ch1/Ch2. 2, HFS delivered to Ch2. 3, HFS delivered to Ch1. 4, Opto and Ch2 stimulation paired. 5, Opto and Ch1 stimulation paired. Slices in 3μM picrotoxin in ACSF. Slice physiology performed by Brian Trieu.

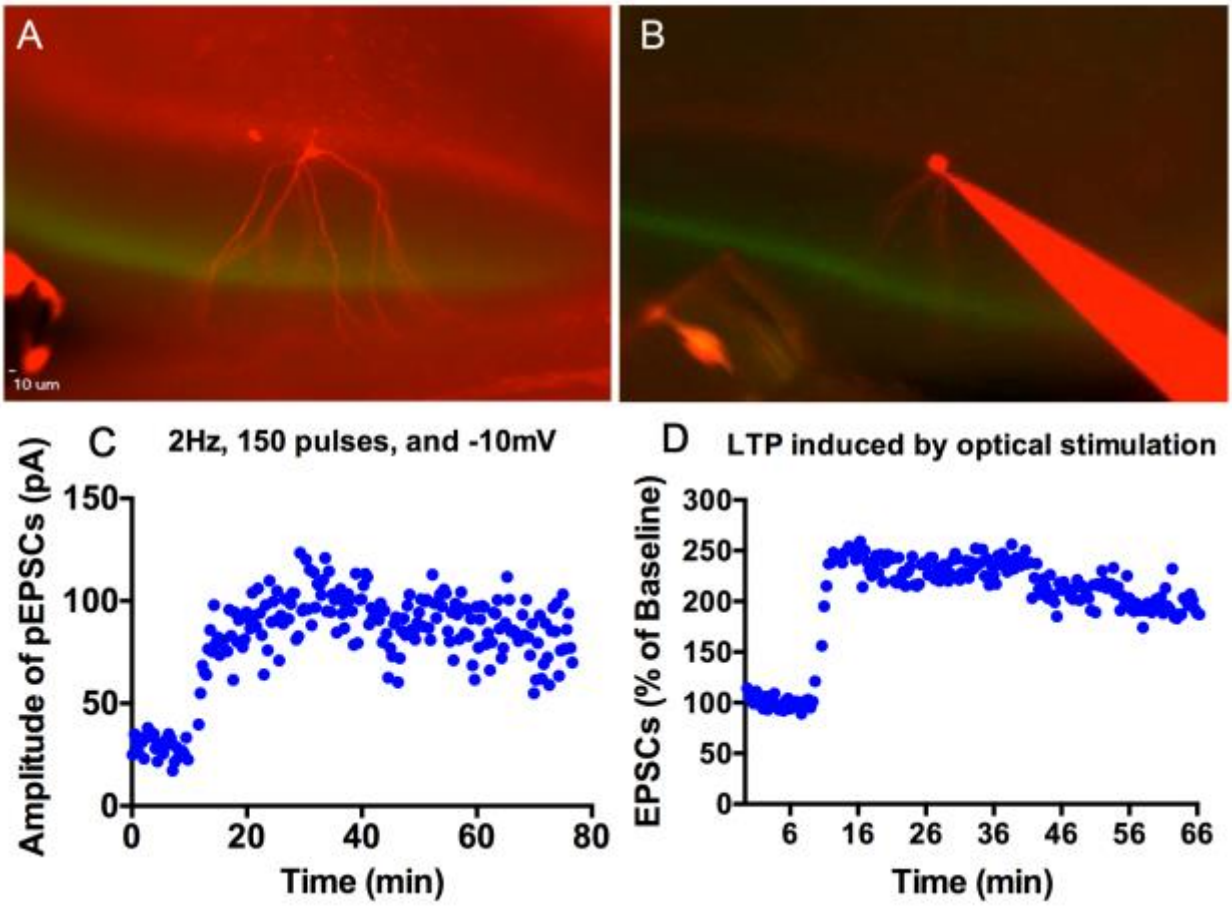

Figure 4.4 Induction of excitatory postsynaptic currents (EPSCs) following optogenetic stimulation. EPSCs were recorded at -70mV using intracellular solution containing $CsMeSO_3$, QX314, and Alexa Fluor 594. Picrotoxin included in ACSF. **A,** Image of granule cell in the dentate gyrus used for patch clamp recording filled with AF 594. **B,** Image of granule cell in a different slice. **C,** Plot of EPSCs over time course of the experiment. Observed a 305% increase in opto EPSC following induction of LTP. **D,** Average LTP induced by optical stimulation (n=5). Whole-cell recordings performed by Yousheng Jia.

Discussion

The present set of experiments demonstrates that injection of AAV8-CAG-ChR2-GFP to the medial entorhinal cortex results in transport of ChR2 to medial perforant path synapses. Transport of ChR2 to perforant path synapses allows for selective activation of a subset of synapses with which extracellular recordings evoked fEPSPs. Induction of LTP using electrical stimulation also resulted in potentiation of the opto-induced fEPSP when stimulation electrodes shared overlapping subsets of synapses. Furthermore, whole-cell recordings demonstrate that optogenetic stimulation elicits EPSCs and that induction of LTP following optical stimulation results in enhanced potentiation of EPSCs. Together, these results illustrate the feasibility of the using optogenetic stimulation to study underlying mechanisms of mRNA targeting at activated synapses.

The discovery of optogenetics has provided the field with powerful tools to explore underlying mechanisms involved in synaptic plasticity. For example, several studies have used optogenetics in awake behaving animals to define cell ensembles involved in specific memory-related tasks. One group performed an intriguing study where they targeted activated neuronal ensembles following contextual fear conditioning to test the hypothesis that the dentate gyrus is an ideal target for the formation of contextual fear memory engrams that represent discrete environments (Ramirez et al., 2014). This study used TetTag mice harboring the transgene c-fos-tetracycline transactivator (tTA). This transgene contains the c-fos promoter, which drives the expression of tTA. The binding of tTA is blocked by Dox, so if Dox is removed from the diet, a window of activity-dependent labeling opens where tTA can bind to the tetracycline-responsive element (TRE) to turn on the expression of ChR2-EYFP in activated granule cells. Taking advantage of this system,

they allowed animals to explore a novel environment (context A) while on Dox diets and thus no ChR2-EYFP was expressed. They later fear conditioned the mice in context B, while off Dox and then place them back on the Dox diet immediately after training. A day later, animals were placed back in context A and stimulated with light to activate the neurons labeled during fear conditioning in context B. Interestingly, they found that optogenetic stimulation of these cells resulted in increased freezing indicative of fear memory recall (Ramirez et al., 2014). This study illustrates how optogenetic stimulation can also be used in awake behaving animals and furthermore how an animal's environment is represented in neuronal ensembles in the hippocampus. Using optogenetics to understand the contribution of cell ensembles moves the field closer to establishing a circuit and functional mapping of multiple memory engrams throughout the brain.

The present set of experiments demonstrates the feasibility of using transport of ChR2 to perforant path synapses to study mRNA targeting mechanisms at activated synapses following the induction of LTP. There are currently several questions remaining about synaptic plasticity mechanisms underlying the induction of LTP and learning and memory. Understanding what is happening at the synapses level at activated synapses may provide the field with answers about synaptic modifications occurring during memory consolidation. The continuous development of new powerful tools, like optogenetic stimulation, will continue to enhance our understanding of mechanisms underlying learning and memory.

References

Bliss TV, Lomo T (1973) Long-lasting potentiation of synaptic transmission in the dentate area of the anaesthetized rabbit following stimulation of the perforant path. J Physiol (Lond) 232:331-356.

Huang F, Chotiner JK, Steward O (2005) The mRNA for elongation factor 1alpha is localized in dendrites and translated in response to treatments that induce long-term depression. J Neurosci 25:7199-7209.

Morris RG, Anderson E, Lynch GS, Baudry M (1986) Selective impairment of learning and blockade of long-term potentiation by an N-methyl-D-aspartate receptor antagonist, AP5. Nature 319:774-776.

Nagel G, Szellas T, Huhn W, Kateriya S, Adeishvili N, Berthold P, Ollig D, Hegemann P, Bamberg E (2003) Channelrhodopsin-2, a directly light-gated cation-selective membrane channel. Pro Natl Acad Sci USA 100:13940-13945.

Ouyang Y, Rosenstein A, Kreiman G, Schuman EM, Kennedy MB (1999) Tetanic stimulation leads to increased accumulation of Ca(2+)/calmodulin-dependent protein kinase II via dendritic protein synthesis in hippocampal neurons. J Neurosci 19:7823-7833.

Ramirez S, Tonegawa S, Liu X (2014) Identification and optogenetic manipulation of memory engrams in the hippocampus. Frontiers in Behavioral Neuroscience 7.

Steward O (1976) Topographic organization of the projections from the entorhinal area to the hippocampal formation of the rat. J Comp Neurol 167:285-314.

Steward O, Halpain S (1999) Lamina-specific synaptic activation causes domain-specific alterations in dendritic immunostaining for MAP2 and CAM kinase II. J Neurosci 19:7834-7845.

Steward O, Wallace C, Lyford G, Worley P (1998) Synaptic activation causes the mRNA for the IEG Arc to localize selectively near activated postsynaptic sites on dendrites. Neuron 21:741-751.

Trieu BH, Kramar EA, Cox CD, Jia Y, Wang W, Gall CM, Lynch G (2015) Pronounced differences in signal processing and synaptic plasticity between piriform-hippocampal network stages: a prominent role for adenosine. J Physiol 593:2889-2907.

Tsokas P (2005) Local Protein Synthesis Mediates a Rapid Increase in Dendritic Elongation Factor 1A after Induction of Late Long-Term Potentiation. J Neurosci 25:5833-5843.

CHAPTER 5

Summary and Conclusions

Compelling evidence demonstrates that LTP results in a persistent increase in synaptic strength between synapses. This enhanced synaptic transmission is believed to serve as a cellular and molecular mechanism that parallels synaptic modifications observed in learning and memory. Key mediators of LTP-induced synaptic plasticity have been identified, for example, NMDA receptors, calcium, and CaMKII have all been shown to be required for the induction of LTP. But precise molecular mechanisms linking NMDA receptor activation and signal transduction pathways to specific synaptic modifications remains elusive.

A leading hypothesis in the field describing how synaptic stimulation can result in synaptic modifications selectively at activated synapses is activity-dependent local protein synthesis. The process of synthesizing new proteins is highly energy-dependent. The ability of a cell to locally translate mRNAs would provide an efficient mechanism to satisfy a dynamic requirement for protein synthesis at specific subcellular compartments in response to stimulation. The discovery of polyribosomes and other translation-related factors near dendritic spines provided critical evidence to support the existence of mechanisms regulating local protein synthesis. It has been a little over 30 years since the discovery of polyribosomes, and the evidence supporting local protein synthesis continues to grow. The number of dendritic mRNAs identified using deep sequencing techniques is reported to be in the thousands in the synaptic neuropil of the hippocampus. Despite the growing list of mRNAs identified, the field is still unclear as to how each of these mRNAs is regulated by activity and how they contribute to specific synaptic modifications. A great

number of studies also report connections linking signal transduction pathways to LTP-induced synaptic modifications and processes underlying learning and memory. In fact, activation of critical substrates, such as PI3-kinase/mTOR and MAPK/ERK reported as key regulators of translation following synaptic activation. But whether they exert translational control independently or synergistically by targeting a common key regulator of translational control remains unclear.

Phosphorylation of rpS6 emerges as a potential candidate by which translation may be regulated at activated synapses in response to synaptic activation induced by HFS and in response to neural activity following a behavioral learning task. There is compelling evidence indicating that rpS6 phosphorylation is involved in the initiation of translation. For example, phosphorylation of rpS6 has been shown to correlate with the initiation of protein synthesis and enhanced 5TOP mRNA translation. 40S ribosomal subunits containing phosphorylated rpS6 have been shown to more efficiently mobilize into polysomes and contribute to the stabilization of the pre-initiation complex. Furthermore, rpS6 is in a prime location, at the interface between the small and large ribosomal subunit, to regulate the initiation of translation and interact with mRNAs, tRNA and initiation factors. The results of the studies detailed in this body of work further add to studies in the field by supporting a role for phosphorylation of rpS6 as a mechanism to regulate the initiation of translation in response to synaptic activity.

A large number of studies to date report findings for rpS6 phosphorylation using experimental methods in cells in culture. The field lacks studies investigating the role of rpS6 phosphorylation in neurons. This body of work sheds light on the role of rpS6 phosphorylation in dentate granule cells in response to synaptic activity. A previous study

done by Panja et al. (2009), reported the finding that HFS induced robust phosphorylation of rpS6 in dentate granule cell bodies and dendrites. This body of work extends that finding, as detailed in Chapter 2, by revealing the previously unknown finding that phosphorylation of rpS6 accumulates selectively at the region of activated synapses. Furthermore, this effect predominately occurs at ser235/236. Most notably, the results show that synaptically-driven rpS6 phosphorylation is NMDA receptor-dependent. Given the importance of NMDA receptor activation in the induction of LTP and synaptic plasticity underlying learning and memory, this finding implicates that phosphorylation of rpS6 may also contribute to these processes.

Phosphorylation of rpS6 is commonly associated with increases in protein synthesis; specifically, it has been shown to regulate global protein synthesis as a downstream effector of mTOR, and it has been implicated in the translation of eIF4E-sensitive mRNAs (cap-dependent translation) and 5'TOP mRNA translation. This study specifically explored the role of rpS6 phosphorylation in regulating global protein synthesis. Surprisingly, robust phosphorylation of rpS6 did not result in increased levels of protein synthesis in the cell bodies of dentate granule cells or dendrites. This finding further confirms that phosphorylation of rpS6 in not involved in general or global protein synthesis but may, in fact, be responsible for the regulation of a specific class of mRNAs. The present set of studies did not directly test the role of rpS6 phosphorylation in regulating 5'TOP mRNA translation, but it is evident that these experiments need to be done in neurons. One intriguing study took advantage of the inducible phosphorylation of rpS6 and captured phosphorylated ribosomes to identify mRNAs expressed in discrete subpopulations of activated cells in the hypothalamus. Taking advantage of this technique

following HFS of the medial perforant path would provide the necessary identification of key mRNAs directly regulated by rpS6 phosphorylation following synaptic activity. Currently, there is speculation as to which mRNAs rpS6 phosphorylation may regulate and the Knight et al. (2012) study provides a detailed list of mRNAs regulated in the hypothalamus, but it is possible that these mRNAs may be different in specific cell types and in response to stimulation paradigms.

The current experiments also demonstrate that phosphorylation of rpS6 at ser235/236 is selectively activated in the portion of dendrite contacted by active synapses following medial perforant path stimulation. Interestingly, phosphorylation of rpS6 at ser236/236 has been shown to be regulated by multiple signal transduction pathways, including mTOR, cAMP, Wnt, and MAPK/ERK. In the hippocampus, the PI3-kinase/mTOR and the MAPK/ERK pathway have both been shown to be important for LTP and behavioral learning tasks. Both PI3-kinase/mTOR and MAPK/ERK-dependent substrates have been identified in dendrites following synaptic activation. Accumulating evidence also points to a potential interaction between these signal transduction pathways in regulating translation. In fact, it has been proposed that MAPK/ERK controls translation by directly activating mTOR-dependent substrates implicated in translational control. Specific mechanisms of how these pathways interact remain unclear, but it has been suggested that RSK, a downstream kinase directly activated by ERK, also phosphorylates PDK1, which is an upstream kinase of mTOR that activates Akt. It has also been suggested that PI3-kinase directly activates MEK, as treatment with the PI3-kinase inhibitor, wortmannin has been shown to inhibit phosphorylation of both MEK and ERK. Experiments detailing these

interactions remain controversial. Additional studies are required to identify upstream interactions between PI3-kinase/mTOR and MAPK/ERK signaling pathways.

It is evident that additional studies are required to clarify precisely how PI3-kinase/mTOR and MAPK/ERK signaling pathways interact, but the results of Chapter 3 reveal the surprising previously unknown results that phosphorylation of rpS6 is differentially regulated at cell bodies and dendrites by these signal transduction pathways. Specifically, the results demonstrate that PI3-kinase/mTOR signaling is involved in phosphorylation of rpS6 in granule cell bodies, while MAPK/ERK regulates phosphorylation of rpS6 selectively in the dendrites. This finding has not been observed before and provides compelling evidence supporting a role for regulation of mRNA translation at specific subcellular compartments in response to synaptic activity. Further studies are needed to explore precisely how these signaling pathways interact. Currently, it is unknown whether one pathway is dominant over the other, perhaps under specific conditions, or whether the interaction between these pathways creates a synergistic effect that is necessary to lead to enhanced protein synthesis.

The present study also reveals the finding that induction of rpS6 phosphorylation is observed in Arc protein-positive cells and astrocytes in response to a learning experience. The results show that rpS6 phosphorylation is activated in the same neurons in which Arc is translated. Arc is a unique immediate early gene that has been shown to be critical for memory consolidation and the high percentage of Arc-positive neurons that were also p-rpS6-positive suggest that phosphorylation of rpS6 may contribute to similar processes or may contribute to Arc mRNA translation. The detection of rpS6 phosphorylation in astrocytes points to a potential interaction between phosphorylated rpS6-positive neurons

and phosphorylated rpS6-positive astrocytes during a learning experience. A hypothesis that emerges is that rpS6 may also initiate similar translation-related processes in astrocytes. The mechanisms detailing a potential role for rpS6 phosphorylation in astrocytes was not directly explored in these studies. But it is interesting to speculate that phosphorylation of rpS6 may mediate astrocyte-neuron interactions during a learning experience. The activation of rpS6 phosphorylation in dentate granule cells and p-rpS6-positive astrocytes following exploration of a novel environment offer an interesting model in which to study astrocyte-neuron interactions involved in synaptic plasticity. Overall, the finding that rpS6 phosphorylation is activated in various cell types, including neurons, astrocytes, and interneurons point to rpS6 phosphorylation as a key regulator of processes that occur in a wide range of cell types. For example, phosphorylation of rpS6 is implicated in translational control of 5'TOP mRNAs, which encode for proteins involved in the translational apparatus. If phosphorylation of rpS6 is specifically involved in 5'TOP mRNA translation, it makes sense that phosphorylation of rpS6 may initiate this process in a wide range of cell types and in response to a wide range of stimuli. In order to meet increased protein synthesis demands, a cell may upregulate the synthesis of the translational apparatus to accommodate for the increased synthesis. But definitive evidence remains elusive. It is also possible that phosphorylation of rpS6 may enhance the translation of certain mRNAs while downregulating the translation of others. Overall, it is unclear whether rpS6 phosphorylation is involved in a similar function in all cell types or whether its function may vary depending on cell type or in response to specific stimulation patterns. These are important questions that are beyond the scope of the current body of work and require further research.

The experiments in Chapter 4 provide evidence of a feasible model to study mRNA targeting at activated synapses using optogenetic stimulation. As mentioned, there are many unanswered questions in the field regarding regulation of local mRNA translation in response to activity. The experiments in Chapter 4 show that optogenetic stimulation results in the induction of LTP using whole-cell recordings. This model provides the opportunity to study signals involved in mRNA targeting and perhaps translation. Furthermore, various techniques can be incorporated to allow for studies on single mRNAs labeled with fluorescent markers to investigate their contribution to synaptic modifications following synaptic stimulation.

Collectively, the results presented in this body of work highlight that synaptic stimulation triggers robust phosphorylation of rpS6 extending previous findings by showing the selective localization of rpS6 phosphorylation near activated dendritic domains. These findings support a role for rpS6 phosphorylation in the initiation of translation at activated synapses. Notably, synaptically-driven induction of rpS6 is dependent on NMDA receptor activation suggesting a role for rpS6 phosphorylation in LTP-induced synaptic plasticity and memory formation. Most surprisingly, the results suggest that phosphorylation of rpS6 may serve as a mechanism to regulate translation at specific subcellular compartments in response to synaptic activation. The differential regulation of rpS6 phosphorylation was mediated by PI3-kinase/mTOR and MAPK/ERK signal transduction pathways. Specifically, it was observed that PI3-kinase regulates phosphorylation of rpS6 throughout the postsynaptic cell but plays a minimal role at activated synapses. The MAPK/ERK pathway was found to regulate phosphorylation of rpS6 primarily in the dendrites. Together, these findings provide critical support for

activity-dependent control of mRNA translation mediated by signal transduction pathways. It suggests that signal transduction pathways may regulate functions by specifically targeting subcellular compartments in neurons allowing neurons to accommodate a dynamic requirement for increased protein synthesis in response to synaptic activity. Altogether, the findings reported here highlight the importance of phosphorylation events in synaptic plasticity.